

4. Mathematical models used in engineering structural analysis

In this chapter we pursue a formidable task – to present the most important mathematical models in structural mechanics. In order to best situate our present objectives, let us review some previous developments.

In Chapter 1, the hierarchical modeling process was introduced. The central idea of this process is to provide a rational framework to select appropriate mathematical models to address well defined questions of engineering interest. For structural analysis, there are a number of mathematical models and there is the need to “know” these models to perform the hierarchical modeling process (see Chapter 1).

In Chapter 2, we discussed fundamental conditions that should be met whichever structural mechanics mathematical model is established and solved.

In Chapter 3, we motivated the need for a 3-D formulation of structural problems and presented the highest hierarchical mathematical model for an isotropic material and linear analysis – the 3-D elasticity model. In the current chapter, based on our earlier discussion of the 3-D elasticity model, we present the remaining most relevant mathematical models of structural mechanics. We start with plane elasticity and then move on to bars, plates and shells.

4.1 Plane elasticity

We refer to plane elasticity as the set of mathematical models which describe the behavior of a body using only displacements in a plane. The out-of-plane behavior is assumed or inferred from the in-plane behavior. In the following, we present the plane strain, the plane stress and the axisymmetric mathematical models.

4.1.1 The plane strain model

The plane strain model could have been discussed at the end of Chapter 3 as an example of a model which leads to the exact solution of the 3-D elasticity problem when some geometric and loading restrictions apply.

In order to motivate the plane strain assumptions let us consider the dam schematically shown in Figure 4.1. The dam corresponds geometrically to a

prismatic solid. The loading due to the water and gravity is the same for every cross-sectional plane. Now, suppose that at the end sections the out-of-plane displacements $w(x, y)$ are prevented but the in-plane displacements $u(x, y)$ and $v(x, y)$ are free. At the base all displacements are prevented. Under these conditions, by symmetry, the displacements are clearly the same for every section of the dam. Hence, the complete behavior of the dam can be described by the displacements $u(x, y)$ and $v(x, y)$ at a typical section.

Much aligned with the semi-inverse method, which was introduced for the torsion problem, we formulate the plane strain problem by introducing displacement assumptions for a prismatic solid.

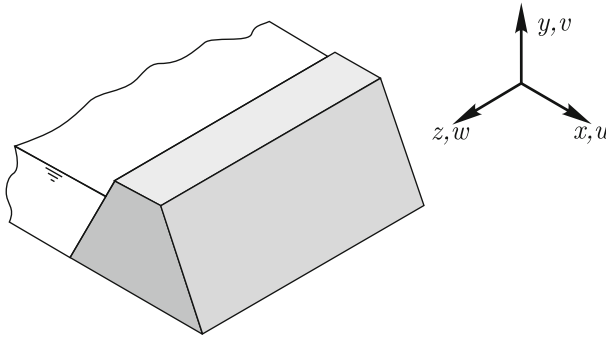


Fig. 4.1. Schematic representation of a dam

Kinematics

Formally, let us consider a prismatic solid as shown in Figure 4.2, whose cross-sections are parallel to the xy plane. Motivated by the above discussion, we introduce the following displacement assumptions

$$u = u(x, y) \quad (4.1)$$

$$v = v(x, y) \quad (4.2)$$

$$w = 0. \quad (4.3)$$

Strain compatibility

Using the compatibility relations

$$\varepsilon_{xx} = \frac{\partial u}{\partial x} \quad \varepsilon_{yy} = \frac{\partial v}{\partial y} \quad \gamma_{xy} = \frac{\partial u}{\partial y} + \frac{\partial v}{\partial x}$$

we obtain

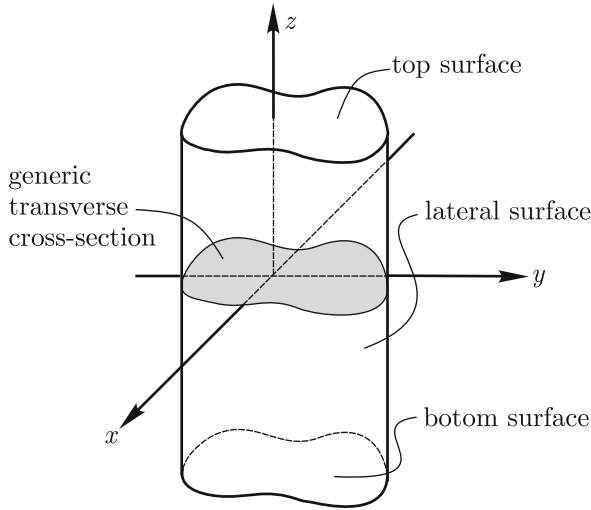


Fig. 4.2. Generic prismatic solid

$$\varepsilon_{xx} = \varepsilon_{xx}(x, y) \quad (4.4)$$

$$\varepsilon_{yy} = \varepsilon_{yy}(x, y) \quad (4.5)$$

$$\gamma_{xy} = \gamma_{xy}(x, y) \quad (4.6)$$

due to the assumptions implicitly given in equations (4.1) and (4.2). Still considering the strain compatibility relations and equations (4.1) to (4.3), we obtain

$$\gamma_{yz} = \frac{\partial v}{\partial z} + \frac{\partial w}{\partial y} = 0$$

$$\gamma_{zx} = \frac{\partial w}{\partial x} + \frac{\partial u}{\partial z} = 0$$

$$\varepsilon_{zz} = \frac{\partial w}{\partial z} = 0.$$

Constitutive relations

Let us consider next the constitutive equations, *i.e.*, the generalized Hooke's law (recall equation (3.110)). Starting with the component ε_{zz}

$$\varepsilon_{zz} = 0 = \frac{\tau_{zz}}{E} - \frac{\nu}{E}(\tau_{xx} + \tau_{yy})$$

which leads to

$$\tau_{zz} = \nu(\tau_{xx} + \tau_{yy}) \quad (4.7)$$

and considering the in-plane normal strain components, we can write

$$\varepsilon_{xx} = \frac{\tau_{xx}}{E} - \frac{\nu}{E}(\tau_{yy} + \tau_{zz}) = \frac{(1 - \nu^2)}{E}\tau_{xx} - \frac{\nu(1 + \nu)}{E}\tau_{yy} \quad (4.8)$$

$$\varepsilon_{yy} = \frac{\tau_{yy}}{E} - \frac{\nu}{E}(\tau_{xx} + \tau_{zz}) = \frac{(1 - \nu^2)}{E}\tau_{yy} - \frac{\nu(1 + \nu)}{E}\tau_{xx}. \quad (4.9)$$

Of course, we have used (4.7) to derive the final forms of equations (4.8) and (4.9). Considering the shear strains and stresses, we obtain

$$\gamma_{xy} = \frac{\tau_{xy}}{G} = \frac{2(1 + \nu)}{E}\tau_{xy} \quad (4.10)$$

and

$$\tau_{xz} = 0 \quad (4.11)$$

$$\tau_{yz} = 0 \quad (4.12)$$

since $\gamma_{xz} = 0$ and $\gamma_{yz} = 0$. It is convenient to define the following column matrices

$$\boldsymbol{\tau} = \begin{bmatrix} \tau_{xx} \\ \tau_{yy} \\ \tau_{xy} \end{bmatrix}, \quad \boldsymbol{\varepsilon} = \begin{bmatrix} \varepsilon_{xx} \\ \varepsilon_{yy} \\ \gamma_{xy} \end{bmatrix}.$$

Therefore, from (4.8), (4.9) and (4.10)

$$\boldsymbol{\varepsilon} = \mathbf{D}\boldsymbol{\tau} \quad (4.13)$$

where

$$\mathbf{D} = \frac{(1 + \nu)}{E} \begin{bmatrix} (1 - \nu) & -\nu & 0 \\ -\nu & (1 - \nu) & 0 \\ 0 & 0 & 2 \end{bmatrix}$$

which can be inverted leading to

$$\boldsymbol{\tau} = \mathbf{D}^{-1}\boldsymbol{\varepsilon} = \mathbf{C}\boldsymbol{\varepsilon} \quad (4.14)$$

where

$$\mathbf{C} = \frac{E(1 - \nu)}{(1 + \nu)(1 - 2\nu)} \begin{bmatrix} 1 & \frac{\nu}{1 - \nu} & 0 \\ \frac{\nu}{1 - \nu} & 1 & 0 \\ 0 & 0 & \frac{1 - 2\nu}{2(1 - \nu)} \end{bmatrix}.$$

We note that the same notation (τ , ε , \mathbf{D} and \mathbf{C}) was used for the 3-D problem for which we have, in general, all non zero stress and strain components and additional entries in the constitutive matrices. Of course, the correct meaning of these matrices is implied by the context. We also note that τ_{zz} , ε_{zz} were not considered in the above definitions, since $\varepsilon_{zz} = 0$ and τ_{zz} is obtained from τ_{xx} and τ_{yy} by equation (4.7). Therefore τ and ε , as defined, fully characterize the stress and strain states. We remark that equations (4.14), (4.4), (4.5) and (4.6) imply that the stress components τ_{xx} , τ_{yy} and τ_{xy} are functions of x , y only, *i.e.*, $\tau_{xx} = \tau_{xx}(x, y)$, $\tau_{yy} = \tau_{yy}(x, y)$ and $\tau_{xy} = \tau_{xy}(x, y)$.

Equilibrium

We need to enforce the equilibrium conditions which read

$$\frac{\partial \tau_{xx}}{\partial x} + \frac{\partial \tau_{xy}}{\partial y} + \frac{\partial \tau_{xz}}{\partial z} + f_x^B = 0 \quad (4.15)$$

$$\frac{\partial \tau_{xy}}{\partial x} + \frac{\partial \tau_{yy}}{\partial y} + \frac{\partial \tau_{yz}}{\partial z} + f_y^B = 0 \quad (4.16)$$

$$\frac{\partial \tau_{xz}}{\partial x} + \frac{\partial \tau_{yz}}{\partial y} + \frac{\partial \tau_{zz}}{\partial z} + f_z^B = 0. \quad (4.17)$$

Introducing (4.7), (4.11), (4.12) and taking into account that $\tau_{xx} = \tau_{xx}(x, y)$, $\tau_{yy} = \tau_{yy}(x, y)$, $\tau_{xy} = \tau_{xy}(x, y)$, we conclude that $f_x^B = f_x^B(x, y)$, $f_y^B = f_y^B(x, y)$ and $f_z^B = 0$. Otherwise, we would not be able to satisfy the equilibrium conditions, which are then expressed by

$$\frac{\partial \tau_{xx}}{\partial x} + \frac{\partial \tau_{xy}}{\partial y} + f_x^B = 0$$

$$\frac{\partial \tau_{xy}}{\partial x} + \frac{\partial \tau_{yy}}{\partial y} + f_y^B = 0.$$

Note that as long as $f_z^B = 0$, equation (4.17) is identically satisfied. Also, we should interpret the conditions on f_x^B , f_y^B and f_z^B as restrictions on the loading such that the displacement assumptions given in (4.1) to (4.3) are appropriate.

Boundary conditions

We need to consider next the boundary conditions. Although, when we introduced the plane strain problem, we did not distinguish between displacement and force boundary conditions, we can now consider the most general set of boundary conditions which would be compatible with the basic assumptions expressed by equations (4.1) to (4.3). Referring to Figure 4.2, let us consider first the lateral surface. On part of the lateral surface, S_u , we can prescribe displacements as long as S_u is given by the extrusion along the z

direction of a curve L_u defined at a cross-section boundary as schematically shown in Figure 4.3. The prescribed displacements are defined by

$$u(x, y, z) = \hat{u}(x, y) \tag{4.18}$$

$$v(x, y, z) = \hat{v}(x, y) \tag{4.19}$$

for any point on S_u .

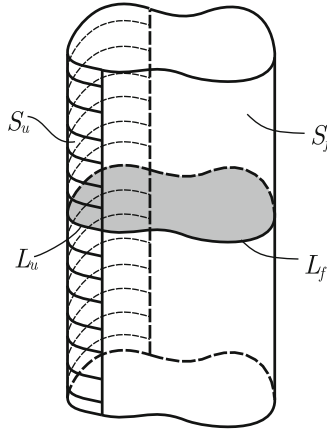


Fig. 4.3. Schematic representation of S_u , S_f and L_u , L_f

Let S_f be the complementary part of the lateral surface defined by the extrusion along z of L_f , the complementary curve to L_u , as also shown in Figure 4.3. Since the solid is prismatic, the normal unit vector at every point on the lateral surface is given by $\mathbf{n} = n_x \mathbf{e}_x + n_y \mathbf{e}_y$ and the force boundary condition reads

$$\mathbf{T}\mathbf{n} = \mathbf{f}^S$$

for every point on S_f , which in components is given by

$$\begin{bmatrix} \tau_{xx} & \tau_{xy} & 0 \\ \tau_{xy} & \tau_{yy} & 0 \\ 0 & 0 & \tau_{zz} \end{bmatrix} \begin{bmatrix} n_x \\ n_y \\ 0 \end{bmatrix} = \begin{bmatrix} f_x^S \\ f_y^S \\ f_z^S \end{bmatrix}.$$

Hence

$$f_x^S = \tau_{xx}n_x + \tau_{xy}n_y \tag{4.20}$$

$$f_y^S = \tau_{xy}n_x + \tau_{yy}n_y \tag{4.21}$$

$$f_z^S = 0. \tag{4.22}$$

The above equations establish additional restrictions for the external load. In fact, besides the restriction given by equation (4.22), equations (4.20) and (4.21) imply that $f_x^S = f_x^S(x, y)$ and $f_y^S = f_y^S(x, y)$ since τ_{xx} and τ_{yy} are functions of x, y only and the normal unit vector at a point on the lateral surface does not change with the coordinate z .

The top and bottom surfaces are peculiar¹ with respect to the imposition of boundary conditions. In fact, in order to be compatible with the displacement assumption $w = 0$ we should consider that $w = \hat{w} = 0$ at the top and bottom surfaces. The in-plane displacements, however, can not be restrained. For example, on the top surface $\mathbf{n} = \mathbf{e}_z$ and the surface tractions $\mathbf{f}^S = \mathbf{Tn}$ are given by

$$\begin{bmatrix} \tau_{xx} & \tau_{xy} & 0 \\ \tau_{xy} & \tau_{yy} & 0 \\ 0 & 0 & \tau_{zz} \end{bmatrix} \begin{bmatrix} 0 \\ 0 \\ 1 \end{bmatrix} = \begin{bmatrix} f_x^S \\ f_y^S \\ f_z^S \end{bmatrix}.$$

Therefore

$$\begin{aligned} f_x^S &= 0 \\ f_y^S &= 0 \\ f_z^S &= \tau_{zz} = \nu(\tau_{xx} + \tau_{yy}) \end{aligned} \quad (4.23)$$

which shows that there can not be any surface tractions applied tangentially to the plane and the surface traction in the direction \mathbf{e}_z is given by (4.23). Here f_z^S can be interpreted as a reactive surface traction compatible with the restriction given by $w = 0$. Analogous derivations would lead for the bottom surface for which $\mathbf{n} = -\mathbf{e}_z$ to

$$\begin{aligned} f_x^S &= 0 \\ f_y^S &= 0 \\ f_z^S &= -\tau_{zz} = -\nu(\tau_{xx} + \tau_{yy}). \end{aligned}$$

Hence, we may say that the top and bottom surfaces behave as if supported on rollers, free to roll into the x and y directions.

Differential formulation

Now we can summarize the formulation of the plane strain problem. Let us consider a prismatic solid as shown in Figure 4.3. On the lateral surface S_u we have prescribed displacements as given by (4.18) and (4.19). On the lateral surface S_f we have prescribed forces defined by

¹ In fact, this is an example in which at a point on the surface the displacement is restricted in a direction and the surface tractions are prescribed in the remaining directions (see Section 2.1.1)

$$\begin{aligned}
 f_x^S &= \hat{f}_x^S(x, y) \\
 f_y^S &= \hat{f}_y^S(x, y) \\
 f_z^S &= 0
 \end{aligned}
 \tag{4.24}$$

and on the top and bottom surfaces w is prescribed to be zero and $f_x^S = f_y^S = 0$.

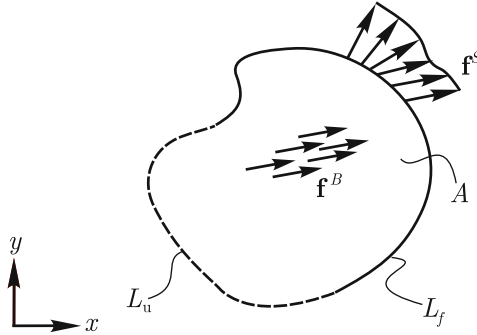


Fig. 4.4. Domain of unit thickness representing the prismatic solid, $A =$ cross-section, $V =$ volume $= 1 \times A$, $S_u = L_u \times 1$, $S_f = L_f \times 1$

Under these conditions the solution of the 3-D elasticity problem can be formulated in a plane as defined in Figure 4.4, for the indicated solid of unit thickness.

Differential formulation of the plane strain model

Given $f_x^B = f_x^B(x, y)$ and $f_y^B = f_y^B(x, y)$ defined in V , find $u(x, y)$, $v(x, y)$; $\tau_{xx} = \tau_{xx}(x, y)$, $\tau_{yy} = \tau_{yy}(x, y)$ and $\tau_{xy} = \tau_{xy}(x, y)$; $\varepsilon_{xx} = \varepsilon_{xx}(x, y)$, $\varepsilon_{yy} = \varepsilon_{yy}(x, y)$ and $\gamma_{xy} = \gamma_{xy}(x, y)$ such that

$$\frac{\partial \tau_{xx}}{\partial x} + \frac{\partial \tau_{xy}}{\partial y} + f_x^B = 0
 \tag{4.25}$$

$$\frac{\partial \tau_{xy}}{\partial x} + \frac{\partial \tau_{yy}}{\partial y} + f_y^B = 0
 \tag{4.26}$$

$$\varepsilon_{xx} = \frac{\partial u}{\partial x} \quad (4.27)$$

$$\varepsilon_{yy} = \frac{\partial v}{\partial y} \quad (4.28)$$

$$\gamma_{xy} = \frac{\partial u}{\partial y} + \frac{\partial v}{\partial x} \quad (4.29)$$

$$\tau = \mathbf{C}\varepsilon \quad (4.30)$$

for every point in V ;

$$f_x^S = \hat{f}_x^S(x, y) \quad (4.31)$$

$$f_y^S = \hat{f}_y^S(x, y) \quad (4.32)$$

for every point in S_f and

$$u = \hat{u}(x, y) \quad (4.33)$$

$$v = \hat{v}(x, y) \quad (4.34)$$

for every point in S_u ².

Once the solution to this plane problem has been found, the solution for the 3-D problem is given by appending

$$w = 0 \quad (4.35)$$

$$\varepsilon_{zz} = \gamma_{xz} = \gamma_{yz} = 0 \quad (4.36)$$

$$\tau_{xz} = \tau_{yz} = 0 \quad (4.37)$$

$$\tau_{zz} = \nu(\tau_{xx} + \tau_{yy}). \quad (4.38)$$

4.1.2 The plane stress model

The motivation for the formulation of the plane stress model is the analysis of a thin plate subjected to loading in its own plane. Consider the plate shown in Figure 4.5 with its mid-surface in the xy plane. We assume that both \mathbf{f}^B and \mathbf{f}^S have no component into the z direction, the top and the bottom surfaces are free from any imposed surface tractions and the thickness of the plate, denoted by h , is small when compared to a characteristic length dimension on the plane of the plate that is $\frac{h}{L} \ll 1$.

² Note that in each of the problem formulations given in Section 3.5 and Chapter 4, we assume that continuous displacements are sought and that sufficient boundary conditions on S_u are prescribed to make the solution possible

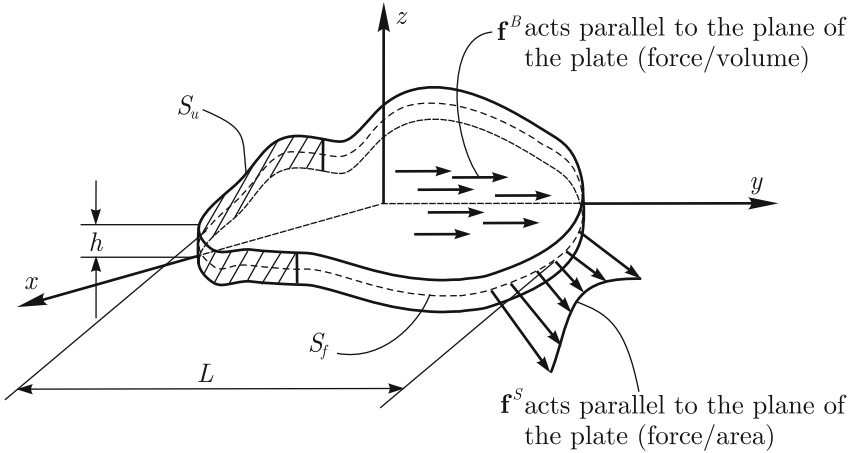


Fig. 4.5. Thin plate subjected to loading in its plane

Based on this problem description, specific assumptions can now be introduced regarding the stress field and the loading.

Stress assumptions

For the plate characterized in Figure 4.5, we assume that

$$\tau_{zz} = \tau_{xz} = \tau_{yz} = 0 \tag{4.39}$$

and taking into account that the plate is thin, we further assume that

$$\tau_{xx} = \tau_{xx}(x, y), \tau_{yy} = \tau_{yy}(x, y), \tau_{xy} = \tau_{xy}(x, y). \tag{4.40}$$

Equilibrium

The equilibrium equations given in (3.114) can be simplified and become

$$\frac{\partial \tau_{xx}}{\partial x} + \frac{\partial \tau_{xy}}{\partial y} + f_x^B = 0 \tag{4.41}$$

$$\frac{\partial \tau_{xy}}{\partial x} + \frac{\partial \tau_{yy}}{\partial y} + f_y^B = 0. \tag{4.42}$$

Therefore equations (4.41) and (4.42) are now phrased in a two-dimensional domain leading also to the restrictions $f_x^B = f_x^B(x, y)$ and $f_y^B = f_y^B(x, y)$.

Constitutive relations

In light of the stress assumptions (4.39), the constitutive equation can be simplified leading to

$$\begin{aligned}
\varepsilon_{xx} &= \frac{\tau_{xx}}{E} - \frac{\nu}{E}\tau_{yy} \\
\varepsilon_{yy} &= \frac{\tau_{yy}}{E} - \frac{\nu}{E}\tau_{xx} \\
\varepsilon_{zz} &= -\frac{\nu}{E}(\tau_{xx} + \tau_{yy}) \\
\gamma_{xy} &= \frac{\tau_{xy}}{G} = \frac{2(1+\nu)}{E}\tau_{xy} \\
\gamma_{xz} &= \frac{\tau_{xz}}{G} = 0 \\
\gamma_{yz} &= \frac{\tau_{yz}}{G} = 0.
\end{aligned}$$

We can organize the constitutive relations in matrix form as given by (4.13) and (4.14) where

$$\mathbf{D} = \frac{1}{E} \begin{bmatrix} 1 & -\nu & 0 \\ -\nu & 1 & 0 \\ 0 & 0 & 2(1+\nu) \end{bmatrix} \quad (4.43)$$

and

$$\mathbf{C} = \frac{E}{1-\nu^2} \begin{bmatrix} 1 & \nu & 0 \\ \nu & 1 & 0 \\ 0 & 0 & \frac{1-\nu}{2} \end{bmatrix}. \quad (4.44)$$

Note that we use the same stress and strain column matrix definitions as for the plane strain problem.

Differential formulation

Now we are ready to characterize the plane stress problem. Let us consider the 3-D problem described in Figure 4.5 where a plate is subjected to a field of body forces

$$\begin{aligned}
f_x^B &= f_x^B(x, y) \\
f_y^B &= f_y^B(x, y) \\
f_z^B &= 0.
\end{aligned}$$

Displacements are prescribed in S_u according to

$$\begin{aligned}
u(x, y, z) &= \hat{u}(x, y) \\
v(x, y, z) &= \hat{v}(x, y)
\end{aligned}$$

and the tractions are prescribed on S_f as

$$f_x^S = \hat{f}_x^S(x, y)$$

$$f_y^S = \hat{f}_y^S(x, y)$$

$$f_z^S = 0.$$

The top and bottom surfaces are free from any surface tractions.

The plane stress problem associated with the 3-D problem described above admits a formulation in a plane domain as generically described in Figure 4.4, but now the thickness is h .

Differential formulation of the plane stress model

Given $f_x^B = f_x^B(x, y)$ and $f_y^B = f_y^B(x, y)$ defined in $V = A \cdot h$, find $u(x, y)$, $v(x, y)$; $\tau_{xx} = \tau_{xx}(x, y)$, $\tau_{yy} = \tau_{yy}(x, y)$ and $\tau_{xy} = \tau_{xy}(x, y)$; $\varepsilon_{xx} = \varepsilon_{xx}(x, y)$, $\varepsilon_{yy} = \varepsilon_{yy}(x, y)$, $\gamma_{xy} = \gamma_{xy}(x, y)$ such that

$$\frac{\partial \tau_{xx}}{\partial x} + \frac{\partial \tau_{xy}}{\partial y} + f_x^B = 0 \quad (4.45)$$

$$\frac{\partial \tau_{xy}}{\partial x} + \frac{\partial \tau_{yy}}{\partial y} + f_y^B = 0 \quad (4.46)$$

$$\varepsilon_{xx} = \frac{\partial u}{\partial x} \quad (4.47)$$

$$\varepsilon_{yy} = \frac{\partial v}{\partial y} \quad (4.48)$$

$$\gamma_{xy} = \frac{\partial u}{\partial y} + \frac{\partial v}{\partial x} \quad (4.49)$$

$$\tau = \mathbf{C}\varepsilon \quad (4.50)$$

for every point in V ;

$$f_x^S = \hat{f}_x^S(x, y) \quad (4.51)$$

$$f_y^S = \hat{f}_y^S(x, y) \quad (4.52)$$

for every point in S_f ; and

$$u = \hat{u}(x, y) \quad (4.53)$$

$$v = \hat{v}(x, y) \quad (4.54)$$

for every point in S_u .

We note that the solution of the plane stress problem appended by

$$\tau_{zz} = \tau_{xz} = \tau_{yz} = 0 \quad (4.55)$$

$$\gamma_{xz} = \gamma_{yz} = 0 \quad (4.56)$$

$$\varepsilon_{zz} = -\frac{\nu}{E}(\tau_{xx} + \tau_{yy}) \quad (4.57)$$

and by $w(x, y, z)$ obtained by the integration of (4.57) with respect to z is not the exact solution of the 3-D problem just described. The reason is that we started from some assumptions on the stress field and did not impose all the compatibility relations (3.115). The 3-D strain field given by the ε_{xx} , ε_{yy} and γ_{xy} solution of the plane stress problem appended by (4.56) and (4.57) does not always lead to a compatible 3-D displacement field, that is, continuous displacements $u(x, y, z)$, $v(x, y, z)$ and $w(x, y, z)$ that satisfy the displacement boundary conditions (with w on S_u free).

Namely, in general, the solution of the plane stress problem leads to stresses τ_{xx} and τ_{yy} which vary with (x, y) . Hence, from (4.57)

$$\varepsilon_{zz} = \varepsilon_{zz}(x, y)$$

and

$$\frac{\partial w}{\partial z} = \varepsilon_{zz}(x, y)$$

which integrated with respect to z leads to

$$w(x, y, z) = z\varepsilon_{zz}(x, y) + f(x, y)$$

where $f(x, y)$ is an arbitrary function of x and y . Assuming that $w(x, y, z)$ is zero at $z = 0$, we obtain $f(x, y) = 0$ and

$$w(x, y, z) = z\varepsilon_{zz}(x, y).$$

Now, we can evaluate

$$\gamma_{yz} = \frac{\partial w}{\partial y} + \frac{\partial v}{\partial z} = z \frac{\partial \varepsilon_{zz}}{\partial y}$$

which is, in general, zero only for $z = 0$. Analogously

$$\gamma_{xz} = \frac{\partial w}{\partial x} + \frac{\partial v}{\partial z} = z \frac{\partial \varepsilon_{zz}}{\partial x}.$$

Hence the transverse shear strains obtained from the displacement field are not zero showing that, in general, the plane stress solution is not the exact solution of the 3-D elasticity problem. However, it is possible to show (Timoshenko and Goodier, 1970) that the solutions of the plane stress problem and of the related 3-D problem are “close” as long as the plate is thin.

The 3-D solution has additional terms which are proportional to z^2 leading to small differences for the solution variables when the thickness is small.

We can appreciate from the above description that the plane strain and plane stress models represent quite distinct behaviors and they each need to be used considering the assumptions contained in the models. In particular, the kind of restrictions imposed on the out-of-plane displacements, *i.e.*, w in the notation used above, helps to identify which model reflects best the behavior of the physical problem. However, although there are distinctly different behaviors, the mathematical formulations of these models lend themselves to a unified presentation.

Consider the differential formulations of the plane strain and plane stress problems given by equations (4.25) to (4.34) and (4.45) to (4.54), respectively. We recognize that the equations for $u(x, y)$, $v(x, y)$, $\varepsilon_{xx}(x, y)$, $\varepsilon_{yy}(x, y)$, $\gamma_{xy}(x, y)$, $\tau_{xx}(x, y)$, $\tau_{yy}(x, y)$ and $\tau_{xy}(x, y)$ are identical except that \mathbf{C} , which expresses the constitutive equation, is different. However, if we define, for $\nu < 0.5$,

$$E_* = \frac{E}{1 - \nu^2} \quad (4.58)$$

and

$$\nu_* = \frac{\nu}{1 - \nu}$$

as the effective Young's modulus and effective Poisson's ratio and introduce these in place of E and ν in the \mathbf{C} matrix for the plane stress model, we obtain

$$\mathbf{C} = \frac{E_*}{1 - \nu_*^2} \begin{bmatrix} 1 & \nu_* & 0 \\ \nu_* & 1 & 0 \\ 0 & 0 & \frac{1 - \nu_*}{2} \end{bmatrix}. \quad (4.59)$$

Then introducing the definitions of E_* and ν_* , we obtain

$$\mathbf{C} = \frac{\frac{E}{1 - \nu^2}}{\left(1 - \frac{\nu}{1 - \nu}\right)\left(1 + \frac{\nu}{1 - \nu}\right)} \begin{bmatrix} 1 & \frac{\nu}{1 - \nu} & 0 \\ \frac{\nu}{1 - \nu} & 1 & 0 \\ 0 & 0 & \frac{1 - \frac{\nu}{1 - \nu}}{2} \end{bmatrix}$$

which gives

$$\mathbf{C} = \frac{E(1 - \nu)}{(1 + \nu)(1 - 2\nu)} \begin{bmatrix} 1 & \frac{\nu}{1 - \nu} & 0 \\ \frac{\nu}{1 - \nu} & 1 & 0 \\ 0 & 0 & \frac{1 - 2\nu}{2(1 - \nu)} \end{bmatrix}$$

i.e., the \mathbf{C} matrix for the plane strain model.

Therefore, both the plane stress and the plane strain models can be formulated with the same set of equations, for example (4.45) to (4.54), using the definition of \mathbf{C} given in (4.14) for plane stress and (4.59) for plane strain. Of course, having the solution for the in-plane variables of the plane stress model, we can readily obtain the solution for the in-plane variables of the plane strain model by replacing E by E_* and ν by ν_* in the analytical expressions for these variables. The solution for the remaining variables is given by (4.35) to (4.38) for the plane strain model and by (4.55) to (4.57) for the plane stress model.

Since E_* and ν_* are larger than E and ν the plane strain model is stiffer than the plane stress model. This fact is expected because the out-of-plane displacements in the plane strain model are constrained to be zero.

Example 4.1

Study the solution of a thin plate subjected to its own weight as shown in Figure 4.6. At the edge $y = a$ a uniform distribution of surface tractions $\mathbf{f}^S = f_y^S \mathbf{e}_y = \rho g a \mathbf{e}_y$ is applied (ρ is the density and g the acceleration due to gravity) and at the three edges $y = 0$, $x = -b/2$ and $x = b/2$ there are no externally applied surface tractions. To suppress rigid body motions the displacements at point P ($x = 0$, $y = a$) are prevented and the plate is not allowed to rotate about P .

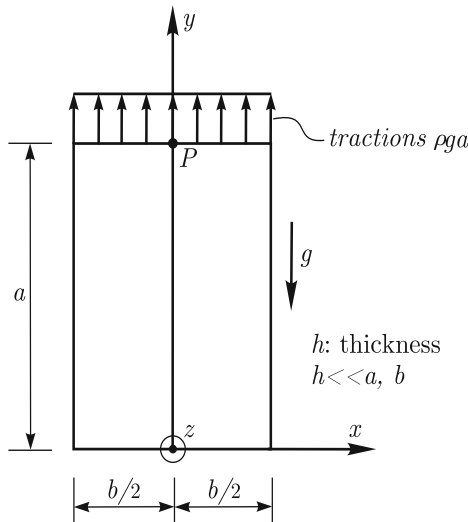


Fig. 4.6. Plate subjected to gravity

Solution

We consider a plane stress model and derive the solution. Due to gravity

$$f_x^B = 0, f_y^B = -\rho g, f_z^B = 0.$$

Since there are no externally applied surface tractions at the three edges $x = -b/2$ and $x = b/2$ the stress components τ_{xx} and τ_{xy} should be zero at these edges. Taking

$$\tau_{xx} = 0 \text{ and } \tau_{xy} = 0$$

for any point in the domain, the equilibrium equation

$$\frac{\partial \tau_{xx}}{\partial x} + \frac{\partial \tau_{xy}}{\partial y} + f_x^B = 0$$

is identically satisfied and

$$\frac{\partial \tau_{xy}}{\partial x} + \frac{\partial \tau_{yy}}{\partial y} + f_y^B = 0$$

leads to

$$\tau_{yy} = \rho g y + f(x)$$

where $f(x)$ is a function of x only. The boundary condition at $y = a$ implies

$$f_y^S = \rho g a = \tau_{yy}(y = a) = \rho g a + f(x) \quad \Rightarrow \quad f(x) = 0$$

and, hence

$$\tau_{yy} = \rho g y. \tag{4.60}$$

The free edge condition at the lower horizontal edge

$$f_y^S(x, 0) = 0 = \tau_{yy}(x, 0)$$

is verified by the τ_{yy} given in (4.60).

We can obtain the strains using the constitutive equations

$$\varepsilon_{xx} = \frac{\tau_{xx}}{E} - \frac{\nu}{E} \tau_{yy} = -\frac{\nu}{E} \tau_{yy} = -\frac{\nu}{E} \rho g y$$

$$\varepsilon_{yy} = \frac{\tau_{yy}}{E} - \frac{\nu}{E} \tau_{xx} = \frac{\rho g y}{E}$$

$$\gamma_{xy} = \frac{\tau_{xy}}{G} = 0$$

where E , ν and $G = \frac{E}{2(1+\nu)}$ are respectively, as usual, the Young modulus, the Poisson ratio and the shear modulus.

To obtain the displacement field, we need to integrate the compatibility relations. Consider

$$\varepsilon_{xx} = \frac{\partial u}{\partial x}$$

which leads to

$$\frac{\partial u}{\partial x} = -\frac{\nu}{E}\rho g y \quad \Rightarrow \quad u(x, y) = -\frac{\nu}{E}\rho g x y + f_1(y) \quad (4.61)$$

where $f_1(y)$ is a function of y only. Also

$$\varepsilon_{yy} = \frac{\partial v}{\partial y}$$

leading to

$$\frac{\partial v}{\partial y} = \frac{\rho g y}{E} \quad \Rightarrow \quad v(x, y) = \frac{\rho g y^2}{2E} + f_2(x) \quad (4.62)$$

where $f_2(x)$ is a function of x only. The shear strain is given by

$$\gamma_{xy} = \frac{\partial u}{\partial y} + \frac{\partial v}{\partial x} = 0 = -\nu k x + \frac{df_1}{dy} + \frac{df_2}{dx}, \quad k = \frac{\rho g}{E}. \quad (4.63)$$

Let us define

$$g_1(x) = -\nu k x + \frac{df_2}{dx}, \quad g_2(y) = \frac{df_1}{dy}. \quad (4.64)$$

Rewriting equation (4.63) using the definitions given in (4.64), we obtain

$$g_1(x) + g_2(y) = 0. \quad (4.65)$$

We note that (4.65) has to hold for any (x, y) in the domain. Therefore

$$g_1 = C_2, \quad g_2 = -C_2$$

where C_2 is a constant. Using (4.64) yields

$$-\nu k x + \frac{df_2}{dx} = C_2$$

which by integration leads to

$$f_2(x) = C_2 x + \frac{\nu k x^2}{2} + C_3$$

and from (4.64)

$$\frac{df_1}{dy} = -C_2 \quad \Rightarrow \quad f_1(y) = -C_2 y + C_4.$$

Therefore

$$u = -\nu kxy - C_2y + C_4 \quad (4.66)$$

$$v = \frac{k}{2}y^2 + C_2x + \frac{\nu kx^2}{2} + C_3. \quad (4.67)$$

Let us impose the kinematic boundary condition at point P

$$u(0, a) = -C_2a + C_4 = 0 \quad (4.68)$$

and

$$v(0, a) = \frac{ka^2}{2} + C_3 = 0. \quad (4.69)$$

In order to impose that there is no rigid body rotation about point P , we enforce that the horizontal infinitesimal fiber with origin at point P remains horizontal. This condition is given by

$$\frac{\partial v}{\partial x}(0, a) = 0.$$

From equation (4.67)

$$\frac{\partial v}{\partial x}(0, a) = C_2 \quad \Rightarrow \quad C_2 = 0.$$

Therefore equation (4.68) gives

$$C_4 = 0$$

and from (4.69)

$$C_3 = -\frac{ka^2}{2}.$$

Introducing all the determined constant values into (4.66) and (4.67) leads to

$$u = -\frac{\nu\rho g}{E}xy$$

$$v = \frac{\rho g}{2E}(y^2 + \nu x^2 - a^2).$$

We note, as physically expected, the thickness h of the plate does not enter the solution.

□

Example 4.2

Consider now that Figure 4.6 defines the section of a 3-D prismatic solid of length L in the z direction. At the end sections $z = L/2$ and $z = -L/2$ the displacements $w(x, y) = 0$ and the surface tractions $f_x^S = f_y^S = 0$. The rotation about the line $(x = 0, y = a, z)$ is prevented and the displacements u and v of points on this line are also prevented. At the lateral surfaces $y = 0$, $x = -b/2$ and $x = b/2$ there are no surface tractions. Find the displacement field and the tractions at the end sections $z = L/2$ and $z = -L/2$ when the solid is subjected to its own weight and to a uniform distribution of surface tractions $\mathbf{f}^S = f_y^S \mathbf{e}_y = \rho g a \mathbf{e}_y$ at the surface $y = a$ (ρ is the density and g the acceleration due to gravity).

Solution

Under the stated conditions, we have a plane strain situation with the same load and boundary conditions as for the plane stress problem of Figure 4.6. Therefore, the in-plane solution is directly obtained from the plane stress solution using the effective elastic constants $E_* = \frac{E}{1-\nu^2}$ and $\nu_* = \frac{\nu}{1-\nu}$ in place of E and ν . Hence

$$u = -\frac{\nu(1+\nu)}{E} \rho g x y$$

$$v = \frac{(1-\nu^2) \rho g}{2E} \left(y^2 + \frac{\nu}{1-\nu} x^2 - a^2 \right)$$

and, of course, $w = 0$. At the end section with normal \mathbf{e}_z , we obtain

$$\mathbf{f}^S = \tau_{zz} \mathbf{e}_z = \nu (\tau_{xx} + \tau_{yy}) \mathbf{e}_z = \nu \rho g y \mathbf{e}_z$$

and at the opposite end section

$$\mathbf{f}^S = -\tau_{zz} \mathbf{e}_z = -\nu \rho g y \mathbf{e}_z.$$

□

4.1.3 The axisymmetric model**Cylindrical coordinate system**

For the definition of the axisymmetric model a cylindrical coordinate system is commonly used and effective. In Figure 4.7, a Cartesian and a cylindrical coordinate system are given. As long as the z axis, the horizontal plane and the line from which the angle θ is measured are defined, the location of every point in 3-D space is uniquely given by the coordinates r , θ and z .

Associated with every point, we define orthonormal base vectors \mathbf{e}_r , \mathbf{e}_θ and \mathbf{e}_z . The unit vectors \mathbf{e}_r and \mathbf{e}_z have the direction of r and z , respectively, and \mathbf{e}_θ is orthogonal to the plane of \mathbf{e}_r and \mathbf{e}_z . Therefore, from point to point, \mathbf{e}_r and \mathbf{e}_θ change directions, different from using a Cartesian coordinate system for which \mathbf{e}_x , \mathbf{e}_y and \mathbf{e}_z are always the same for every point.

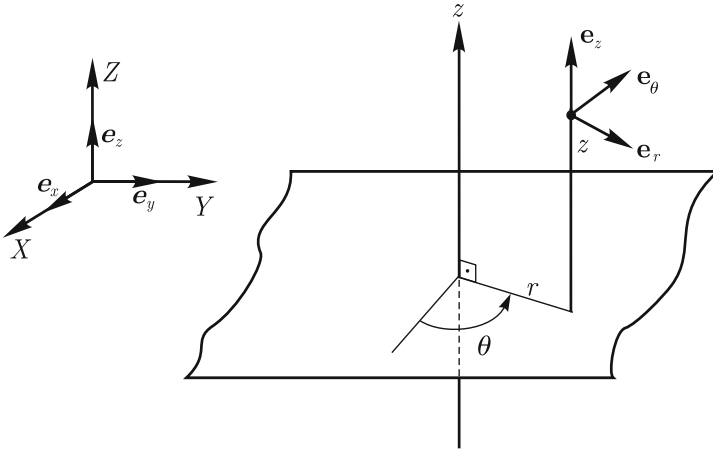


Fig. 4.7. Definition of a cylindrical coordinate system

The stress components in a cylindrical system are referred to the local system $(\mathbf{e}_r, \mathbf{e}_\theta, \mathbf{e}_z)$ which changes from point to point.

Equilibrium

A differential element of a solid at a given point corresponding to infinitesimal increments dr , $d\theta$ and dz and the stress components are shown in Figure 4.8. Further, in Figure 4.9 a top view is given. We have also in this system that $\tau_{r\theta} = \tau_{\theta r}$, $\tau_{rz} = \tau_{zr}$ and $\tau_{\theta z} = \tau_{z\theta}$. Equilibrium in the direction \mathbf{e}_r requires

$$\begin{aligned} & \left(\tau_{rr} + \frac{\partial \tau_{rr}}{\partial r} dr \right) (r + dr) d\theta dz - \tau_{rr} r d\theta dz \\ & - \left(2\tau_{\theta\theta} + \frac{\partial \tau_{\theta\theta}}{\partial \theta} d\theta \right) dr dz \frac{d\theta}{2} \\ & + \left(\tau_{r\theta} + \frac{\partial \tau_{r\theta}}{\partial \theta} d\theta \right) dr dz - \tau_{r\theta} dr dz \\ & + \left(\tau_{rz} + \frac{\partial \tau_{rz}}{\partial z} dz \right) \left(r + \frac{dr}{2} \right) d\theta dr - \tau_{rz} \left(r + \frac{dr}{2} \right) d\theta dr \end{aligned}$$

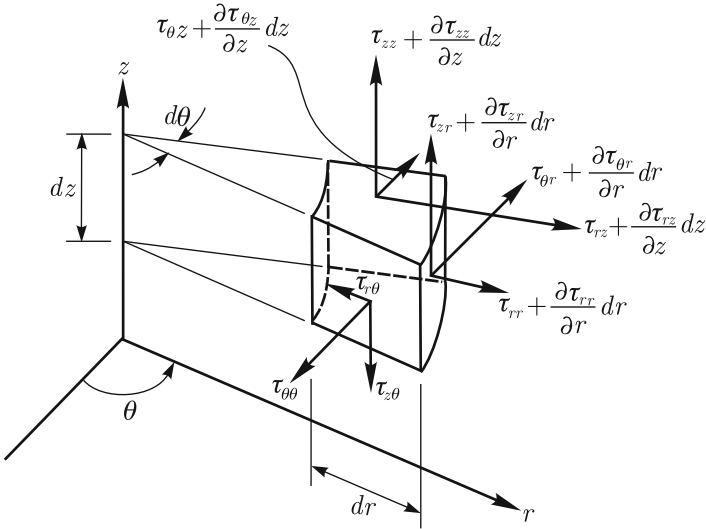


Fig. 4.8. Stresses on a differential element described by cylindrical coordinates. Stresses are shown only on visible faces

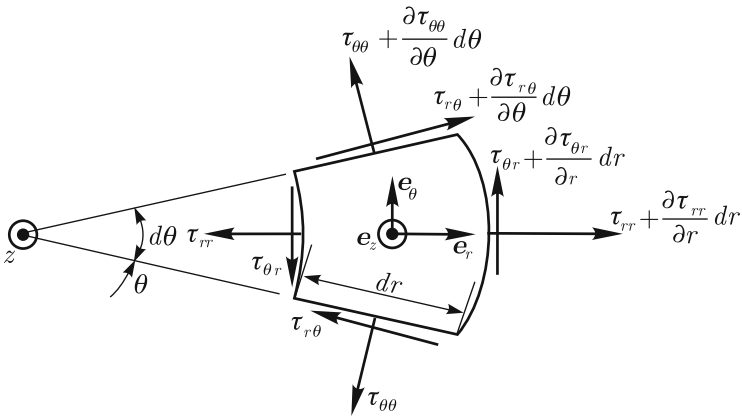


Fig. 4.9. Stresses on a differential element described by cylindrical coordinates. Stresses are shown only on visible faces

$$+f_r^B \left(r + \frac{dr}{2} \right) d\theta dr dz = 0.$$

Neglecting infinitesimals of fourth order, we obtain

$$\frac{\partial \tau_{rr}}{\partial r} + \frac{1}{r} \frac{\partial \tau_{r\theta}}{\partial \theta} + \frac{\partial \tau_{rz}}{\partial z} + \frac{\tau_{rr} - \tau_{\theta\theta}}{r} + f_r^B = 0. \tag{4.70}$$

Equilibrium in the direction \mathbf{e}_θ requires

$$\begin{aligned}
& \left(\tau_{\theta r} + \frac{\partial \tau_{\theta r}}{\partial r} dr \right) (r + dr) d\theta dz - \tau_{\theta r} r d\theta dz \\
& + \left(\tau_{\theta\theta} + \frac{\partial \tau_{\theta\theta}}{\partial \theta} d\theta \right) dr dz - \tau_{\theta\theta} dr dz \\
& + \left(\tau_{r\theta} + \frac{\partial \tau_{r\theta}}{\partial \theta} d\theta \right) dr dz \frac{d\theta}{2} - \tau_{r\theta} dr dz \frac{d\theta}{2} \\
& + \left(\tau_{\theta z} + \frac{\partial \tau_{\theta z}}{\partial z} dz \right) \left(r + \frac{dr}{2} \right) d\theta dr - \tau_{\theta z} \left(r + \frac{dr}{2} \right) d\theta dr \\
& + f_{\theta}^B \left(r + \frac{dr}{2} \right) d\theta dr dz = 0
\end{aligned}$$

leading to

$$\frac{\partial \tau_{\theta r}}{\partial r} + \frac{1}{r} \frac{\partial \tau_{\theta\theta}}{\partial \theta} + \frac{\partial \tau_{\theta z}}{\partial z} + \frac{\tau_{\theta r}}{r} + \frac{\tau_{r\theta}}{r} + f_{\theta}^B = 0. \quad (4.71)$$

And for the direction z

$$\begin{aligned}
& \left(\tau_{zr} + \frac{\partial \tau_{zr}}{\partial r} dr \right) (r + dr) d\theta dz - \tau_{zr} r d\theta dz \\
& + \left(\tau_{z\theta} + \frac{\partial \tau_{z\theta}}{\partial \theta} d\theta \right) dr dz - \tau_{z\theta} dr dz \\
& + \left(\tau_{zz} + \frac{\partial \tau_{zz}}{\partial z} dz \right) \left(r + \frac{dr}{2} \right) d\theta dr - \tau_{zz} \left(r + \frac{dr}{2} \right) d\theta dr \\
& + f_z^B \left(r + \frac{dr}{2} \right) d\theta dr dz = 0
\end{aligned}$$

which leads to

$$\frac{\partial \tau_{zr}}{\partial r} + \frac{1}{r} \frac{\partial \tau_{z\theta}}{\partial \theta} + \frac{\partial \tau_{zz}}{\partial z} + \frac{\tau_{zr}}{r} + f_z^B = 0. \quad (4.72)$$

Summarizing, the equilibrium conditions in the cylindrical coordinate system are

$$\begin{aligned}
\frac{\partial \tau_{rr}}{\partial r} + \frac{1}{r} \frac{\partial \tau_{r\theta}}{\partial \theta} + \frac{\partial \tau_{rz}}{\partial z} + \frac{\tau_{rr} - \tau_{\theta\theta}}{r} + f_r^B &= 0 \\
\frac{\partial \tau_{\theta r}}{\partial r} + \frac{1}{r} \frac{\partial \tau_{\theta\theta}}{\partial \theta} + \frac{\partial \tau_{\theta z}}{\partial z} + 2 \frac{\tau_{\theta r}}{r} + f_{\theta}^B &= 0 \\
\frac{\partial \tau_{zr}}{\partial r} + \frac{1}{r} \frac{\partial \tau_{z\theta}}{\partial \theta} + \frac{\partial \tau_{zz}}{\partial z} + \frac{\tau_{zr}}{r} + f_z^B &= 0.
\end{aligned}$$

Let us now introduce axisymmetric conditions, *i.e.*, we consider a solid of revolution which is subjected to an axisymmetric load distribution. A typical situation is presented in Figure 4.10. We note that under these conditions

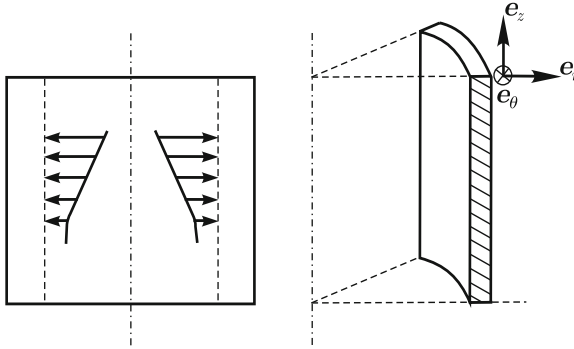


Fig. 4.10. A typical solid with an axisymmetric geometry and loading

$$f_\theta^B = 0$$

$$\frac{\partial(\cdot)}{\partial\theta} = 0 \text{ for any stress component}$$

$$\tau_{r\theta} = \tau_{z\theta} = 0$$

and the equilibrium conditions simplify to

$$\frac{\partial\tau_{rr}}{\partial r} + \frac{\partial\tau_{rz}}{\partial z} + \frac{\tau_{rr} - \tau_{\theta\theta}}{r} + f_r^B = 0 \tag{4.73}$$

$$\frac{\partial\tau_{zr}}{\partial r} + \frac{\partial\tau_{zz}}{\partial z} + \frac{\tau_{zr}}{r} + f_z^B = 0 \tag{4.74}$$

and, of course, equation (4.71) is identically satisfied.

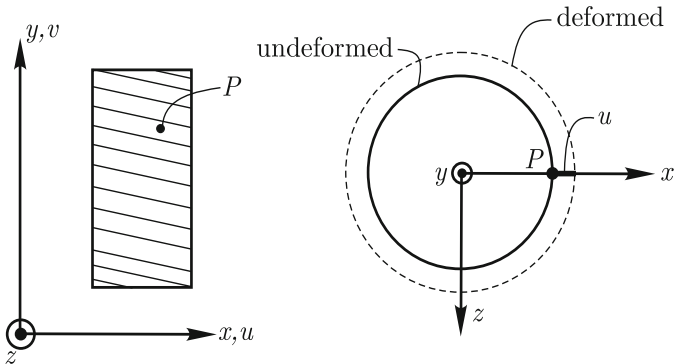


Fig. 4.11. Displacement of a generic point under axisymmetric conditions

When we have axisymmetric conditions, the displacements, stresses and strains are the same for any plane which contains the axis of symmetry.

Therefore, the problem can be formulated in a plane and it is customary to use a Cartesian coordinate system for that plane, as shown in Figure 4.11. Here y is now the axis of symmetry. In the coordinate system of Figure 4.11, the equilibrium equations (4.73) and (4.74) are

$$\frac{\partial \tau_{xx}}{\partial x} + \frac{\partial \tau_{xy}}{\partial y} + \frac{\tau_{xx} - \tau_{zz}}{x} + f_x^B = 0 \quad (4.75)$$

$$\frac{\partial \tau_{xy}}{\partial x} + \frac{\partial \tau_{yy}}{\partial y} + \frac{\tau_{xy}}{x} + f_y^B = 0. \quad (4.76)$$

Note that these equilibrium equations are the plane stress and plane strain equilibrium equations with $\frac{\tau_{xx} - \tau_{zz}}{x}$ added in the first equation and $\frac{\tau_{xy}}{x}$ in the second equation.

Strain compatibility

Due to the axisymmetric conditions, the displacements for material particles in the xy plane in Figure 4.11 are given by

$$u = u(x, y)$$

$$v = v(x, y)$$

$$w = 0$$

and the strains

$$\varepsilon_{xx} = \frac{\partial u}{\partial x}$$

$$\varepsilon_{yy} = \frac{\partial v}{\partial y}$$

$$\gamma_{xy} = \frac{\partial u}{\partial y} + \frac{\partial v}{\partial x}$$

$$\gamma_{xz} = \gamma_{yz} = 0$$

Figure 4.11 also shows that a displacement $u(x, y)$ actually means that a circumference of radius x of material points of the solid deforms into a circumference of radius $x + u$ as shown. Therefore, we can evaluate the *circumferential* or *hoop* strain ε_{zz} by

$$\varepsilon_{zz} = \frac{2\pi(x + u) - 2\pi x}{2\pi x} = \frac{u}{x}.$$

Constitutive relations

It is convenient to define stress and strain column matrices without including the zero stress and strain components, *i.e.*,

$$\boldsymbol{\tau} = \begin{bmatrix} \tau_{xx} \\ \tau_{yy} \\ \tau_{xy} \\ \tau_{zz} \end{bmatrix}, \quad \boldsymbol{\varepsilon} = \begin{bmatrix} \varepsilon_{xx} \\ \varepsilon_{yy} \\ \gamma_{xy} \\ \varepsilon_{zz} \end{bmatrix}$$

The constitutive equation is given by $\boldsymbol{\tau} = \mathbf{C}\boldsymbol{\varepsilon}$ with

$$\mathbf{C} = \frac{E(1-\nu)}{(1+\nu)(1-2\nu)} \begin{bmatrix} 1 & \frac{\nu}{1-\nu} & 0 & \frac{\nu}{1-\nu} \\ \frac{\nu}{1-\nu} & 1 & 0 & \frac{\nu}{1-\nu} \\ 0 & 0 & \frac{1-2\nu}{2(1-\nu)} & 0 \\ \frac{\nu}{1-\nu} & \frac{\nu}{1-\nu} & 0 & 1 \end{bmatrix}. \quad (4.77)$$

which is obtained from the \mathbf{C} for 3-D conditions given by (3.113).

Differential formulation

Let us consider a solid of revolution for which a generic cross-section A is shown in Figure 4.12 subjected to axisymmetric loads and displacement boundary conditions. The volume V of the solid corresponds to revolving A about the y axis. Usually one radian is considered, see Section 5.2.4. On the lateral surface S_u , which corresponds to revolving the boundary line L_u , the displacements are prescribed. On the lateral surface S_f , which corresponds to revolving the boundary line L_f , surface tractions are applied. Body forces \mathbf{f}^B are also present. Under these conditions the solution of the 3-D elasticity problem can be formulated in the plane domain described in Figure 4.12.

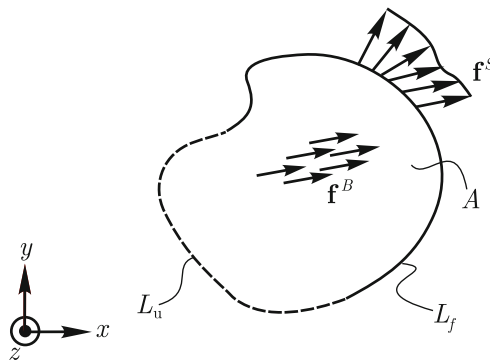


Fig. 4.12. Domain representing a generic cross-section of the solid of revolution

Differential formulation of the axisymmetric model

Given $f_x^B = f_x^B(x, y)$ and $f_y^B = f_y^B(x, y)$ defined in V , find $u(x, y)$, $v(x, y)$; $\tau_{xx} = \tau_{xx}(x, y)$, $\tau_{yy} = \tau_{yy}(x, y)$, $\tau_{xy} = \tau_{xy}(x, y)$ and $\tau_{zz} = \tau_{zz}(x, y)$; $\varepsilon_{xx} = \varepsilon_{xx}(x, y)$, $\varepsilon_{yy} = \varepsilon_{yy}(x, y)$, $\gamma_{xy} = \gamma_{xy}(x, y)$ and $\varepsilon_{zz} = \varepsilon_{zz}(x, y)$ such that

$$\frac{\partial \tau_{xx}}{\partial x} + \frac{\partial \tau_{xy}}{\partial y} + \frac{\tau_{xx} - \tau_{zz}}{x} + f_x^B = 0$$

$$\frac{\partial \tau_{xy}}{\partial x} + \frac{\partial \tau_{yy}}{\partial y} + \frac{\tau_{xy}}{x} + f_y^B = 0$$

$$\varepsilon_{xx} = \frac{\partial u}{\partial x}, \quad \varepsilon_{yy} = \frac{\partial v}{\partial y}$$

$$\gamma_{xy} = \frac{\partial u}{\partial y} + \frac{\partial v}{\partial x}, \quad \varepsilon_{zz} = \frac{u}{x}$$

$$\boldsymbol{\tau} = \mathbf{C}\boldsymbol{\varepsilon}$$

for every point in V and for the \mathbf{C} given in (4.77). The boundary conditions are

$$f_x^S = \hat{f}_x^S(x, y), \quad f_y^S = \hat{f}_y^S(x, y)$$

for every point in S_f and

$$u = \hat{u}(x, y), \quad v = \hat{v}(x, y)$$

for every point in S_u .

We note that this solution gives the exact solution of the 3-D problem with

$$w = 0$$

and

$$\tau_{xz} = \tau_{yz} = 0$$

$$\gamma_{xz} = \gamma_{yz} = 0.$$

Example 4.3

Consider a disc with a central circular hole. The disc is subjected to internal pressure p_i and external pressure p_e . The problem description is given in Figure 4.13. Determine the stress distribution and the displacements.

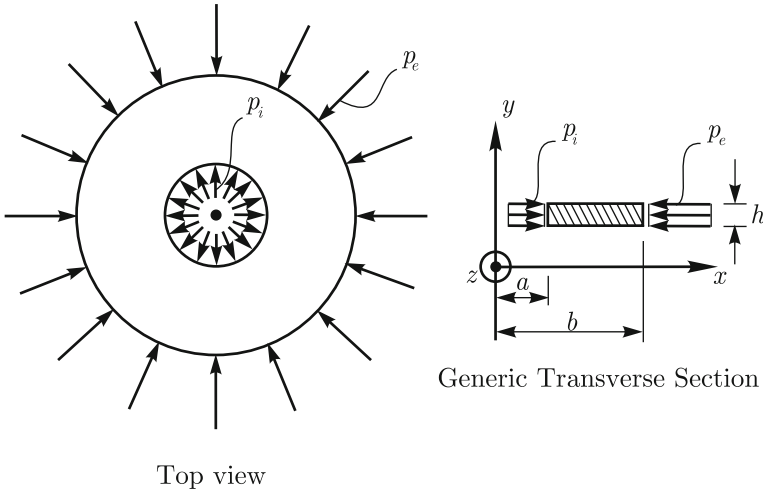


Fig. 4.13. Schematic description of disc problem

Solution

The disc is a solid of revolution subjected to axisymmetric loading. Considering the load given and that the disc is thin, plane stress conditions also apply.

Therefore

$$\tau_{xy} = 0, \tau_{yy} = 0$$

and the equilibrium condition given in equation (4.75) simplifies to

$$\frac{d\tau_{xx}}{dx} + \frac{\tau_{xx} - \tau_{zz}}{x} = 0. \quad (4.78)$$

Since there are no body forces, Equation (4.76) is identically satisfied. The relevant strain components are

$$\varepsilon_{xx} = \frac{du}{dx} \quad (4.79)$$

and

$$\varepsilon_{zz} = \frac{u}{x}. \quad (4.80)$$

The plane stress constitutive equation with the shear strain (stress) zero can be directly used, *i.e.*

$$\tau_{xx} = \frac{E}{1 - \nu^2} (\varepsilon_{xx} + \nu \varepsilon_{zz}) \quad (4.81)$$

$$\tau_{zz} = \frac{E}{1 - \nu^2} (\varepsilon_{zz} + \nu \varepsilon_{xx}). \quad (4.82)$$

Introducing (4.79) and (4.80) into (4.81) and (4.82) yields

$$\tau_{xx} = \frac{E}{1 - \nu^2} \left(\frac{du}{dx} + \nu \frac{u}{x} \right) \quad (4.83)$$

$$\tau_{zz} = \frac{E}{1 - \nu^2} \left(\frac{u}{x} + \nu \frac{du}{dx} \right) \quad (4.84)$$

and substituting (4.83) and (4.84) into the equilibrium equation (4.78) leads to

$$\frac{d^2 u}{dx^2} + \frac{1}{x} \frac{du}{dx} - \frac{u}{x^2} = 0.$$

The above ordinary differential equation has a general solution given by

$$u = C_1 x + \frac{C_2}{x} \quad (4.85)$$

where C_1 and C_2 are constants to be determined. The general expression for the stresses can be obtained by introducing (4.85) into (4.83) and (4.84) leading to

$$\tau_{xx} = \frac{E}{1 - \nu^2} \left[C_1 (1 + \nu) - C_2 \frac{(1 - \nu)}{x^2} \right] \quad (4.86)$$

$$\tau_{zz} = \frac{E}{1 - \nu^2} \left[C_1 (1 + \nu) + C_2 \frac{(1 - \nu)}{x^2} \right]. \quad (4.87)$$

We are now ready to impose the force boundary conditions. At the internal surface of the disc we have

$$\tau_{xx}|_{x=a} = -p_i \quad (4.88)$$

and at the external surface

$$\tau_{xx}|_{x=b} = -p_e. \quad (4.89)$$

Equation (4.86) subjected to the conditions given by (4.88) and (4.89) leads to

$$C_1 = \frac{1 - \nu}{E} \frac{a^2 p_i - b^2 p_e}{b^2 - a^2}$$

$$C_2 = \frac{1 + \nu}{E} \frac{a^2 b^2 (p_i - p_e)}{b^2 - a^2}.$$

Hence, the stresses are given by

$$\tau_{xx} = \frac{a^2 p_i - b^2 p_e}{b^2 - a^2} - \frac{(p_i - p_e) a^2 b^2}{x^2 (b^2 - a^2)}$$

$$\tau_{zz} = \frac{a^2 p_i - b^2 p_e}{b^2 - a^2} + \frac{(p_i - p_e) a^2 b^2}{x^2 (b^2 - a^2)}.$$

Note that

$$\tau_{xx} + \tau_{zz} = 2 \left(\frac{a^2 p_i - b^2 p_e}{b^2 - a^2} \right)$$

is a constant, *i.e.*, independent of the point where it is evaluated. Therefore

$$\varepsilon_{yy} = -\nu (\tau_{xx} + \tau_{zz}) \quad (4.90)$$

is also a constant. Hence, the out-of-plane displacements v are independent of x and any horizontal plane remains horizontal after deformation (this also means that the distortion γ_{xy} is indeed zero and, of course, $\gamma_{yz} = \gamma_{xz} = 0$ due to the axisymmetric conditions). Hence, we conclude that we obtained the exact 3-D solution and the assumptions of the plane stress model in this case did not lead to an approximate solution.

We also note that, since horizontal planes remain horizontal after deformation the derived solution is also valid for any thickness of the disc, *i.e.*, it is valid not only for a thin disc but also for long cylinders, as long as the out-of-plane displacements are not restricted. In case we prevent the out-of-plane displacements, a plane strain condition develops and the solution can be readily obtained by using the effective material constants, *i.e.*, by replacing E by E_* and ν by ν_* in the solution of the in-plane variables, that is, $\tau_{xx}(x)$, $\tau_{zz}(x)$ and $u(x)$. Note that ε_{yy} is not an in-plane variable for the plane stress problem considered here and hence it is not obtained by replacing ν by ν_* in (4.90). Of course, $\varepsilon_{yy} = 0$ for plane strain conditions.

To conclude this example solution the radial displacements can be evaluated by substituting the value of the constants C_1 and C_2 into equation (4.85) leading to

$$u(x) = \frac{1 - \nu}{E} \frac{a^2 p_i - b^2 p_e}{b^2 - a^2} x + \frac{1 + \nu}{E} \frac{a^2 b^2 (p_i - p_e)}{(b^2 - a^2) x}$$

□

Before we move to the next section and embark on the discussion of the mathematical models of bars, it is timely to place such bar models and

the forthcoming plate and shell models in the larger context of structural mechanics mathematical modeling.

If we look at the developments presented in this section and compare, from the hierarchical modeling perspective, the 2-D models with the 3-D elasticity model – our highest order mathematical model in linear analysis – there is an important point. As long as the geometric, loading and boundary condition restrictions are satisfied, the plane strain and axisymmetric models lead to the exact solution of the 3-D elasticity problem. Therefore, the modeling considerations should only focus on judging whether the assumptions used in the plane strain or, respectively the axisymmetric model, with respect to the 3-D model are (sufficiently) satisfied in the actual physical problem.

Such situation contrasts with the plane stress model. In such model even if the geometric, loading and boundary condition restrictions are exactly satisfied, its solution is not, in general, the solution of the associated 3-D model, *i.e.* that for which the plate is modeled as a 3-D solid. Hence, the plane stress model is what we refer to be a structural model. In what follows we will be formulating bars, plates and shell models which considering the interpretations given above are characterized also as structural models. We summarize these observations in Figure 4.14.

4.2 Bar models

There are a number of bar models which are associated with different geometric, loading and kinematic boundary conditions. Also, there are different nomenclatures in the technical literature associated with bar models, and hence we adopt a terminology which best fits the aim to use the models in the hierarchical modeling process.

Generically, a bar can be understood to be a slender 3-D solid which has one dimension much larger than the other two dimensions, which are of the same order of magnitude. We could say that if a , b and c are characteristic dimensions of a solid in three orthogonal directions, such solid can be assumed to be a bar if a is of the order of b , *i.e.*, $\frac{1}{5} \leq \frac{a}{b} \leq 5$ and $\frac{c}{\max(a,b)} \geq 10$. Then, it is usual to characterize the bar's geometry from the definition of a curve called the bar axis. At any point of the bar axis, a plane region, orthogonal to the bar axis, is defined. Such plane region is referred to as the transverse cross-section of the bar at this point. The collection of these transverse cross-sections characterize the bar's geometry, where the bar axis is taken to pass through the centers of gravity of the cross-sections. In Figure 4.15, a generic bar is shown.

We can identify a number of different situations. For example, the bar axis can be a three-dimensional curve, a planar curve or a straight line. The cross-sections may have a constant or varying shape. Moreover, of course, the bar can be loaded by various different external forces. Depending on the

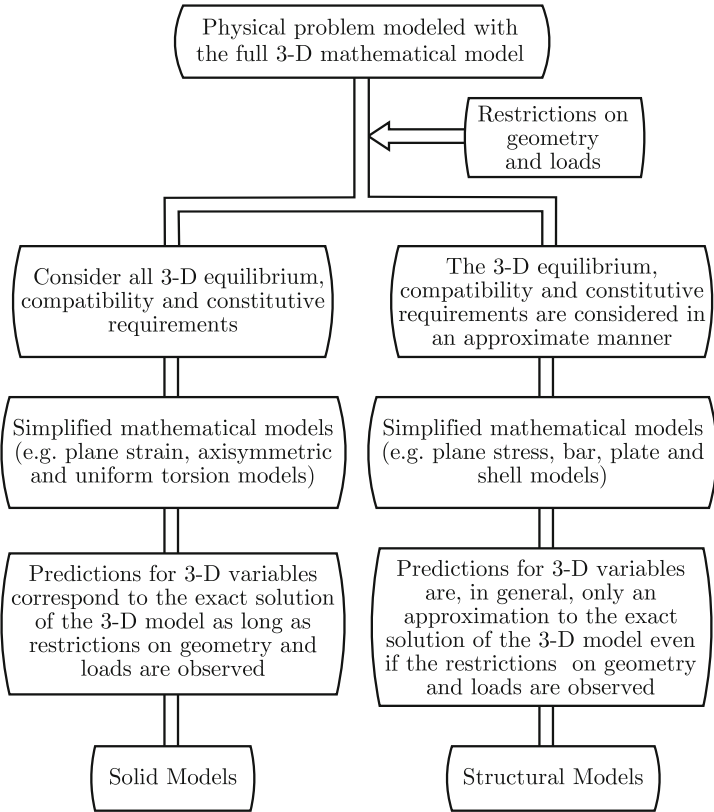


Fig. 4.14. Summary of mathematical modeling in solid and structural mechanics

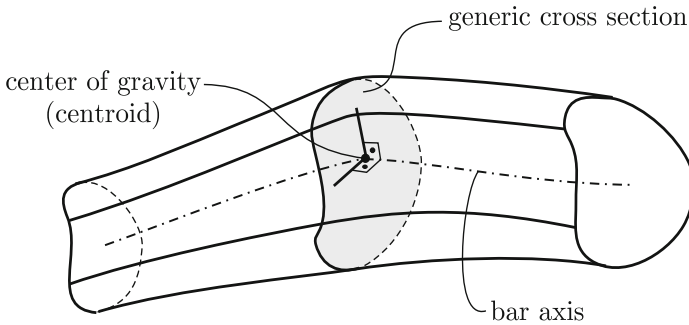


Fig. 4.15. A generic bar geometry

combination of the geometric and loading characteristics of the problem, the bar structural behavior may be different. Therefore, there are a number of mathematical models for bars which are associated with specific geometric and loading conditions.

As a first approach to formulate bar models, we consider the bar as a 3-D solid and impose geometric and loading restrictions. Also, we introduce assumptions for the stress and displacement fields. Then, the 3-D elasticity equations are used to obtain the differential formulation of the bar model.

This is the approach that we followed to obtain the plane elasticity models and which we now use to derive the bar models. The approach gives insight into how well the bar solutions satisfy the 3-D equations.

4.2.1 Prismatic bar subjected to axial loading

The assumptions used for the mathematical model are (see also Figure 4.16):

- *Geometry*: The solid is a prismatic bar (a bar of constant cross-section and straight axis).
- *Kinematics*: The cross-sections remain plane and displace only in the axial direction (they do not rotate). The section displacements are given by $u = u(x)$.
- *External loading and boundary conditions*: The body forces per unit of volume are given by $\mathbf{f}^B = f_x^B(x)\mathbf{e}_x$.
At the section $x = 0$ either $f_x^S = f_0^S$ or $u = u_0$, and $f_y^S = f_z^S = 0$.
At the section $x = L$ either $f_x^S = f_L^S$ or $u = u_L$, and $f_y^S = f_z^S = 0$.
On the lateral surfaces of the bar $\mathbf{f}^S = \mathbf{0}$.
- *Stresses*: The normal stress τ_{xx} is the only nonzero stress component.

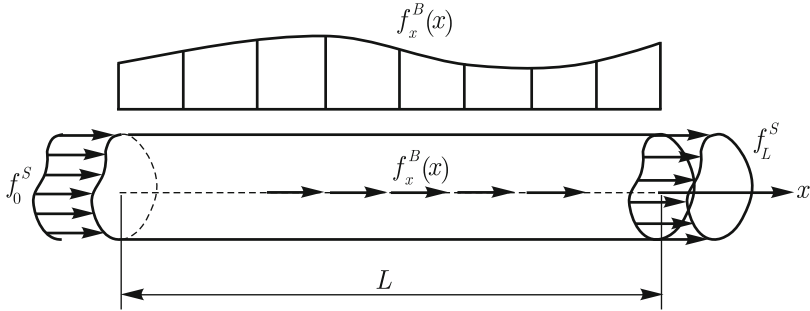


Fig. 4.16. Schematic representation of the model. Either displacement or force boundary conditions should be specified at the end sections. Bar cross-sectional area A

Now let us consider the 3-D elasticity equations.

Equilibrium

Considering the differential equilibrium equations (3.114), the first equation leads to

$$\frac{\partial \tau_{xx}}{\partial x} + f_x^B = 0 \quad (4.91)$$

and the remaining equations are identically satisfied.

Constitutive equations

Considering the generalized Hooke's law given in (3.116), we obtain

$$\varepsilon_{xx} = \frac{\tau_{xx}}{E}, \quad \varepsilon_{yy} = -\frac{\nu}{E}\tau_{xx}, \quad \varepsilon_{zz} = -\frac{\nu}{E}\tau_{xx} \quad (4.92)$$

$$\gamma_{xy} = 0, \quad \gamma_{yz} = 0, \quad \gamma_{zx} = 0. \quad (4.93)$$

Strain-displacement relations

Introducing (4.92) and (4.93) into (3.115) we obtain

$$\frac{\partial u}{\partial x} = \frac{\tau_{xx}}{E} \quad (4.94)$$

$$\frac{\partial v}{\partial y} = -\frac{\nu}{E}\tau_{xx} \quad (4.95)$$

$$\frac{\partial w}{\partial z} = -\frac{\nu}{E}\tau_{xx} \quad (4.96)$$

$$\frac{\partial u}{\partial y} + \frac{\partial v}{\partial x} = 0 \quad (4.97)$$

$$\frac{\partial v}{\partial z} + \frac{\partial w}{\partial y} = 0. \quad (4.98)$$

$$\frac{\partial u}{\partial z} + \frac{\partial w}{\partial x} = 0 \quad (4.99)$$

Boundary conditions

On the surface given by $x = 0$

$$\text{either } f_0^S = -\tau_{xx}(0) \text{ or } u(0) = u_0 \\ f_y^S = -\tau_{yx} = 0, \quad f_z^S = -\tau_{zx} = 0 \text{ (identically satisfied).}$$

On that given by $x = L$

$$\text{either } f_L^S = \tau_{xx}(L) \text{ or } u(L) = u_L \\ f_y^S = \tau_{yx} = 0, \quad f_z^S = \tau_{zx} = 0 \text{ (identically satisfied).}$$

On the lateral surface

$$\mathbf{Tn} = \mathbf{0}$$

or

$$\begin{bmatrix} \tau_{xx} & 0 & 0 \\ 0 & 0 & 0 \\ 0 & 0 & 0 \end{bmatrix} \begin{bmatrix} 0 \\ n_y \\ n_z \end{bmatrix} = \begin{bmatrix} 0 \\ 0 \\ 0 \end{bmatrix}$$

which is identically satisfied.

We can obtain a solution solving (4.91) for τ_{xx} and then (4.94) for $u(x)$. Note, however, that when $f_x^B(x) \neq 0$, we obtain $\tau_{xx} = \tau_{xx}(x)$ and from (4.92)

$$\varepsilon_{yy} = \frac{\partial v}{\partial y} = -\frac{\nu}{E}\tau_{xx}(x) \quad (4.100)$$

$$\varepsilon_{zz} = \frac{\partial w}{\partial z} = -\frac{\nu}{E}\tau_{xx}(x) \quad (4.101)$$

which for varying x means a varying Poisson effect with x , unless $\nu = 0$. Since this induced extension/contraction of the fibers in the plane of the section is different for neighboring sections, the sections have to warp to keep the transverse shear strains ($\gamma_{yz} = \gamma_{xz} = 0$) equal to zero. Then, of course, $u = u(x)$ is violated, that is, the kinematic assumption “the cross-sections remain plane and displace only in the axial direction (they do not rotate)” is violated. However, in the bar model this effect is neglected and, hence, using this model we in essence assume that the physical link between two neighboring sections is given by rollers *i.e.* the contraction/extension of the fibers in the section does not affect the deformation of neighboring sections.

More formally, integrating of (4.100) with respect to y leads to

$$v = -\frac{\nu}{E}\tau_{xx}(x)y + F(x, z)$$

where $F(x, z)$ is a function of x and z only. This equation substituted into (4.97) gives

$$\frac{\partial u}{\partial y} = \frac{\nu}{E} \frac{\partial \tau_{xx}}{\partial x} y - \frac{\partial F}{\partial x}(x, z)$$

which can not be satisfied if $u = u(x)$ unless $\nu = 0$. A similar conclusion would arise if (4.101) and (4.99) were considered.

Now the 1-D bar model can be detailed.

Let $\tau = \tau_{xx}$ and $f = f_x^B A$ be the distributed axial force per unit of length. Also let $N = \tau A$ be the axial force. Hence, the equilibrium equation (4.91) can be re-written as

$$\frac{dN}{dx} + f = 0.$$

Defining $\varepsilon = \varepsilon_{xx}$, the strain compatibility relation is given by

$$\varepsilon = \frac{du}{dx}$$

and the constitutive relation by

$$\tau = E\varepsilon.$$

The boundary condition at $x = 0$ is either a displacement boundary condition

$$u(0) = u_0$$

where u_0 is the prescribed displacement, or a force boundary condition

$$N(0) = \tau(0)A = -f_0^S A = -R_0$$

where R_0 is the prescribed concentrated force with positive sense given by the x axis. Analogously, at $x = L$, we have either

$$u(L) = u_L$$

where u_L is the prescribed displacement at L , or

$$N(L) = \tau(L)A = f_L^S A = R_L$$

where R_L is the prescribed concentrated force at $x = L$ with the same sense convention as that adopted for R_0 . The differential formulation is summarized below.

Differential formulation of bar subjected to axial loading

Given the axial distributed loading $f(x)$, find $N(x)$, $\varepsilon(x)$, $u(x)$ such that

$$\frac{dN}{dx} + f = 0 \quad (4.102)$$

$$\varepsilon = \frac{du}{dx} \quad (4.103)$$

$$N = EA\varepsilon \quad (4.104)$$

for all x within the bar. At $x = 0$ we have either

$$u(0) = u_0 \quad \text{or} \quad N(0) = -R_0$$

and at $x = L$, either

$$u(L) = u_L \quad \text{or} \quad N(L) = R_L.$$

It is usual to write the differential formulation in terms of displacements only, by introducing (4.103) and (4.104) into (4.102) and using that

$$N(0) = EA\varepsilon(0) = EA\frac{du}{dx}(0)$$

and

$$N(L) = EA\varepsilon(L) = EA\frac{du}{dx}(L).$$

Differential formulation of bar subjected to axial loading in terms of displacements only

Given $f(x)$, find $u(x)$ such that

$$EA\frac{d^2u}{dx^2} + f = 0 \quad (4.105)$$

for all x within the bar. At $x = 0$, we have either

$$u(0) = u_0 \quad \text{or} \quad \frac{du}{dx}(0) = -\frac{R_0}{EA} \quad (4.106)$$

and at $x = L$, either

$$u(L) = u_L \quad \text{or} \quad \frac{du}{dx}(L) = \frac{R_L}{EA}. \quad (4.107)$$

Of course, when the problem is solved for $u(x)$, we can obtain $\varepsilon(x)$ and $N(x)$ using equations (4.103) and (4.104).

Once the 1-D differential formulation is solved, the solution for the 3-D problem based on the 1-D solution can be obtained:

$$\begin{aligned} u &= u(x) \\ \tau_{xx} &= \tau, \quad \tau_{yy} = \tau_{zz} = \tau_{xy} = \tau_{xz} = \tau_{yz} = 0 \\ \varepsilon_{xx} &= \varepsilon = \frac{du}{dx}, \quad \varepsilon_{yy} = -\frac{\nu}{E}\tau, \quad \varepsilon_{zz} = -\frac{\nu}{E}\tau \\ \gamma_{xy} &= \gamma_{xz} = \gamma_{yz} = 0 \end{aligned}$$

and the displacements associated with the extension/contraction of the fibers in the cross-section can be evaluated using

$$v = -\frac{\nu}{E}\tau y \quad (4.108)$$

$$w = -\frac{\nu}{E}\tau z \quad (4.109)$$

which satisfies (4.95), (4.96), (4.98) and the condition that the bar axis has no transverse displacements.

Note that when $f_x^B(x) = 0$ or $\nu = 0$ the 1-D model leads to the exact solution of the 3-D problem.

Example 4.4

Consider a steel bar subjected to its own weight as shown in Figure 4.17.

The solution of the 3-D elasticity problem is given by

$$u = \frac{\rho g}{2E}(2Lx - x^2 - \nu(y^2 + z^2))$$

$$v = -\nu \frac{\rho g}{E}(L - x)y$$

$$w = -\nu \frac{\rho g}{E}(L - x)z$$

- (i) Find the solution for the bar using the 1-D model.
- (ii) Compare the solution obtained in (i) with the exact solution.

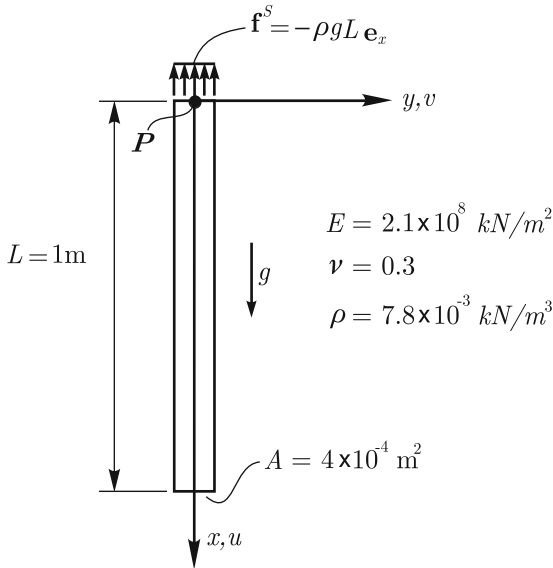


Fig. 4.17. Bar problem definition. Point P is fixed and the bar cannot rotate with respect to P

Solution

- (i) The differential formulation for the 1-D model in terms of displacements is given by

$$EA \frac{d^2 u}{dx^2} + \rho g A = 0$$

$$u(0) = 0$$

$$\frac{du}{dx}(L) = 0.$$

Solving, we obtain

$$u(x) = \frac{\rho g}{2E} (2Lx - x^2) \quad (4.110)$$

and the axial stress is given by

$$\tau = E \frac{du}{dx} = \rho g(L - x)$$

using equations (4.108) and (4.109), we obtain

$$v = -\nu \frac{\rho g}{E} (L - x)y \quad (4.111)$$

$$w = -\nu \frac{\rho g}{E} (L - x)z. \quad (4.112)$$

(ii) Comparing the 1-D solution with the exact solution, we observe that the predictions for v and w are exactly the same. The u displacements differ by the warping of the cross-section. In fact, we can write

$$u_{exact} = u_{one-dimensional} + u_{warp}$$

where $u_{one-dimensional}$ is the solution of the 1-D bar model and

$$u_{warp} = -\nu \frac{\rho g}{2E} (y^2 + z^2)$$

is the warping displacement. Of course, when $\nu = 0$ the solutions of both models coincide. We note that for bar problems the warping displacements are small when compared to those predicted by the 1-D model. For example, considering the square cross-section for the bar in Figure 4.17, the ratio between the maximum warping displacement and that of the 1-D model at $x = L$ is 6×10^{-5} .

□

4.2.2 Prismatic bar subjected to transverse loading; the Bernoulli-Euler beam model.

This model plays a fundamental role in the formulation and understanding of mathematical models for structural analysis. The model serves as a reference for many structural models.

The external loading and geometry are selected to lead to bending in one plane only and to not induce torsion. The term beam is used to describe a bar when there is transverse loading that is transferred to the supports by bending.

The assumptions used for the mathematical model are (see also Figure 4.18):

- *Geometry*: The solid is a prismatic bar (a bar of constant cross-section and straight axis). The plane xz is a plane of symmetry.

- *Kinematics*: The cross-sections remain plane and orthogonal to the deformed bar axis. The bar axis goes through the centroid of the section, remains in the xz plane and the in-plane deformation of the cross-sections is neglected.
- *External loading and boundary conditions*: The load is transverse to the bar, that is, in the z direction and we choose to model it as body forces per unit of volume given by $\mathbf{f}^B = f_z^B(x)\mathbf{e}_z$. At the end sections either displacements or surface tractions are prescribed. On the lateral surfaces of the bar $\mathbf{f}^S = \mathbf{0}$.
- *Stresses*: The normal stress τ_{xx} and the transverse shear stress τ_{xz} are the only nonzero stress components.

We choose a bar of rectangular cross-section (see Figure 4.18) and consider the 3-D elasticity equations.

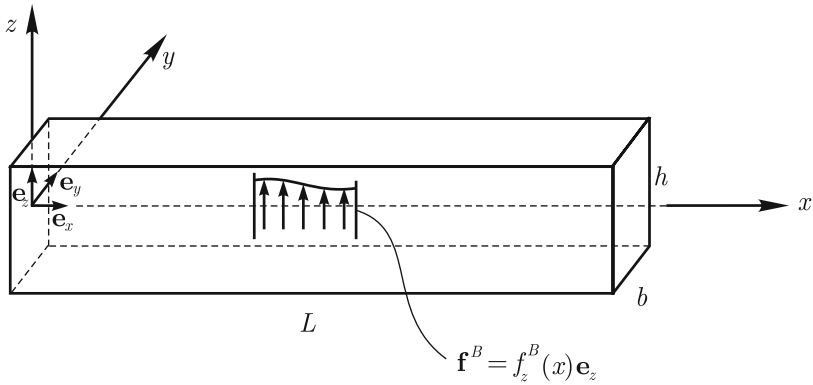


Fig. 4.18. Bar subjected to transverse loading

Equilibrium

Considering the differential equilibrium equations (3.114), the first and third equations lead to

$$\frac{\partial \tau_{xx}}{\partial x} + \frac{\partial \tau_{xz}}{\partial z} = 0 \quad (4.113)$$

$$\frac{\partial \tau_{xz}}{\partial x} + f_z^B(x) = 0 \quad (4.114)$$

and the second equation is identically satisfied.

Constitutive equations

Considering the generalized Hooke's law given in (3.116), we obtain

$$\varepsilon_{xx} = \frac{\tau_{xx}}{E}, \varepsilon_{yy} = -\frac{\nu}{E}\tau_{xx}, \varepsilon_{zz} = -\frac{\nu}{E}\tau_{xx} \quad (4.115)$$

$$\gamma_{xy} = 0, \gamma_{yz} = 0, \gamma_{zx} = \frac{\tau_{xz}}{G} \quad (4.116)$$

Strain-displacement relations

Introducing (4.115) and (4.116) into (3.115) we obtain

$$\frac{\partial u}{\partial x} = \frac{\tau_{xx}}{E} \quad (4.117)$$

$$\frac{\partial v}{\partial y} = -\frac{\nu}{E}\tau_{xx} \quad (4.118)$$

$$\frac{\partial w}{\partial z} = -\frac{\nu}{E}\tau_{xx} \quad (4.119)$$

$$\frac{\partial u}{\partial y} + \frac{\partial v}{\partial x} = 0 \quad (4.120)$$

$$\frac{\partial v}{\partial z} + \frac{\partial w}{\partial y} = 0. \quad (4.121)$$

$$\frac{\partial u}{\partial z} + \frac{\partial w}{\partial x} = \frac{\tau_{xz}}{G} \quad (4.122)$$

Let us now consider the kinematic assumptions which are pictorially described in Figure 4.19. Since we are assuming infinitesimally small displacements and we neglect the in-plane deformation of the cross-sections

$$w = w(x) \quad (4.123)$$

and from the hypothesis “the cross-sections remain plane and orthogonal to the deformed bar axis”, we obtain

$$u = -z \frac{dw}{dx} \quad (4.124)$$

where we have also used that the displacements are infinitesimally small. Considering that “the bar axis remains in the xz plane” and again that “the in-plane deformation of the cross-sections is neglected”

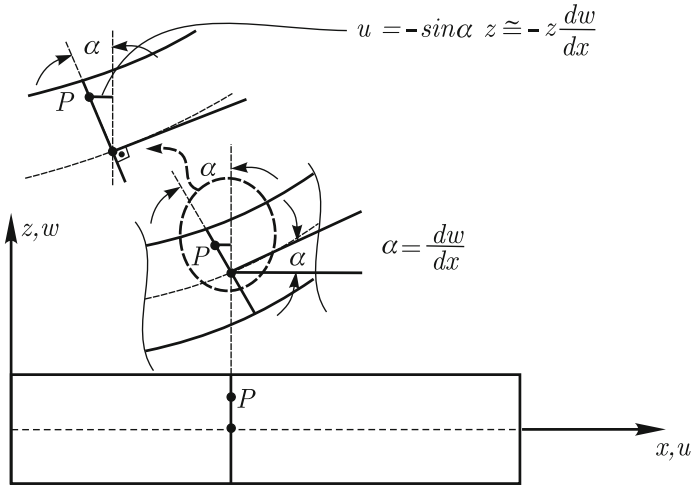


Fig. 4.19. Kinematics of beam sections

$$v = 0.$$

Note that considering the kinematic assumptions, equations (4.118), (4.119) and (4.122) can not be exactly satisfied. In fact, the violation of (4.118) and (4.119) means that we are neglecting the contraction/extension of the fibers in the plane of the cross-section due to Poisson's effect. And from (4.123) and (4.124)

$$\gamma_{xz} = \frac{\partial u}{\partial z} + \frac{\partial w}{\partial x} = -\frac{dw}{dx} + \frac{dw}{dx} = 0 \tag{4.125}$$

which corresponds to a violation of (4.122). This means that we are neglecting the induced shear strain γ_{xz} due to the shear stress τ_{xz} .

We also note that the displacements are fully determined once $w(x)$ is known.

From (4.117) and (4.124), we obtain

$$\tau_{xz} = -zE \frac{d^2 w}{dx^2} \tag{4.126}$$

which substituted into (4.113) yields

$$-zE \frac{d^3 w}{dx^3} + \frac{\partial \tau_{xz}}{\partial z} = 0.$$

Integrating the above equation with respect to z , we obtain

$$\tau_{xz} = \frac{z^2}{2} E \frac{d^3 w}{dx^3} + f(x, y) \tag{4.127}$$

where $f(x, y)$ is a function of x and y only. Since the top and bottom surfaces of the bar are free of surface tractions, we have

$$\tau_{xz} \left(x, y, \frac{h}{2} \right) = 0 \quad (4.128)$$

$$\tau_{xz} \left(x, y, -\frac{h}{2} \right) = 0. \quad (4.129)$$

Considering (4.128), that is, the condition at the top surface and (4.127), we obtain

$$\frac{h^2}{8} E \frac{d^3 w}{dx^3} + f(x, y) = 0$$

which leads to

$$f(x, y) = g(x) = -\frac{h^2}{8} E \frac{d^3 w}{dx^3}$$

and with this $f(x, y) = g(x)$, (4.127) also satisfies (4.129). Hence

$$\tau_{xz} = \frac{E}{2} \frac{d^3 w}{dx^3} \left(z^2 - \left(\frac{h}{2} \right)^2 \right). \quad (4.130)$$

Substituting (4.130) into (4.114) yields

$$\frac{E}{2} \frac{d^4 w}{dx^4} \left(z^2 - \left(\frac{h}{2} \right)^2 \right) + f_z^B(x) = 0$$

which can be satisfied pointwise only at $z = 0$, that is, at the bar axis. We can integrate the above equation over the cross-section to impose that it should be satisfied in average to obtain

$$\frac{d^4 w}{dx^4} = \frac{f_z^B(x) A}{EI} \quad (4.131)$$

where $A = bh$ is the area of the cross-section and $I = \frac{bh^3}{12}$ is the moment of inertia of the cross-section with respect to the y axis. The boundary conditions at the lateral surfaces ($y = \pm \frac{b}{2}$) are satisfied since there are no surface tractions applied and $\tau_{yy} = \tau_{yz} = 0$.

We still have to consider the boundary conditions at the end surfaces given by $x = 0$ and $x = L$.

Since the only nonzero stress components are τ_{xx} and τ_{xz} , the surface tractions at $x = 0$ are $f_x^S = -\tau_{xx}$, $f_y^S = 0$, $f_z^S = -\tau_{xz}$ and at $x = L$ $f_x^S = \tau_{xx}$, $f_y^S = 0$, $f_z^S = \tau_{xz}$. Note that the stress components τ_{xx} and τ_{xz} are given in (4.126) and (4.130), and they are fully determined when the values of $\frac{d^2 w}{dx^2}$ and $\frac{d^3 w}{dx^3}$ have been obtained.

Hence, the differential formulation of the Bernoulli-Euler beam model is based on the solution of (4.131) for $w(x)$ subject to boundary conditions at $x = 0$ and $x = L$. Before we detail this differential formulation we define the section stress resultants

$$M(x) = \int_A -\tau_{xz} z \, dA \quad (4.132)$$

$$V(x) = \int_A -\tau_{xz} \, dA \quad (4.133)$$

where, of course, $M(x)$ is the bending moment and $V(x)$ is the shear force. Using (4.126) and (4.130), we obtain

$$M(x) = EI \frac{d^2 w}{dx^2} \quad (4.134)$$

$$V(x) = EI \frac{d^3 w}{dx^3} \quad (4.135)$$

and, hence,

$$\frac{dM}{dx} = V.$$

Also, we can define the transverse loading per unit of length

$$p(x) = f_z^B(x) A$$

which using (4.131) and (4.134) yields

$$\frac{d^2 M}{dx^2} = p.$$

We summarize below the differential formulation of the beam mathematical model.

Differential formulation of the Bernoulli-Euler beam model in terms of displacement only

Given the transverse distributed loading $p(x)$, find $w = w(x)$ such that

$$\frac{d^4 w}{dx^4} = \frac{p(x)}{EI} \quad (4.136)$$

for all x within the bar. At $x = 0$, we have either

$$w(0) = w_0 \quad \text{or} \quad EI \frac{d^3 w}{dx^3}(0) = Q_0 \quad (4.137)$$

and either

$$\frac{dw}{dx}(0) = \varphi_0 \quad \text{or} \quad EI \frac{d^2w}{dx^2}(0) = M_0. \quad (4.138)$$

At $x = L$, we have either

$$w(L) = w_L \quad \text{or} \quad EI \frac{d^3w}{dx^3}(L) = -Q_L \quad (4.139)$$

and either

$$\frac{dw}{dx}(L) = \varphi_L \quad \text{or} \quad EI \frac{d^2w}{dx^2}(L) = -M_L. \quad (4.140)$$

where M_0 and M_L are externally applied moments measured positive as moments about the y -axis, and Q_0 and Q_L are externally applied forces measured positive into the z -direction.

We note that

$$M_0 \mathbf{e}_y = \left(\int_A f_x^S(0, y, z) z \, dA \right) \mathbf{e}_y$$

that is, $M_0 \mathbf{e}_y$ is the moment which is equivalent to the surface tractions $f_x^S(0, y, z)$. Note that since $f_x^S(0, y, z) = -\tau_{xx}(0, y, z)$

$$M_0 = \int_A -\tau_{xx}(0, y, z) z \, dA = M(0) = EI \frac{d^2w}{dx^2}(0)$$

which gives the second equation of (4.138).

Also

$$Q_0 \mathbf{e}_z = \left(\int_A f_z^S(0, y, z) \, dA \right) \mathbf{e}_z$$

that is, $Q_0 \mathbf{e}_z$ is the force which is equivalent to the surface tractions $f_z^S(0, y, z)$. Note that since $f_z^S(0, y, z) = -\tau_{xz}(0, y, z)$

$$Q_0 = \int_A -\tau_{xz}(0, y, z) \, dA = V(0) = EI \frac{d^3w}{dx^3}(0)$$

which is the second equation of (4.137). Analogous interpretations hold for $x = L$. In summary, at the bar end sections we should prescribe either a displacement or a force and either a rotation or a moment.

Note that once the differential formulation is solved and $w(x)$ determined, we can obtain the 3-D predictions of the bar mathematical model using (4.124), (4.126), (4.130) and the assumptions $w(x, y, z) = w(x)$, $v(x, y, z) = 0$, $\tau_{yy} = \tau_{zz} = \tau_{xy} = \tau_{yz} = 0$. If the in-plane extension/contraction of

the fibers are of interest, we can improve the predictions for $w(x, y, z)$ and $v(x, y, z)$ substituting τ_{xx} given by (4.126) into (4.118), (4.119) and considering (4.121).

The approach we used to derive the 1-D differential formulation for the Bernoulli-Euler beam model, and also for the bar subjected to axial loading only, in which we considered the 3-D elasticity equations, permits to clearly identify what the model assumptions are and how they affect the satisfaction of the 3-D equations. However, as we consider more complex structural mathematical models such as curved beam, plate and shell models this approach becomes difficult to follow and we consider for the formulation of the remaining models a classical approach.

In this classical approach we also start with a 3-D solid and consider geometric, kinematic and mechanical assumptions. Then, we enforce equilibrium, constitutive and compatibility conditions. These conditions are related to the analogous 3-D elasticity conditions but are not exactly those. For example, equilibrium is imposed in terms of stress resultants and constitutive and compatibility conditions are selectively enforced. We exemplify the use of this classical approach with the Bernoulli-Euler model considered already.

We start from the same geometric and kinematic assumptions given above and consider a load $p(x)$ per unit longitudinal length acting into the z direction. Then, we use (4.124) and (4.117) which implicitly consider the compatibility relation

$$\varepsilon_{xx} = \frac{\partial u}{\partial x} \quad (4.141)$$

and the constitutive relation

$$\varepsilon_{xx} = \frac{\tau_{xx}}{E}$$

to obtain (4.126). Note that in using the above constitutive relation, we implicitly assumed that $\tau_{yy} = \tau_{zz} = 0$.

Then we consider equilibrium in terms of the stress resultants of a differential element as summarized in Figure 4.20³.

We note that to represent the actions of the rest of the beam on the end cross-sections of this differential element we have introduced the bending moment $M(x)$ and the shear force $V(x)$ which are necessary to equilibrate the transverse load as detailed below.

Equilibrium of the differential element in the z direction yields

$$V - (V + dV) + p(x)dx = 0$$

$$\frac{dV}{dx} = p(x) \quad (4.142)$$

³ Note that this sign convention for the transverse shear V for the beam models (see also Section 4.2.8) is quite common but is opposite to the convention used for plates and shells

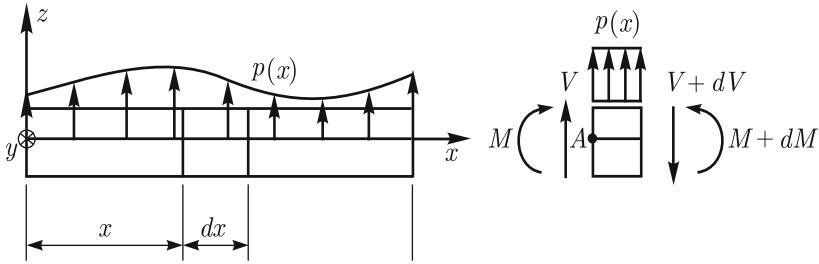


Fig. 4.20. Equilibrium of a generic differential element

and moment equilibrium, which is enforced about point A for instance, gives

$$-(V + dV)dx + p(x)dx \frac{dx}{2} - M + (M + dM) = 0.$$

Neglecting infinitesimals of higher order, we obtain

$$\frac{dM}{dx} = V. \quad (4.143)$$

Equations (4.142) and (4.143) are the bar equilibrium conditions. Of course, equilibrium in the axial direction is trivially satisfied since we are considering transverse loading only and the axial forces are zero.

Taking derivatives of (4.143) with respect to x and substituting the result in (4.142) yields

$$\frac{d^2 M}{dx^2} = p(x). \quad (4.144)$$

Using (4.126) and (4.132), we obtain (4.134) which substituted in (4.144) yields (4.136). Now we could write the same differential formulation obtained above and given in (4.136) to (4.140). Hence, both approaches lead to the same differential formulation.

We state below some classical equations and definitions for the beam model. From (4.126) and (4.134), we obtain

$$\tau_{xx} = -\frac{M}{I}z \quad (4.145)$$

which gives the linear normal stress distribution at the beam cross-section. We note that, since z is measured from the bar axis going through the centroid of the section,

$$\int_A \tau_{xx} dA = 0.$$

Indeed, we want this property and have chosen the location of the bar axis correspondingly. We also define

$$\kappa = \frac{d^2 w}{dx^2} \quad (4.146)$$

where κ gives the curvature of the bar axis since we are considering infinitesimally small displacements. Then, (4.134) gives

$$\kappa = \frac{M}{EI} \quad (4.147)$$

which leads to the important physical interpretation that the bending moment $M(x)$ induces curvature of the beam axis. The product EI is called the bending rigidity of the section (or of the beam, when the beam has a constant cross-section). It gives the stiffness of the section for bending induced curvature.

We can rewrite the differential formulation given in (4.136) to (4.140), now considering (4.144), (4.146) and (4.147) to obtain:

Differential formulation of the Bernoulli-Euler beam model

Given the transverse distributed loading $p(x)$, find $M(x)$, $\kappa(x)$, $w(x)$ such that

$$\frac{d^2 M}{dx^2} = p(x) \quad (4.148)$$

$$\kappa(x) = \frac{d^2 w}{dx^2} \quad (4.149)$$

$$\kappa(x) = \frac{M(x)}{EI} \quad (4.150)$$

for all x within the bar. At $x = 0$ we have

$$w(0) = w_0 \quad \text{or} \quad \frac{dM}{dx}(0) = Q_0 \quad (4.151)$$

and

$$\frac{dw}{dx}(0) = \varphi_0 \quad \text{or} \quad M(0) = M_0. \quad (4.152)$$

At $x = L$

$$w(L) = w_L \quad \text{or} \quad \frac{dM}{dx}(L) = -Q_L \quad (4.153)$$

and

$$\frac{dw}{dx}(L) = \varphi_L \quad \text{or} \quad M(L) = -M_L. \quad (4.154)$$

Of course, the solution of both differential formulations leads to the same transverse displacements and, hence, the same model predictions. We note that the differential formulation given by (4.148)—(4.154) explicitly shows the conditions of equilibrium, compatibility and constitutive behavior. In fact, (4.148) is the equilibrium equation, (4.149) the compatibility relation and (4.150) the constitutive equation.

Considering the variables in the formulation of this bar model and the variables of the bar under axial loading model, we recognize that some of these variables are quite different from those of the 2-D and 3-D elasticity models. For example, in the bending bar model we have stress resultants and curvature variables. This is usually the case for structural mathematical models.

In order to give a unified framework for the presentation of the structural mathematical models, let us make some definitions. There are always *kinematic variables* which fully characterize the kinematics of the model. The kinematic variable for this model is $w = w(x)$. Note that all displacement components for any point in the bar can be obtained from $w(x)$. In fact,

$$\begin{aligned} u(x, y, z) &= -z \frac{dw}{dx} \\ v(x, y, z) &= 0 \\ w(x, y, z) &= w(x). \end{aligned}$$

There are strain type variables which are linked to the straining of the beam fibers. They are referred to as *generalized strain variables*. The curvature $\kappa(x)$ is the generalized strain variable for this model.

There are variables which are linked to the internal actions and are referred to as *generalized internal force variables* or *generalized stress variables*. The moment $M(x)$ is such variable for the beam model.

We note that there is a correspondence between the above defined generalized strain and the usual strains of the 2-D and 3-D elasticity models. Both are obtained from the kinematic variables and are related to the straining of the material fibers.

The correspondence also holds for the generalized internal force or generalized stress in the beam model and the stresses for the 2-D and 3-D elasticity models since both reflect the internal transfer of forces. Finally, the generalized strain and internal force are related by a generalized constitutive equation (see equation (4.150)).

The kinematic, the generalized strain and the generalized stress variables are called *primary variables* of the model since they completely characterize the model and its mathematical formulation can be fully stated considering these variables. Also, the primary variables are used to express the conditions of equilibrium, compatibility and constitutive behavior.

Note that the shear force does not enter directly in the differential formulation of the problem and can be obtained by equation (4.143) after $M(x)$ has been found. It is termed an *auxiliary variable*.

Example 4.5

Obtain the transverse shear stress distribution at a generic cross-section of a beam.

Solution

Due to the kinematic assumptions of the Bernoulli-Euler beam model the transverse shear strain γ_{xz} is zero, see (4.125). Therefore, the constitutive relation would lead to $\tau_{xz} = \tau_{zx} = 0$. However, considering the equilibrium condition (4.143) a nonzero shear force V is in general required. Of course, the shear force is the stress resultant associated with the distribution of τ_{zx} . At a given cross-section

$$V = \int_A (-\tau_{zx}) \, dA \tag{4.155}$$

where the minus sign is a result of the sign convention. Equation (4.155) shows that τ_{zx} can not be zero throughout the cross-section when V is different from zero. This apparent inconsistency is resolved when we recognize that in the Bernoulli-Euler model the shear deformations which would be induced by τ_{zx} are neglected. This assumption is increasingly appropriate as h/L becomes smaller, because for slender beams this shear deformation contributes very little to the overall beam deformation. However, the contribution of τ_{zx} for equilibrium can not be neglected.

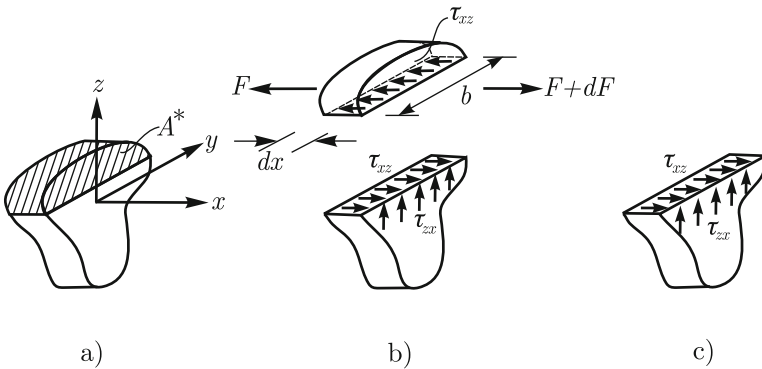


Fig. 4.21. Transverse shear stresses in beams

In order to evaluate an approximate distribution of τ_{zx} (approximate when compared to the 3-D elasticity solution), consider the part of the beam shown in Figure 4.21a which is obtained by cutting the beam at two cross-sections dx apart. In Figure 4.21b, the equilibrium in the x direction of the highlighted part of Figure 4.21a is shown. Of course

$$F = \int_{A^*} \tau_{xx} dA = \int_{A^*} -\frac{M}{I} z dA = -\frac{M}{I} \int_{A^*} z dA. \quad (4.156)$$

Note that a constant distribution of τ_{zx} is assumed at the horizontal plane defined by the cut. Recalling a result for shear stresses acting on orthogonal planes, we note that the shear stress acting on this horizontal plane defines the shear stress acting on the beam cross-section as schematically shown in Figure 4.21c. Considering Figure 4.21b the equilibrium in the x direction leads to

$$dF = \tau_{xz} b dx$$

or

$$\tau_{xz} = \frac{1}{b} \frac{dF}{dx}. \quad (4.157)$$

Let us define

$$\mathfrak{M}_y = \int_{A^*} z dA \quad (4.158)$$

which is the static moment of the area A^* with respect to the y axis. From equations (4.143), (4.156), (4.157) and (4.158) we obtain

$$\tau_{xz} = \tau_{zx} = -\frac{\mathfrak{M}_y}{bI} \frac{dM}{dx} = -\frac{V\mathfrak{M}_y}{bI}. \quad (4.159)$$

In order to obtain insight into the shear stress distribution, consider a beam of rectangular cross-section. Referring to Figure 4.22a, we can write

$$\begin{aligned} \mathfrak{M}_y &= \int_{A^*} z dA = \int_{z^*}^{h/2} \int_{-b/2}^{b/2} z dy dz = b \int_{z^*}^{h/2} z dz = b \frac{z^2}{2} \Big|_{z^*}^{h/2} \\ &= \frac{b}{2} \left(\frac{h^2}{4} - (z^*)^2 \right) \end{aligned}$$

where z^* is the z coordinate associated with the cutting horizontal plane as shown in Figure 4.22a. Then, from (4.159) we obtain

$$\tau_{xz} = -\frac{V}{2I} \left(\frac{h^2}{4} - (z^*)^2 \right) = -\frac{3V}{2bh} \left(1 - \left(\frac{z^*}{h/2} \right)^2 \right) \quad (4.160)$$

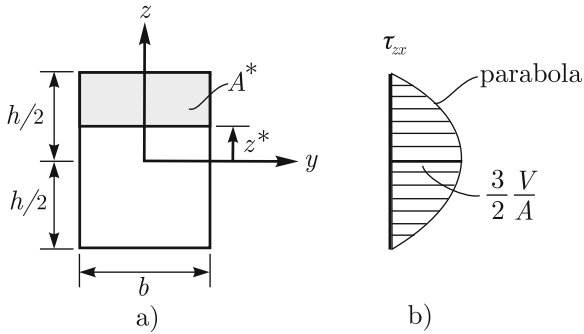


Fig. 4.22. a) Geometric definitions; b) Transverse shear stress distribution for a rectangular cross-section

where we used that $I = bh^3/12$. Of course, we note the agreement between (4.130) and (4.160).

As summarized in Figure 4.22b, the shear stress distribution for a rectangular cross-section is parabolic with the maximum value at the centroid given by $3/2$ times the average shear stress V/A . Note that the condition of zero shear stresses at the top and bottom surfaces of the beam is satisfied.

□

Demonstrative solutions

We give below some example solutions. These examples, besides giving some insight into the use and behavior of the beam model, present solutions in a convenient form to introduce the matrix method of analysis for frames.

Example 4.6

Find the solution of the beam problem described in Figure 4.23.

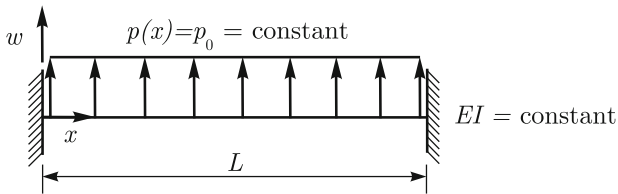


Fig. 4.23. Built-in beam subjected to constant transverse load

Solution

We use the differential formulation

$$\frac{d^4 w}{dx^4} = \frac{p_0}{EI} \quad (4.161)$$

with the following boundary conditions

$$w(0) = \frac{dw}{dx}(0) = w(L) = \frac{dw}{dx}(L) = 0$$

to enforce the kinematic restraints to displacements and rotations at both ends. Integrating equation (4.161) with respect to x yields

$$w(x) = \frac{p_0 x^4}{24EI} + C_1 x^3 + C_2 x^2 + C_3 x + C_4 \quad (4.162)$$

where C_1 , C_2 , C_3 and C_4 are constants to be determined. Imposing the boundary conditions gives

$$w(x) = -\frac{p_0 x^4}{24EI} + \frac{p_0 L}{12EI} x^3 - \frac{p_0 L^2}{24EI} x^2. \quad (4.163)$$

The end-forces and moments are obtained by using (4.134) and (4.135)

$$M(0) = M(L) = -\frac{p_0 L^2}{12}, \quad V(0) = -V(L) = \frac{p_0 L}{2}.$$

□

Example 4.7

Find the solution to the beam problem subjected to an imposed end-displacement as summarized in Figure 4.24.

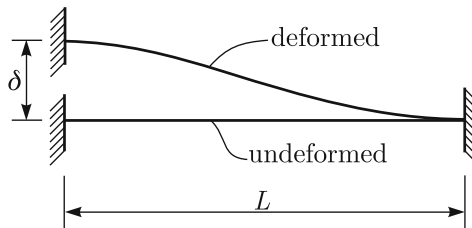


Fig. 4.24. Built-in beam subjected to imposed end transverse displacement

Solution

We use

$$\frac{d^4w}{dx^4} = 0 \quad (4.164)$$

with the following boundary conditions

$$w(0) = \delta, \quad \frac{dw}{dx}(0) = w(L) = \frac{dw}{dx}(L) = 0. \quad (4.165)$$

Integrating (4.164) leads to

$$w(x) = C_1x^3 + C_2x^2 + C_3x + C_4. \quad (4.166)$$

The constants can be determined by imposing the boundary conditions given in (4.165) leading to

$$\begin{aligned} w(x) &= \left(\frac{2x^3}{L^3} - \frac{3x^2}{L^2} + 1 \right) \delta \\ &= h_2(x)\delta \end{aligned} \quad (4.167)$$

where

$$h_2(x) = \frac{2x^3}{L^3} - \frac{3x^2}{L^2} + 1.$$

The function $h_2(x)$ gives the transverse displacement of the beam axis when a unit transverse displacement is imposed at the left end and the remaining end-displacement and rotations are fixed. The corresponding end-forces and moments are

$$M(0) = -M(L) = -\frac{6EI}{L^2}, \quad V(0) = V(L) = \frac{12EI}{L^3}.$$

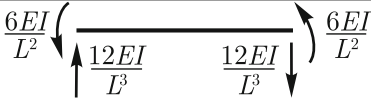
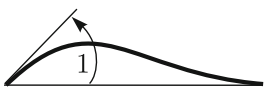
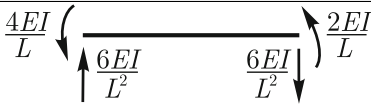
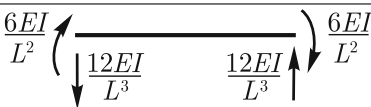
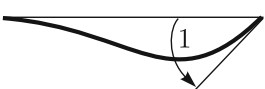
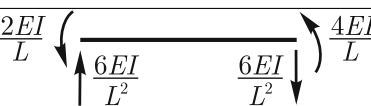
□

Proceeding as in Example 4.7, we can derive the solutions of the beam model for other unit end displacement/rotation conditions as summarized in Table 4.1. The h_i functions are referred to as the beam Hermitian functions. These solutions are very useful since they can be used to find solutions to arbitrarily chosen end displacement/rotation conditions. In fact, let us consider the beam without transverse loading but with imposed end displacement/rotation conditions given by

$$w(0) = w_0, \quad w(L) = w_L, \quad \frac{dw}{dx}(0) = w'_0 \quad \text{and} \quad \frac{dw}{dx}(L) = w'_L. \quad (4.168)$$

The solution to this problem is given by

Table 4.1. Exact solution for unit end displacement/rotation conditions

Problem description	Bar end-forces and solution for $w(x)$
 <p>$w(0) = 1; w(L) = 0; \frac{dw(0)}{dx} = 0; \frac{dw(L)}{dx} = 0$</p>	 <p>$h_2(x) = \frac{2x^3}{L^3} - \frac{3x^2}{L^2} + 1$</p>
 <p>$w(0) = 0; w(L) = 0; \frac{dw(0)}{dx} = 1; \frac{dw(L)}{dx} = 0$</p>	 <p>$h_3(x) = \frac{x^3}{L^2} - \frac{2x^2}{L} + x$</p>
 <p>$w(0) = 0; w(L) = 1; \frac{dw(0)}{dx} = 0; \frac{dw(L)}{dx} = 0$</p>	 <p>$h_5(x) = -\frac{2x^3}{L^3} + \frac{3x^2}{L^2}$</p>
 <p>$w(0) = 0; w(L) = 0; \frac{dw(0)}{dx} = 0; \frac{dw(L)}{dx} = 1$</p>	 <p>$h_6(x) = \frac{x^3}{L^2} - \frac{x^2}{L}$</p>

$$w(x) = h_2(x)w_0 + h_3(x)w'_0 + h_5(x)w_L + h_6(x)w'_L. \tag{4.169}$$

The $w(x)$ defined in (4.169) satisfies (4.136) for $p(x) = 0$ since $h_2(x)$, $h_3(x)$, $h_5(x)$ and $h_6(x)$ also verify (4.136) for $p(x) = 0$, and the $w(x)$ satisfies the boundary conditions given in (4.168) since the $h_i(x)$, $\frac{dh_i(x)}{dx}$ assume the value of 1 for the corresponding end displacement/rotation conditions (see Table 4.1) and the value of zero for the other end conditions. The solution in (4.169) represents of course an application of the principle of superposition (See Section 2.3.6).

Example 4.8

Assume that the end conditions for the problem in Figure 4.23 are those stated in (4.168). Find the solution of the problem.

Solution

Denoting by $w_1(x)$ the solution for the transverse load with zero end displacements/rotations derived in Example 4.6 given by (4.163) and by $w_2(x)$ the solution for the specified displacement/rotation end conditions with no transverse load given by (4.169), the function

$$w(x) = w_1(x) + w_2(x)$$

is the solution sought. In fact

$$\frac{d^4 w}{dx^4} = \frac{d^4}{dx^4}(w_1(x) + w_2(x)) = \frac{d^4 w_1}{dx^4} + \frac{d^4 w_2}{dx^4} = \frac{d^4 w_1}{dx^4} = \frac{p(x)}{EI}$$

and since $w_1(x)$ corresponds to the zero end conditions (it is the solution to the problem of Example 4.6) $w(x)$ satisfies the given boundary conditions. \square

Note that we can obtain the solution to the problem of a beam subjected to a transverse load $p(x)$ and imposed end displacements/rotations by solving a beam clamped at both ends subjected to the $p(x)$ (see Example 4.6) and adding to this solution the response due to the imposed end displacements/rotations (see (4.169)).

In the next example, we examine a situation in which at one end we have a prescribed displacement and no restriction on the section rotation.

Example 4.9

Solve the problem described in Figure 4.25. We note that there is no restriction

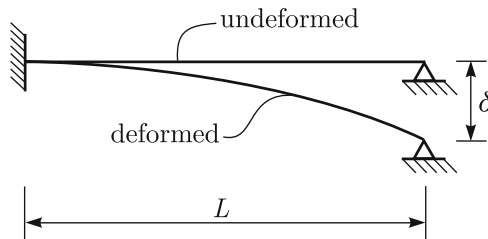


Fig. 4.25. Beam subjected to imposed end transverse displacement. Section rotation at right end is left free

tion on the rotation at the end $x = L$.

Solution

Although we do not have a prescribed rotation at the end $x = L$, we can still take advantage of the general solution for $p(x) = 0$ which is given by (4.169). Of course $w_0 = w'_0 = 0$, $w_L = -\delta$ and w'_L is to be determined. The condition of leaving the section rotation at $x = L$ free is represented by imposing that the bending moment at that section is zero. Hence the solution can be written as

$$w(x) = h_5(x)(-\delta) + h_6(x)w'_L$$

with $M(L) = 0$. This condition corresponds to

$$M(L) = EI \frac{d^2w}{dx^2}(L) = 0$$

and hence

$$\frac{d^2w}{dx^2}(L) = \left. \frac{d^2h_5(x)}{dx^2} \right|_L (-\delta) + \left. \frac{d^2h_6(x)}{dx^2} \right|_L w'_L = 0$$

to give

$$w'_L = -\frac{3\delta}{2L}.$$

Therefore the final solution is

$$w(x) = -\left(h_5(x) + \frac{3}{2L} h_6(x) \right) \delta.$$

□

The *principle of superposition* used in the above solutions is employed abundantly, and we choose to detail it further in the next example.

Example 4.10

Consider the problem described in Figure 4.26a. Show how the principle of superposition can be used to solve this problem.

Solution

In Figure 4.26b we show four simpler problems whose solutions *superimposed* give the solution to the original problem.

We note that for each problem the restraints are those of the original problem and an external action – either a part of the total loading or a support

settlement/rotation – is introduced. Of course, when considered together, the external actions in the simpler problems should represent all external actions on the original structure.

The validity of the principle of superposition rests on the linearity of the differential formulation of the problem. Referring to the differential formulation of the Bernoulli-Euler beam model, we summarize in Table 4.2 the differential formulation of each simple problem. Due to the linearity of the differential formulation

$$w(x) = w_1(x) + w_2(x) + w_3(x) + w_4(x)$$

is the solution of the original problem.

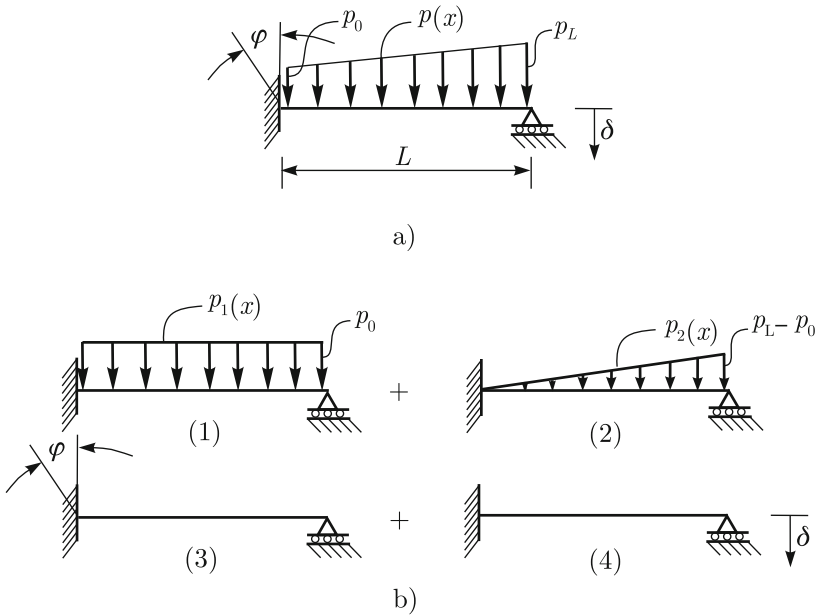


Fig. 4.26. a) Original problem; b) Simpler problems used for the superposition

In fact,

$$\frac{d^4 w}{dx^4} = \frac{d^4 w_1}{dx^4} + \frac{d^4 w_2}{dx^4} + \frac{d^4 w_3}{dx^4} + \frac{d^4 w_4}{dx^4} = \frac{p_1(x)}{EI} + \frac{p_2(x)}{EI} = \frac{p(x)}{EI}$$

$$w(0) = w_1(0) + w_2(0) + w_3(0) + w_4(0) = 0$$

Table 4.2. Differential formulations of simpler problems

(1) $\frac{d^4 w_1}{dx^4} = \frac{p_1(x)}{EI}$ $w_1(0) = 0, \quad w_1(L) = 0$ $\frac{dw_1}{dx}(0) = 0, \quad EI \frac{d^2 w_1}{dx^2}(L) = 0$	(2) $\frac{d^4 w_2}{dx^4} = \frac{p_2(x)}{EI}$ $w_2(0) = 0, \quad w_2(L) = 0$ $\frac{dw_2}{dx}(0) = 0, \quad EI \frac{d^2 w_2}{dx^2}(L) = 0$
(3) $\frac{d^4 w_3}{dx^4} = 0$ $w_3(0) = 0, \quad w_3(L) = 0$ $\frac{dw_3}{dx}(0) = \varphi, \quad EI \frac{d^2 w_3}{dx^2}(L) = 0$	(4) $\frac{d^4 w_4}{dx^4} = 0$ $w_4(0) = 0, \quad w_4(L) = -\delta$ $\frac{dw_4}{dx}(0) = 0, \quad EI \frac{d^2 w_4}{dx^2}(L) = 0$

$$\frac{dw}{dx}(0) = \frac{dw_1}{dx}(0) + \frac{dw_2}{dx}(0) + \frac{dw_3}{dx}(0) + \frac{dw_4}{dx}(0) = \varphi$$

$$w(L) = w_1(L) + w_2(L) + w_3(L) + w_4(L) = -\delta$$

$$EI \frac{d^2 w}{dx^2}(L) = EI \frac{d^2 w_1}{dx^2}(L) + EI \frac{d^2 w_2}{dx^2}(L) + EI \frac{d^2 w_3}{dx^2}(L) + EI \frac{d^2 w_4}{dx^2}(L) = 0$$

which show that $w(x)$ satisfies all field and boundary conditions of the original problem. The solution of the seemingly complex problem has therefore been reduced to the solution of the four simpler problems.

□

Bars subjected to axial and transverse loading

In Section 4.1 we examined the solution of bars subjected to axial loading only and in this section we obtained the solution of bars subjected to transverse loading only. In the linear analysis considered, the axial loading does not induce any rotations of the bar sections and the transverse loading does not induce any axial displacement at the bar axis. Therefore, in the context of infinitesimally small displacements, the solution of a bar subjected to the simultaneous actions of axial and transverse loadings can be obtained by the superposition of the solutions to the axial and bending problems.

Example 4.11

Find the solution of a bar of length L and cross-sectional area A subjected to imposed axial end displacements u_0 at $x = 0$ and u_L at $x = L$.

Solution

Considering the differential formulation of the bar problem subjected to axial loading given by (4.105) to (4.107), we have

$$EA \frac{d^2 u}{dx^2} = 0$$

where E is Young's modulus. Hence,

$$u(x) = C_2 x + C_1$$

and imposing $u(0) = u_0$ and $u(L) = u_L$, we obtain

$$u(x) = u_0 \left(1 - \frac{x}{L}\right) + u_L \frac{x}{L}$$

or

$$u(x) = h_1(x)u_0 + h_4(x)u_L.$$

We note that $h_1(x)$ gives the solution for an imposed unit axial displacement at $x = 0$ with the other end fixed. Analogously, the function $h_4(x)$ gives the solution for an imposed axial unit displacement at $x = L$ with the end $x = 0$ fixed. □

Let us consider a generic bar and number the end degrees of freedom as schematically shown in Figure 4.27.



Fig. 4.27. Numbering of end section degrees of freedom. Young's modulus E , the moment of inertia I and the cross-sectional area A are all constant

Consider that these end displacements are imposed and that there is no distributed axial and transverse loading. Using Examples 4.7 and 4.11, the solution can be written as⁴

$$u(x) = h_1(x)u_1 + h_4(x)u_4 \tag{4.170}$$

⁴ Note that $u(x)$ in (4.170) represents a uniform section displacement (independent of z used in (4.124)) and $w(x)$ in (4.171) results in an additional u -displacement as given in (4.124)

and

$$w(x) = h_2(x)u_2 + h_3(x)u_3 + h_5(x)u_5 + h_6(x)u_6 \quad (4.171)$$

and the numbering used for the functions h_i is now obvious. If in addition a transverse or axial loading is applied, the solutions can be obtained by superposition (see Example 4.10).

4.2.3 Bar models obtained by an assemblage of bars

We have studied so far bar models of only one bar. When bar models are used in structural engineering to model real structures, the resulting models almost always involve an assemblage of bars.

In Chapter 2, we studied truss structures made of several bars. The truss models are simpler than those we consider next since in truss structures each bar only carries an axial force due to pin end conditions. However, the same concepts can be used to analyze structures made of an assemblage of bars carrying bending and axial forces.

Consider the structure in Figure 4.28a. The structure is clearly properly supported since, due to the clamped condition at section A , the structure can not undergo any motion when considered rigid.

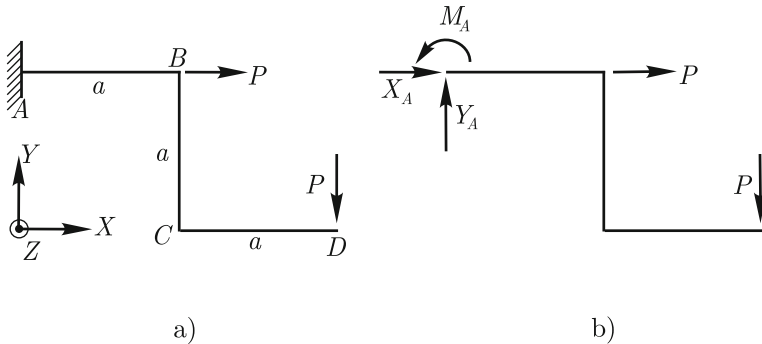


Fig. 4.28. a) Three-bar structure model. Bars AB , BC and CD have constant EI and EA ; b) External actions on the structure with reactions included

This structure is statically determinate since the suppression of any of its restraints would yield a structure that is no longer properly supported.

Associated with each restraint, a reaction force is introduced as schematically shown in Figure 4.28b. Since the structure is statically determinate the reactions can be determined using the global equilibrium conditions below

$$\sum F_X = 0 \quad \Rightarrow \quad X_A = -P$$

$$\sum F_Y = 0 \quad \Rightarrow \quad Y_A = P$$

$$M_A - P \cdot 2a = 0 \quad \Rightarrow \quad M_A = 2Pa.$$

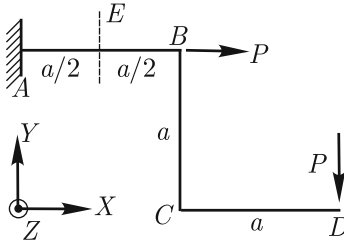


Fig. 4.29. Definition of section *E*

Let us discuss how to determine the internal forces and moment at any section by examining the section *E* shown in Figure 4.29. The structure is conceptually cut at this section and we introduce the section forces and moments acting onto the two resulting parts as shown in Figure 4.30.

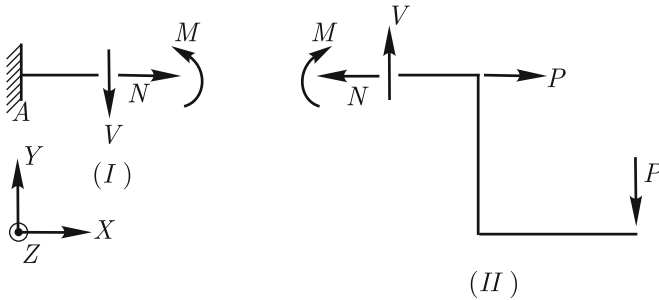


Fig. 4.30. Internal forces at section *E*

Of course, the internal forces and moments at section *E* can be evaluated by enforcing equilibrium of either part (I) or (II). Since in part (II) we have only known external actions, its equilibrium directly gives these internal forces and moments. We obtain

$$\begin{aligned} N &= P \\ V &= P \\ M &= -\frac{3Pa}{2}. \end{aligned}$$

In this way, we can determine N , V and M for any section and obtain the axial, shear and moment diagrams which are shown in Figure 4.31. For a generic point on the bar axis, the magnitude shown orthogonal to the axis indicates the value of the particular internal force/moment at that bar section. For the axial and shear force diagrams the sign convention is indicated next to the diagrams. For the bending moment, the convention is to draw the diagram on the side where the fibers are tensioned due to the action of the bending moment.

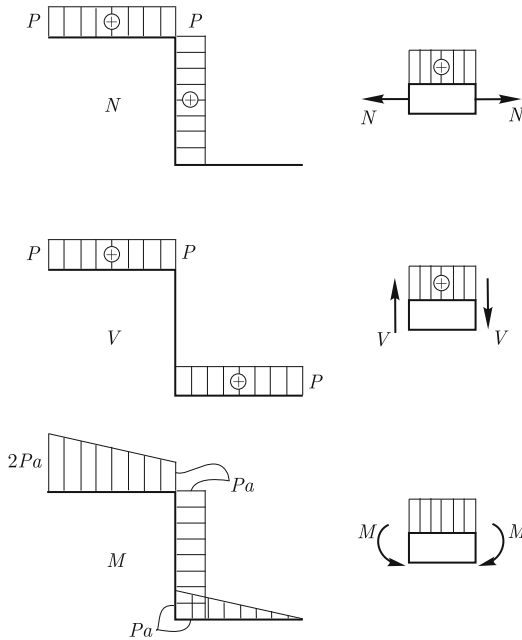


Fig. 4.31. Axial, shear and bending moment diagrams

To illustrate how displacements can be evaluated for an assemblage of bars, we consider the example below.

Example 4.12

Calculate the section displacement indicated in Figure 4.32.

Solution

We need to consider the contributions due to the axial force and the bending moment. Note that the displacement δ_C depends not only on the deforma-

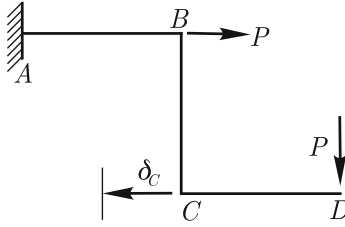


Fig. 4.32. Section displacement to be evaluated

tion of bar BC but also on that of bar AB . Since we know the displacements/rotation at A and the internal forces of bar AB , we can evaluate the displacements/rotation at point B by solving the applicable differential equations for bar AB .

For every bar we adopt a local coordinate system such that the x axis is always axial as described in Figure 4.33a.

The differential formulation for the bending problem of bar AB reads

$$\frac{d^2w}{dx^2} = \frac{M(x)}{EI} = \frac{1}{EI} (Px - 2Pa) \quad (4.172)$$

$$w(0) = 0; \quad w'(0) = 0$$

and for the axial problem

$$\frac{du}{dx} = \frac{N(x)}{EA} = \frac{P}{EA} \quad (4.173)$$

$$u(0) = 0.$$

Solving equations (4.172) and (4.173), we obtain for section B

$$u_B = \frac{Pa}{EA}$$

$$w_B = -\frac{5Pa^3}{6EI}$$

$$w'_B = -\frac{3Pa^2}{2EI}.$$

For bar BC , we have

$$\frac{d^2w}{dx^2} = \frac{M(x)}{EI} = -\frac{Pa}{EI}$$

$$w(0) = u_B = \frac{Pa}{EA}; \quad w'(0) = w'_B = -\frac{3Pa^2}{2EI}$$

and

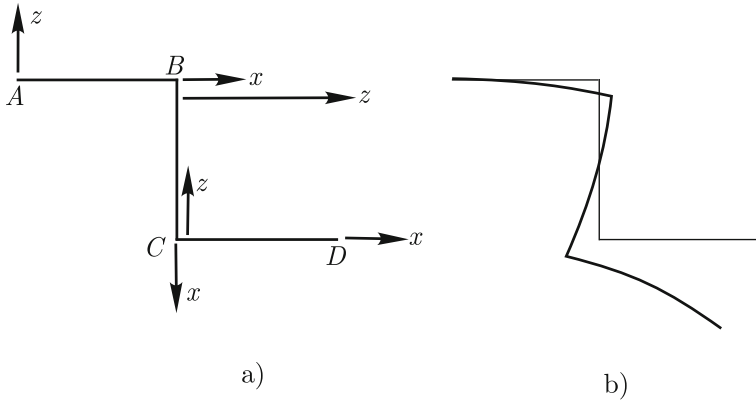


Fig. 4.33. a) Choices of local axes; b) Magnified deformed shape

$$\frac{du}{dx} = \frac{N(x)}{EA} = \frac{P}{EA}$$

$$u(0) = -w_B = \frac{5Pa^3}{6EI}.$$

Of course, the end conditions at $x = 0$ for bar BC have been obtained from the displacements and the rotation at section B considered as the end section of bar AB .

Solving the above equations, we obtain

$$w_C = \frac{Pa}{EA} + \frac{5Pa^3}{6EI} = \frac{5Pa^3}{6EI} \left(1 + \frac{6I}{5Aa^2} \right)$$

and

$$w_C = -\frac{2Pa^3}{EI} + \frac{Pa}{EA} = -\frac{2Pa^3}{EI} \left(1 - \frac{I}{2Aa^2} \right).$$

Therefore

$$\delta_C = -w_C = \frac{2Pa^3}{EI} \left(1 - \frac{I}{2Aa^2} \right). \quad (4.174)$$

A magnified deformed shape of the structure is shown in Figure 4.33b.

We compare the relative contribution of the axial and bending deformations to the calculated displacement. Assuming that the bars are of a rectangular cross-section of height h , expression (4.174) becomes

$$\delta_C = \frac{2Pa^3}{EI} \left(1 - \frac{1}{24} \left(\frac{h}{a} \right)^2 \right)$$

and we see that for a usual range of values for h and a the contribution of the axial deformation is negligible when compared to that of the bending deformation.

□

Although the methodology used in the above example to find displacements/rotations for an assemblage of bars provides insight into the kinematics of the deformation, it is not efficient for a structure of many bars. Moreover, the solution would become even more cumbersome for statically indeterminate structures. Consider, for example, the structure described in Figure 4.34 which was obtained by adding a support at point C to the structure of Figure 4.28.

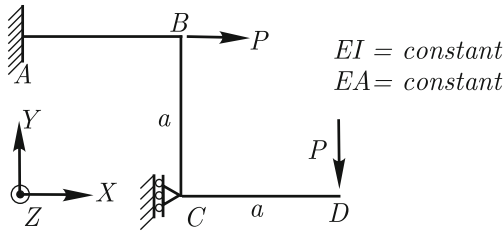


Fig. 4.34. Modified three-bar structure

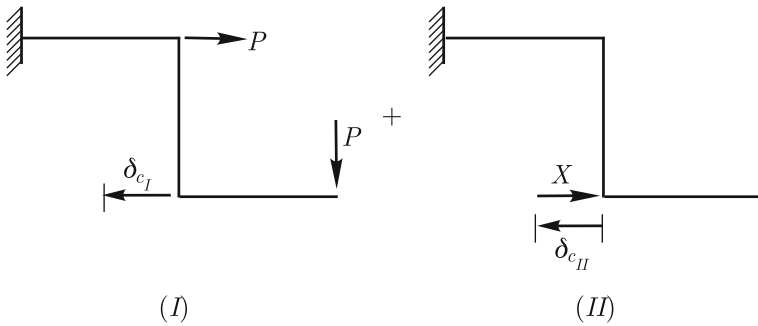


Fig. 4.35. Superposition for three-bar structure

Before we can solve for the displacements we need to find the reaction at C . For that purpose we can use the superposition of effects as shown in Figure 4.35 and impose the compatibility relation

$$\delta_{C_I} + \delta_{C_{II}} = 0.$$

If we define $\delta_{C_{II}}^1$ as $\delta_{C_{II}}$ for $X = 1$ then

$$X = -\frac{\delta_{C_I}}{\delta_{C_{II}}^1}.$$

Of course, δ_{C_I} is the δ_C evaluated above and $\delta_{C_{II}}^1$ can be calculated in a similar way.

The discussion above reinforces the need for a systematic approach to solve engineering structures made of many bars and provides the motivation for the next section.

4.2.4 Matrix displacement method for frames

In this section we introduce a systematic approach to solve structures made of several bars. The methods described in the previous section, which are very useful to obtain insight into the behavior of simple bar structures, are not adequate for solving structures made of several bars.

Analogous to the developments for truss structures, presented in Chapter 2, the matrix method provides a very efficient approach to analyze frame structures of arbitrary complexity.

The main ingredients of the matrix method have already been presented in Section 2.3 and using Table 4.1 we can now directly assemble the bar element stiffness matrix including bending effects.

Stiffness matrix for a bar in a local system

The stiffness matrix of a bar in the local system of axes and corresponding to the nodal degrees of freedom shown in Figure 4.36 is given by the equation

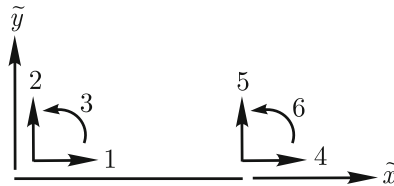


Fig. 4.36. Bar local axes and degrees of freedom

$$\tilde{\mathbf{k}}\tilde{\mathbf{u}} = \tilde{\mathbf{f}} \quad (4.175)$$

where

$$\tilde{\mathbf{u}} = \begin{bmatrix} \tilde{u}_1 \\ \tilde{u}_2 \\ \tilde{u}_3 \\ \tilde{u}_4 \\ \tilde{u}_5 \\ \tilde{u}_6 \end{bmatrix}, \quad \tilde{\mathbf{f}} = \begin{bmatrix} \tilde{f}_1 \\ \tilde{f}_2 \\ \tilde{f}_3 \\ \tilde{f}_4 \\ \tilde{f}_5 \\ \tilde{f}_6 \end{bmatrix}$$

$$\tilde{\mathbf{k}} = \begin{bmatrix} \frac{EA}{L} & 0 & 0 & -\frac{EA}{L} & 0 & 0 \\ 0 & \frac{12EI}{L^3} & \frac{6EI}{L^2} & 0 & -\frac{12EI}{L^3} & \frac{6EI}{L^2} \\ 0 & \frac{6EI}{L^2} & \frac{4EI}{L} & 0 & -\frac{6EI}{L^2} & \frac{2EI}{L} \\ -\frac{EA}{L} & 0 & 0 & \frac{EA}{L} & 0 & 0 \\ 0 & -\frac{12EI}{L^3} & -\frac{6EI}{L^2} & 0 & \frac{12EI}{L^3} & -\frac{6EI}{L^2} \\ 0 & \frac{6EI}{L^2} & \frac{2EI}{L} & 0 & -\frac{6EI}{L^2} & \frac{4EI}{L} \end{bmatrix}. \quad (4.176)$$

The elements in the matrix $\tilde{\mathbf{k}}$ corresponding to bending are, of course, the forces and moments listed in Table 4.1. To illustrate this observation, consider that we impose $\tilde{u}_2 = 1$ and $\tilde{u}_1 = \tilde{u}_3 = \tilde{u}_4 = \tilde{u}_5 = \tilde{u}_6 = 0$. The solution to this problem is given in Table 4.1. and is summarized in Figure 4.37.

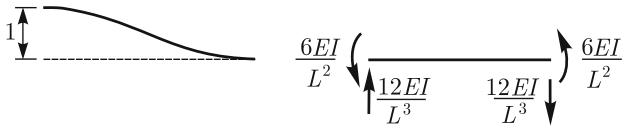


Fig. 4.37. Solution that leads to the second column of $\tilde{\mathbf{k}}$

Of course, from (4.175), we obtain

$$\tilde{\mathbf{f}} = [\tilde{k}_{i2}] = \begin{bmatrix} 0 \\ \frac{12EI}{L^3} \\ \frac{6EI}{L^2} \\ 0 \\ -\frac{12EI}{L^3} \\ \frac{6EI}{L^2} \end{bmatrix}$$

exemplifying how the second column of $\tilde{\mathbf{k}}$ is obtained.

Stiffness matrix of bar in the global system

The stiffness matrix of an arbitrarily inclined bar is now obtained in the global system as for a truss element in Chapter 2. Using the nodal displacement/rotation and force/moment conventions in Figure 4.38, we obtain

$$u_3 = \tilde{u}_3, u_6 = \tilde{u}_6, f_3 = \tilde{f}_3, f_6 = \tilde{f}_6.$$

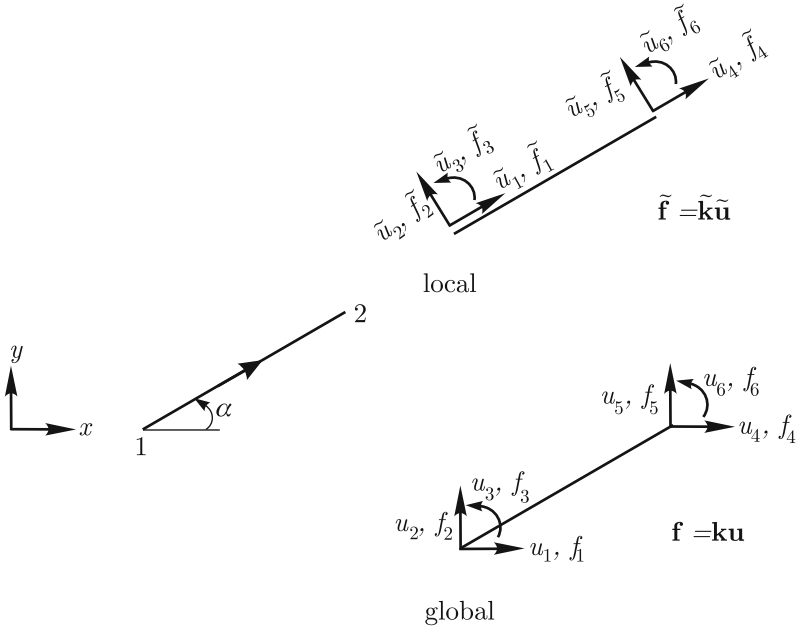


Fig. 4.38. Local and global degrees of freedom of an arbitrarily oriented bar element

We have

$$\mathbf{f} = \mathbf{k}\mathbf{u}$$

with

$$\mathbf{k} = \mathbf{T}^T \tilde{\mathbf{k}} \mathbf{T}$$

$$\mathbf{f} = \begin{bmatrix} f_1 \\ f_2 \\ f_3 \\ f_4 \\ f_5 \\ f_6 \end{bmatrix}, \quad \mathbf{u} = \begin{bmatrix} u_1 \\ u_2 \\ u_3 \\ u_4 \\ u_5 \\ u_6 \end{bmatrix}$$

and

$$\tilde{\mathbf{u}} = \mathbf{T} \mathbf{u}, \quad \tilde{\mathbf{f}} = \mathbf{T} \mathbf{f}$$

where

$$\mathbf{T} = \begin{bmatrix} \cos \alpha & \sin \alpha & 0 & 0 & 0 & 0 \\ -\sin \alpha & \cos \alpha & 0 & 0 & 0 & 0 \\ 0 & 0 & 1 & 0 & 0 & 0 \\ 0 & 0 & 0 & \cos \alpha & \sin \alpha & 0 \\ 0 & 0 & 0 & -\sin \alpha & \cos \alpha & 0 \\ 0 & 0 & 0 & 0 & 0 & 1 \end{bmatrix}. \quad (4.177)$$

Formulation of the matrix method for frames and a demonstrative example

From this point onwards, the formulation of the matrix method is as in the analysis of truss structures. In other words, we can define $\mathbf{F}^{(m)}$, $\mathbf{U}^{(m)}$ and $\mathbf{K}^{(m)}$ in an analogous manner considering that for the frame bar we have six degrees of freedom per element. Then equilibrium at all degrees of freedom is enforced by

$$\mathbf{R} = \sum_{m=1}^{n_e} \mathbf{F}^{(m)}$$

where n_e = number of elements in the structure. Element equilibrium, compatibility, the stress strain behavior, and the nodal compatibility are enforced by using

$$\mathbf{F}^{(m)} = \mathbf{K}^{(m)} \mathbf{U}.$$

Hence, we arrive at

$$\mathbf{K} \mathbf{U} = \mathbf{R}$$

with

$$\mathbf{K} = \sum_{m=1}^{n_e} \mathbf{K}^{(m)}.$$

The assemblage process is implemented using the $\mathbf{LM}^{(m)}$ array which, for this case, has six entries instead of four. In the next example we explore the definitions above.

Example 4.13

Consider the bar structure defined in Figure 4.39. Find the nodal displacements, the reactions and draw the internal force diagrams for the structure.

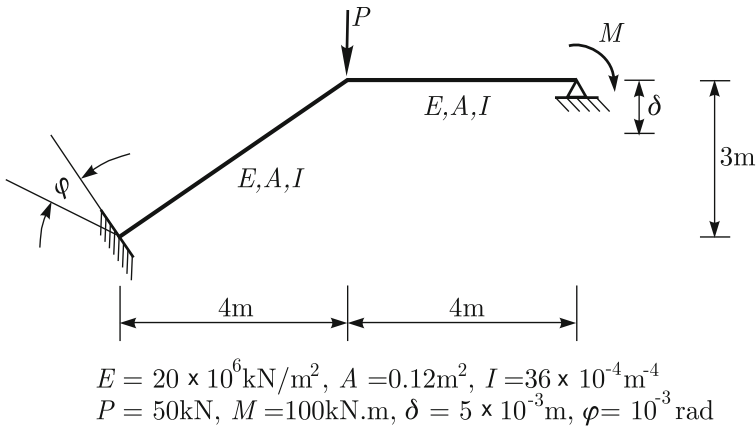


Fig. 4.39. Problem description. $E \equiv$ Young's modulus, $A \equiv$ cross-sectional area and $I \equiv$ moment of inertia. The δ is a vertical settlement and φ is an imposed support rotation

Solution

The matrix method will be used and, since the objective of this example is to illustrate this method, the solution is presented in detail.

Step 1 – Number nodes and bars. Also number degrees of freedom, numbering first the free ones. Establish bar orientations.

The result of this step is summarized in Figure 4.40.

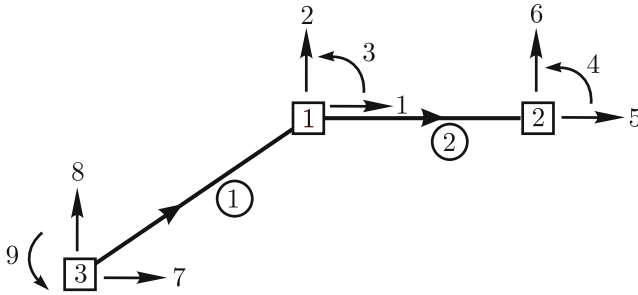


Fig. 4.40. Numbering definitions for the structure and bar orientations

Step 2 – Evaluate $\tilde{\mathbf{k}}$ and \mathbf{T} for every bar.

Note that the $\tilde{\mathbf{k}}$ matrix has always the form given in (4.176). The only changes from bar to bar are due to different geometric and material properties of the bars, *i.e.*, E , A and L .

The matrix \mathbf{T} is defined by (4.177) and for each bar the angle α has to be introduced. The bar orientation is used to arrive at the correct α where the first bar node defines the origin of the \tilde{x} axis. We obtain

$$\tilde{\mathbf{k}}^{(1)} = \begin{bmatrix} 480000 & 0 & 0 & -480000 & 0 & 0 \\ 0 & 6912 & 17280 & 0 & -6912 & 17280 \\ 0 & 17280 & 57600 & 0 & -17280 & 28800 \\ -480000 & 0 & 0 & 480000 & 0 & 0 \\ 0 & -6912 & -17280 & 0 & 6912 & -17280 \\ 0 & 17280 & 28800 & 0 & -17280 & 57600 \end{bmatrix}$$

and

$$\mathbf{T}^{(1)} = \begin{bmatrix} 0.8 & 0.6 & 0 & 0 & 0 & 0 \\ -0.6 & 0.8 & 0 & 0 & 0 & 0 \\ 0 & 0 & 1 & 0 & 0 & 0 \\ 0 & 0 & 0 & 0.8 & 0.6 & 0 \\ 0 & 0 & 0 & -0.6 & 0.8 & 0 \\ 0 & 0 & 0 & 0 & 0 & 1 \end{bmatrix}$$

where we have used $\alpha_1 = \arctg(3/4)$. For bar 2

$$\tilde{\mathbf{k}}^{(2)} = \begin{bmatrix} 600000 & 0 & 0 & -600000 & 0 & 0 \\ 0 & 13500 & 27000 & 0 & -13500 & 27000 \\ 0 & 27000 & 72000 & 0 & -27000 & 36000 \\ -600000 & 0 & 0 & 600000 & 0 & 0 \\ 0 & -13500 & -27000 & 0 & 13500 & -27000 \\ 0 & 27000 & 36000 & 0 & -27000 & 72000 \end{bmatrix}$$

and

$$\mathbf{T}^{(2)} = \begin{bmatrix} 1 & 0 & 0 & 0 & 0 & 0 \\ 0 & 1 & 0 & 0 & 0 & 0 \\ 0 & 0 & 1 & 0 & 0 & 0 \\ 0 & 0 & 0 & 1 & 0 & 0 \\ 0 & 0 & 0 & 0 & 1 & 0 \\ 0 & 0 & 0 & 0 & 0 & 1 \end{bmatrix}$$

where we have used $\alpha_1 = 0$. $\mathbf{T}^{(2)}$ is the identity matrix, since the global and local axes are coincident for this bar.

Step 3 – Evaluate \mathbf{k} for each bar using $\mathbf{k} = \mathbf{T}^T \tilde{\mathbf{k}} \mathbf{T}$.

We obtain

$$\mathbf{k}^{(1)} = \begin{bmatrix} 309688 & 227082 & -10368 & -309688 & -227082 & -10368 \\ 227082 & 177224 & 13824 & -227082 & -177224 & 13824 \\ -10368 & 13824 & 57600 & 10368 & -13824 & 28800 \\ -309688 & -227082 & 10368 & 309688 & 227082 & 10368 \\ -227082 & -177224 & -13824 & 227082 & 177224 & -13824 \\ -10368 & 13824 & 28800 & 10368 & -13824 & 57600 \end{bmatrix}$$

$$\mathbf{k}^{(2)} = \begin{bmatrix} 600000 & 0 & 0 & -600000 & 0 & 0 \\ 0 & 13500 & 27000 & 0 & -13500 & 27000 \\ 0 & 27000 & 72000 & 0 & -27000 & 36000 \\ -600000 & 0 & 0 & 600000 & 0 & 0 \\ 0 & -13500 & -27000 & 0 & 13500 & -27000 \\ 0 & 27000 & 36000 & 0 & -27000 & 72000 \end{bmatrix}$$

Step 4 – Construct the **LM** array for each bar.

Referring to Figure 4.40

$$\mathbf{LM}^{(1)} = \begin{bmatrix} 7 & 8 & 9 & 1 & 2 & 3 \end{bmatrix}$$

$$\mathbf{LM}^{(2)} = \begin{bmatrix} 1 & 2 & 3 & 5 & 6 & 4 \end{bmatrix}$$

Step 5 – Assemble the structure stiffness matrix **K**, given below.

From the element stiffness matrices, $\mathbf{k}^{(m)}$, we obtain **K** using the $\mathbf{LM}^{(m)}$ arrays as discussed in Chapter 2. We construct explicitly only the upper part of the matrix and take advantage of symmetry to obtain the lower part.

We note that since there is no direct physical connection between nodes 2 and 3, *i.e.*, no bar linking nodes 2 and 3, the stiffness terms coupling the degrees of freedom of node 2 (4, 5, 6) and node 3 (7, 8, 9) should be zero, as obtained. The solid lines shown in the matrix below identify the partitions associated with the free and restrained degrees of freedom. Since we have first numbered all free degrees of freedom, there is no need to exchange rows to arrive at \mathbf{K}_{aa} , \mathbf{K}_{ab} , \mathbf{K}_{ba} and \mathbf{K}_{bb} .

Step 6 – Construct the load column matrix for the free degrees of freedom \mathbf{R}_a .

Considering the load given, we obtain

$$\mathbf{R}_a = \begin{bmatrix} R_1 \\ R_2 \\ R_3 \\ R_4 \end{bmatrix} = \begin{bmatrix} 0 \\ -50 \\ 0 \\ -100 \end{bmatrix}$$

Step 7 – Construct the displacement column matrix for the restrained degrees of freedom \mathbf{U}_b .

$$\mathbf{U}_b = \begin{bmatrix} U_5 \\ U_6 \\ U_7 \\ U_8 \\ U_9 \end{bmatrix} = \begin{bmatrix} 0 \\ -0.005 \\ 0 \\ 0 \\ 0.001 \end{bmatrix}$$

$$\mathbf{K} = \begin{bmatrix} 909688 & 227082 & 10368 & 0 & -600000 & 0 & -309688 & -227082 & 10368 \\ 227082 & 190724 & 13176 & 27000 & 0 & -13500 & -227082 & -177224 & -13824 \\ 10368 & 13176 & 129600 & 36000 & 0 & -27000 & -10368 & 13824 & 28800 \\ 0 & 27000 & 36000 & 72000 & 0 & -27000 & 0 & 0 & 0 \\ -600000 & 0 & 0 & 0 & 600000 & 0 & 0 & 0 & 0 \\ 0 & -13500 & -27000 & -27000 & 0 & 13500 & 0 & 0 & 0 \\ -309688 & -227082 & -10368 & 0 & 0 & 0 & 309688 & 227082 & -10368 \\ -227082 & -177224 & 13824 & 0 & 0 & 0 & 227082 & 177224 & 13824 \\ 10368 & -13824 & 28800 & 0 & 0 & 0 & -10368 & 13824 & 57600 \end{bmatrix}$$

Step 8 – Construct and solve the linear system of algebraic equations given by

$$\mathbf{K}_{aa}\mathbf{U}_a = \mathbf{R}_a - \mathbf{K}_{ab}\mathbf{U}_b$$

$$\begin{bmatrix} 909688 & 227082 & 10368 & 0 \\ 227082 & 190724 & 13176 & 27000 \\ 10368 & 13176 & 129600 & 36000 \\ 0 & 27000 & 36000 & 72000 \end{bmatrix} \begin{bmatrix} U_1 \\ U_2 \\ U_3 \\ U_4 \end{bmatrix} = \begin{bmatrix} 0 \\ -50 \\ 0 \\ -100 \end{bmatrix} - \begin{bmatrix} -600000 & 0 & -309688 & -227082 & 10368 \\ 0 & -13500 & -227082 & -177224 & -13824 \\ 0 & -27000 & -10368 & 13824 & 28800 \\ 0 & -27000 & 0 & 0 & 0 \end{bmatrix} \begin{bmatrix} 0 \\ -0.005 \\ 0 \\ 0 \\ 0.001 \end{bmatrix}$$

$$\mathbf{U}_a = \begin{bmatrix} U_1 \\ U_2 \\ U_3 \\ U_4 \end{bmatrix} = \begin{bmatrix} 2.192 \times 10^{-5} \\ -1.144 \times 10^{-4} \\ -4.172 \times 10^{-4} \\ -3.012 \times 10^{-3} \end{bmatrix}$$

Step 9 – Evaluate the reactions given by \mathbf{R}_b using

$$\mathbf{R}_b = \mathbf{K}_{ba}\mathbf{U}_a + \mathbf{K}_{bb}\mathbf{U}_b$$

$$\begin{bmatrix} R_5 \\ R_6 \\ R_7 \\ R_8 \\ R_9 \end{bmatrix} = \begin{bmatrix} -600000 & 0 & 0 & 0 \\ 0 & -13500 & -27000 & -27000 \\ -309688 & -227082 & -10368 & 0 \\ -227082 & -177224 & 13824 & 0 \\ 10368 & -13824 & 28800 & 0 \end{bmatrix} \begin{bmatrix} U_1 \\ U_2 \\ U_3 \\ U_4 \end{bmatrix} + \begin{bmatrix} 600000 & 0 & 0 & 0 & 0 \\ 0 & 13500 & 0 & 0 & 0 \\ 0 & 0 & 309688 & 227082 & -10368 \\ 0 & 0 & 227082 & 177224 & 13824 \\ 0 & 0 & -10368 & 13824 & 57600 \end{bmatrix} \begin{bmatrix} 0 \\ -0.005 \\ 0 \\ 0 \\ 0.001 \end{bmatrix}$$

$$\mathbf{R}_b = \begin{bmatrix} -13.15 \\ 26.64 \\ 13.15 \\ 23.36 \\ 47.39 \end{bmatrix}$$

Step 10 – Evaluate the nodal forces in each bar.

From the nodal displacements of the structure, we extract, for each bar, the bar nodal displacements. This can be systematically accomplished using the **LM** arrays. In fact, for bar 1

$$u_1 = U_7, \quad u_2 = U_8, \quad u_3 = U_9$$

$$u_4 = U_1, \quad u_5 = U_2, \quad u_6 = U_3.$$

Therefore, with $\mathbf{u}^{(1)}$ determined, we can evaluate $\mathbf{f}^{(1)}$ using $\mathbf{f}^{(1)} = \mathbf{k}^{(1)}\mathbf{u}^{(1)}$ which yields

$$\mathbf{f}^{(1)T} = \begin{bmatrix} 13.15 & 23.36 & 47.39 & -13.15 & -23.36 & 6.58 \end{bmatrix}.$$

For bar 2, using $\mathbf{LM}^{(2)}$ we directly write

$$\mathbf{u}^{(2)T} = \begin{bmatrix} 2.192 \times 10^{-5} & -1.144 \times 10^{-4} & -4.172 \times 10^{-4} & 0 & -5 \times 10^{-3} & -3.012 \times 10^{-3} \end{bmatrix}$$

and considering $\mathbf{f}^{(2)} = \mathbf{k}^{(2)}\mathbf{u}^{(2)}$ we arrive at

$$\mathbf{f}^{(2)T} = \begin{bmatrix} 13.15 & -26.64 & -6.58 & -13.15 & 26.64 & -100 \end{bmatrix}.$$

Step 11 – Evaluate bar nodal forces in the bar's local system.

Although we could find the internal force diagrams from the bar nodal forces in the global system, they are more easily determined from the bar nodal forces in the local system.

We have

$$\tilde{\mathbf{f}}^{(1)} = \mathbf{T}^{(1)}\mathbf{f}^{(1)} = \begin{bmatrix} 24.54 \\ 10.79 \\ 47.39 \\ -24.54 \\ -10.79 \\ 6.58 \end{bmatrix}.$$

Analogously

$$\tilde{\mathbf{f}}^{(2)} = \mathbf{T}^{(2)}\mathbf{f}^{(2)} = \begin{bmatrix} 13.15 \\ -26.64 \\ -6.58 \\ -13.15 \\ 26.64 \\ -100 \end{bmatrix}.$$

Step 12 – Construct the internal force diagrams.

These diagrams can be constructed bar by bar using $\tilde{\mathbf{f}}^{(m)}$ and they are shown in Figure 4.41. Only as a verification, we can check that the equilibrium

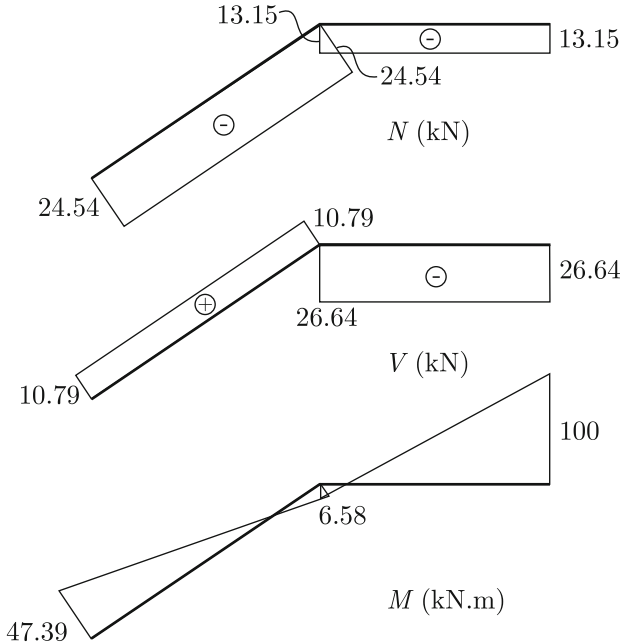


Fig. 4.41. Internal force diagrams

of node 1 holds. Figure 4.42 summarizes this situation.

Regarding the units, although we did not show these explicitly, all obtained displacements are in meters, rotations in radians, forces in kN and moments in $kN \cdot m$. These units are those used in the physical problem, see Figure 4.39, and were used throughout the solution.

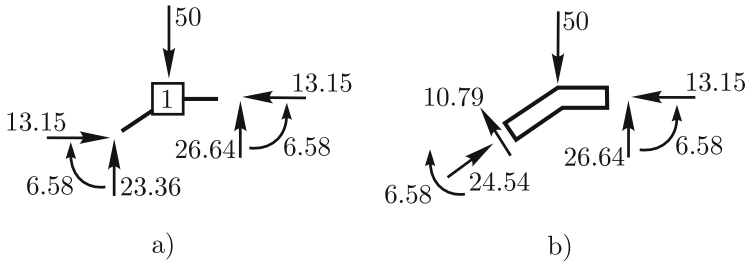


Fig. 4.42. Equilibrium of node 1. a) bar end forces in the global system acting onto node; b) Internal forces at “node” sections

□

External loads applied to the bars

So far, the matrix method was formulated considering external loads applied only to the nodes. However, in practice we frequently find structures in which loads are not applied to the nodes. Therefore, we need to extend our formulation to consider loads applied to the bars.

The central idea behind the procedure to be presented is to take advantage of the superposition of effects and construct a solution strategy based on the formulation of the matrix method which considers loads applied to the nodes only.

For that consider that the solution will be obtained by superimposing the solutions for two problems: (I) and (II). Problem (I) is defined considering the external loads which are applied directly onto the bars (*i.e.* not to the nodes) and restraining all degrees of freedom to have zero displacements/rotations. The external reactions which should be introduced to guarantee that all displacements/rotations are zero when we consider the loads applied directly onto the bars are given by \mathbf{R}_0 with $\mathbf{R}_{0,a}$ being the partition associated with the degrees of freedom that are free in the original structure and $\mathbf{R}_{0,b}$ with those that are restrained.

Since the loads given by \mathbf{R}_0 do not exist in the original structure, they are introduced in problem (II) with the reversed sense, *i.e.*, $-\mathbf{R}_0$. In problem (II), we consider in addition the external loads of the original structure which are applied directly to the nodes.

We note that problem (II) can be solved in the usual way since the external loads are applied to the nodes only. The nodal displacement/rotation solution for problem (II) is already the solution for the original structure since for structure (I) all degrees of freedom were fixed.

Now the solution strategy is apparent. The solution of problem (II) will lead to the displacements/rotations and reactions of the original problem. The matrix equation for problem (II) can be written as

$$\begin{bmatrix} \mathbf{K}_{aa} & \mathbf{K}_{ab} \\ \mathbf{K}_{ba} & \mathbf{K}_{bb} \end{bmatrix} \begin{bmatrix} \mathbf{U}_a \\ \mathbf{U}_b \end{bmatrix} = \begin{bmatrix} \mathbf{R}_a - \mathbf{R}_{0,a} \\ \mathbf{R}_b - \mathbf{R}_{0,b} \end{bmatrix}.$$

The first set of equations

$$\mathbf{K}_{aa}\mathbf{U}_a = \mathbf{R}_a - \mathbf{R}_{0,a} - \mathbf{K}_{ab}\mathbf{U}_b \tag{4.178}$$

can be solved for \mathbf{U}_a and the second set leads to the reactions, *i.e.*,

$$\mathbf{R}_b = \mathbf{R}_{0,b} + \mathbf{K}_{ba}\mathbf{U}_a + \mathbf{K}_{bb}\mathbf{U}_b. \tag{4.179}$$

We emphasize that

$$\mathbf{U}^T = \begin{bmatrix} \mathbf{U}_a & \mathbf{U}_b \end{bmatrix}$$

is the solution for the original problem. Note that, if there are imposed nodal displacements/rotations they should be introduced in problem (II) only and the above equations are already taking into account this possibility. We also assumed that no external concentrated forces and moments are applied at the restraint degrees of freedom. These concentrated forces/moments would have to be added (with appropriate senses) to the reactions calculated in (4.179).

Regarding the calculation of the bar nodal forces, we need to be particularly careful. We note that, although there are no nodal displacements for problem (I), in general, the bar nodal forces are not zero since the external loads applied to the bars should be equilibrated by these bar nodal forces. Let us denote by $\tilde{\mathbf{f}}_0^{(m)}$ the bar (m) nodal forces in the local system for problem (I). Therefore, the bar nodal forces for bar (m) for the original problem are given by

$$\tilde{\mathbf{f}}^{(m)} = \tilde{\mathbf{f}}_0^{(m)} + \tilde{\mathbf{k}}^{(m)}\tilde{\mathbf{u}}^{(m)}.$$

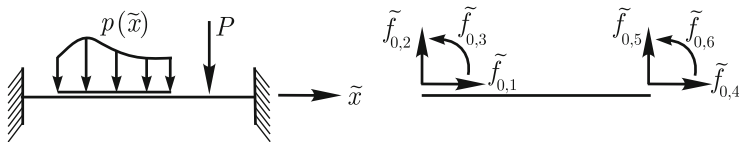


Fig. 4.43. Generic situation to evaluate $\tilde{\mathbf{f}}_0$

Let us show how to obtain \mathbf{R}_0 from the bar nodal forces $\tilde{\mathbf{f}}_0^{(m)}$ of the structure. We first note that $\tilde{\mathbf{f}}_0^{(m)}$ can be obtained by considering bar (m) clamped at both ends subjected to the external load applied to bar (m). A generic situation is shown in Figure 4.43. In the bar global system these forces are given by

$$\mathbf{f}_0^{(m)} = \mathbf{T}^{(m)T} \tilde{\mathbf{f}}_0^{(m)}. \quad (4.180)$$

Now we define $\mathbf{F}_0^{(m)}$ as the $N \times 1$ column matrix, N being the total number of degrees of freedom of the structure, which is obtained from $\mathbf{f}_0^{(m)}$ in the same way as $\mathbf{F}^{(m)}$ is obtained from $\mathbf{f}^{(m)}$, *i.e.*, using the correspondence between the local and global numbering. Then we can enforce equilibrium of every node of problem (I) by

$$\mathbf{R}_0 = \sum_{m=1}^{n_e} \mathbf{F}_0^{(m)} \quad (4.181)$$

which shows how to obtain \mathbf{R}_0 from $\mathbf{F}_0^{(m)}$. Of course, since $\mathbf{F}_0^{(m)}$ has many zero entries, the summation given in (4.181) is efficiently performed directly from the nodal force column matrices $\tilde{\mathbf{f}}_0^{(m)}$ using the $\mathbf{LM}^{(m)}$ arrays.

Typical examples of $\tilde{\mathbf{f}}_0^{(m)}$ are given in Figure 4.44 and Figure 4.45 for which

$$\tilde{\mathbf{f}}_0^{(i)T} = \left[0 \quad \frac{P}{2} \quad \frac{Pa}{8} \quad 0 \quad \frac{P}{2} \quad -\frac{Pa}{8} \right]$$

and

$$\tilde{\mathbf{f}}_0^{(j)T} = \left[0 \quad \frac{pa}{2} \quad \frac{pa^2}{12} \quad 0 \quad \frac{pa}{2} \quad -\frac{pa^2}{12} \right].$$

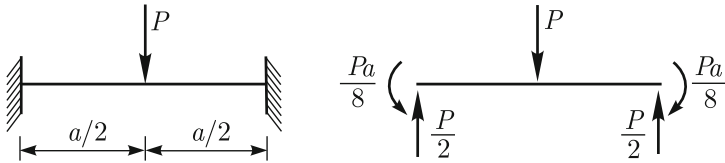


Fig. 4.44. Evaluation of $\tilde{\mathbf{f}}_0^{(i)}$

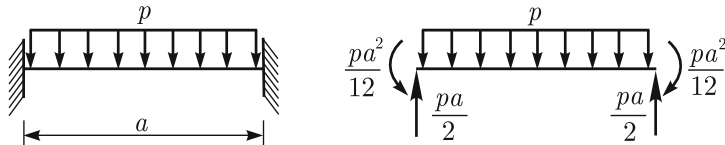


Fig. 4.45. Evaluation of $\tilde{\mathbf{f}}_0^{(j)}$

Example 4.14

Consider the structure defined in Figure 4.39 with the addition of the loads applied to the bars as summarized in Figure 4.46. Find the nodal displacements, the reactions and draw the internal force diagrams for the structure.

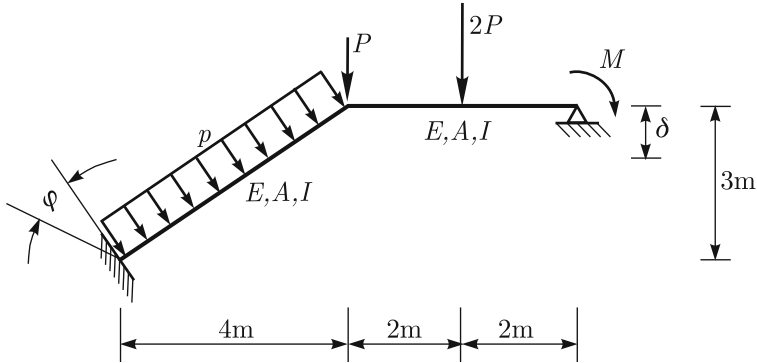


Fig. 4.46. Problem description with the added load. The data given in Figure 4.39 remains unchanged and $p = 60 \text{ kN/m}$

Solution

We need to evaluate \mathbf{R}_0 and use the superposition detailed in this section. We keep the same definitions of Example 4.13.

Using the solutions summarized in Figures 4.44 and 4.45, we can write

$$\tilde{\mathbf{f}}_0^{(1)T} = \begin{bmatrix} 0 & 150 & 125 & 0 & 150 & -125 \end{bmatrix}$$

$$\tilde{\mathbf{f}}_0^{(2)T} = \begin{bmatrix} 0 & 50 & 50 & 0 & 50 & -50 \end{bmatrix}$$

and using (4.180)

$$\mathbf{f}_0^{(1)T} = \begin{bmatrix} -90 & 120 & 125 & -90 & 120 & -125 \end{bmatrix}$$

$$\mathbf{f}_0^{(2)T} = \begin{bmatrix} 0 & 50 & 50 & 0 & 50 & -50 \end{bmatrix}.$$

Taking advantage of the **LM** arrays already defined in Example 4.13, we write

$$\mathbf{R}_{0,a}^T = \begin{bmatrix} -90 & 170 & -75 & -50 \end{bmatrix}$$

$$\mathbf{R}_{0,b}^T = \begin{bmatrix} 0 & 50 & -90 & 120 & 125 \end{bmatrix}.$$

Now \mathbf{U}_a can be evaluated using (4.178) which is written as

$$\begin{bmatrix} 909688 & 227082 & 10368 & 0 \\ 227082 & 190724 & 13176 & 27000 \\ 10368 & 13176 & 129600 & 36000 \\ 0 & 27000 & 36000 & 72000 \end{bmatrix} \begin{bmatrix} U_1 \\ U_2 \\ U_3 \\ U_4 \end{bmatrix} = \begin{bmatrix} 0 \\ -50 \\ 0 \\ -100 \end{bmatrix} - \begin{bmatrix} -90 \\ 170 \\ -75 \\ -50 \end{bmatrix} -$$

$$\begin{bmatrix} -600000 & 0 & -309688 & -227082 & 10368 \\ 0 & -13500 & -227082 & -177224 & -13824 \\ 0 & -27000 & -10368 & 13824 & 28800 \\ 0 & -27000 & 0 & 0 & 0 \end{bmatrix} \begin{bmatrix} 0 \\ -0.005 \\ 0 \\ 0 \\ 0.001 \end{bmatrix}.$$

(4.182)

Of course, the stiffness matrices are the same as for Example 4.13. Solving (4.182), we obtain

$$\mathbf{U}_a^T = \begin{bmatrix} 5.396 \times 10^{-4} & -1.810 \times 10^{-3} & -2.222 \times 10^{-5} & -1.880 \times 10^{-3} \end{bmatrix}.$$

The reactions \mathbf{R}_b can be obtained using (4.179)

$$\mathbf{R}_b = \begin{bmatrix} 0 \\ 50 \\ -90 \\ 120 \\ 125 \end{bmatrix} + \begin{bmatrix} -600000 & 0 & 0 & 0 \\ 0 & -13500 & -27000 & -27000 \\ -309688 & -227082 & -10368 & 0 \\ -227082 & -177224 & 13824 & 0 \\ 10368 & -13824 & 28800 & 0 \end{bmatrix} \begin{bmatrix} U_1 \\ U_2 \\ U_3 \\ U_4 \end{bmatrix} + \begin{bmatrix} 600000 & 0 & 0 & 0 & 0 \\ 0 & 13500 & 0 & 0 & 0 \\ 0 & 0 & 309688 & 227082 & -10368 \\ 0 & 0 & 227082 & 177224 & 13824 \\ 0 & 0 & -10368 & 13824 & 57600 \end{bmatrix} \begin{bmatrix} 0 \\ -0.005 \\ 0 \\ 0 \\ 0.001 \end{bmatrix}$$

leading to

$$\mathbf{R}_b^T = \begin{bmatrix} -323.72 & 58.28 & 143.72 & 331.72 & 212.57 \end{bmatrix}.$$

From \mathbf{U} we obtain the bar nodal displacements $\mathbf{u}^{(1)}$ and $\mathbf{u}^{(2)}$, and in the local system they are given by

$$\tilde{\mathbf{u}}^{(1)} = \mathbf{T}^{(1)} \mathbf{u}^{(1)} = \mathbf{T}^{(1)} \begin{bmatrix} 0 \\ 0 \\ 0.001 \\ 5.396 \times 10^{-4} \\ -1.810 \times 10^{-3} \\ -2.222 \times 10^{-5} \end{bmatrix} = \begin{bmatrix} 0 \\ 0 \\ 0.001 \\ -6.542 \times 10^{-4} \\ -1.771 \times 10^{-3} \\ -2.222 \times 10^{-5} \end{bmatrix}$$

and

$$\tilde{\mathbf{u}}^{(2)} = \mathbf{u}^{(2)} = \begin{bmatrix} 5.396 \times 10^{-4} \\ -1.810 \times 10^{-3} \\ -2.222 \times 10^{-5} \\ 0 \\ -0.005 \\ -1.880 \times 10^{-3} \end{bmatrix}$$

since $\mathbf{T}^{(2)} = \mathbf{I}$.

The bar nodal forces in the local system can be evaluated by

$$\tilde{\mathbf{f}}^{(1)} = \tilde{\mathbf{f}}_0^{(1)} + \tilde{\mathbf{k}}^{(1)}\tilde{\mathbf{u}}^{(1)} = \begin{bmatrix} 314 \\ 179.14 \\ 212.57 \\ -314 \\ 120.86 \\ -66.87 \end{bmatrix}$$

$$\tilde{\mathbf{f}}^{(2)} = \tilde{\mathbf{f}}_0^{(2)} + \tilde{\mathbf{k}}^{(2)}\tilde{\mathbf{u}}^{(2)} = \begin{bmatrix} 323.72 \\ 41.72 \\ 66.87 \\ -323.72 \\ 58.28 \\ -100 \end{bmatrix}.$$

The internal force diagrams are shown in Figure 4.47.

□

Additional bar end conditions

In the frame structures considered so far, continuity of rotations was implied for the bar sections and, in particular, at the nodes. Referring to Figures 4.39 and 4.40, as an example, we can see that the rotation of node 1 (taken as a typical node) is the same as the end section rotation of bar 1 and that of the initial section of bar 2. This continuity is taken into account in the matrix formulation through the compatibility condition

$$U_3 = u_6^{(1)} = u_3^{(2)}.$$

The stiffness matrix given in (4.176) has been derived to model such situations since it provides stiffness with respect to the bar end section rotations which, by compatibility, correspond to the nodal rotations.

In engineering structural analysis we frequently also have an internal rotational hinge (pin type connection) as in Figure 4.48. In this case the bar element sections connected to the hinge no longer have to undergo the same rotation (while the section displacements have to be the same). Hence, the

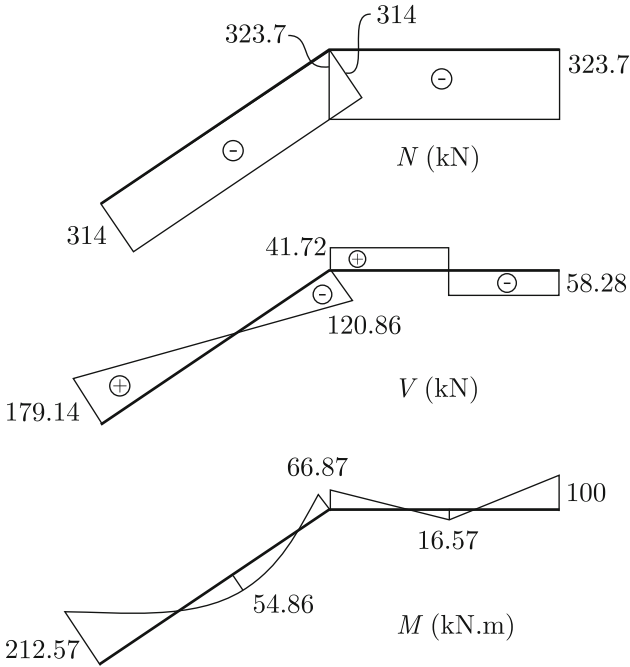


Fig. 4.47. Internal force diagrams

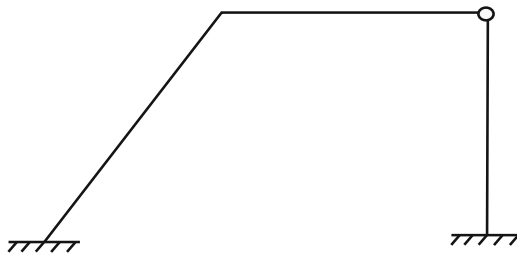


Fig. 4.48. Frame structure with a pin connection

compatibility condition for the rotation no longer exists and there is no moment transferred between the sections connected to the hinge.

There is no unique way to model the rotational hinge. For example, in Figure 4.49a we choose a node to represent each section connected to the hinge and enforce that the section translations are the same, that is, $U_4 = U_7$ and $U_5 = U_8$. This could be efficiently accomplished by choosing as degrees of freedom the translations of the hinge plus the rotations of the sections connected to the hinge, as shown in Figure 4.49b.

An efficient modeling alternative that keeps the number of degrees of freedom per node at three is shown in Figure 4.50. In Figure 4.50a, node 2

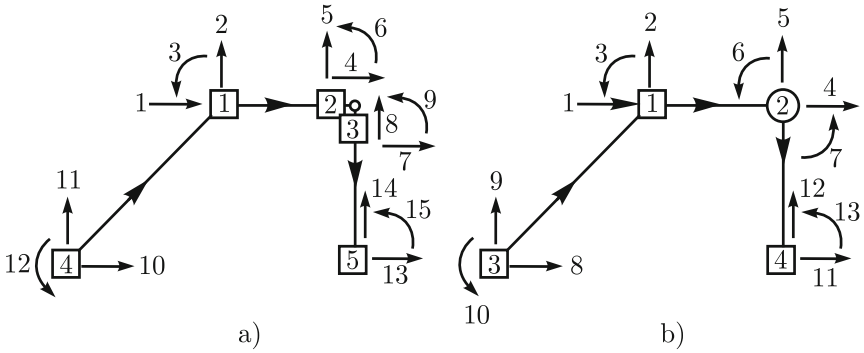


Fig. 4.49. Modeling the rotational hinge

is considered attached to bar 2, *i.e.*, the rotation of node 2 is the same as the rotation of the end section of bar 2. Therefore, the degree of freedom 6 corresponds to the rotation of the end section of bar 2. The translations of node 2, *i.e.*, degrees of freedom 4 and 5, still correspond to the translations of the sections of bars 2 and 3 which connect at node 2. The stiffness matrix of bar 3 has to be modified, as detailed shortly, and the rotation of the section of bar 3 at node 2 will no longer be a direct outcome of the solution of the matrix equations.

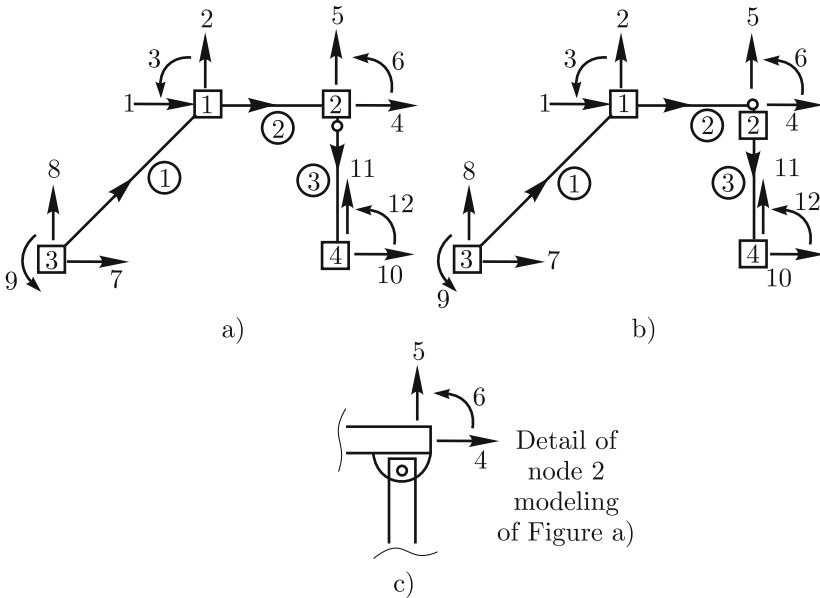


Fig. 4.50. Two modeling choices for the rotational hinge

In Figure 4.50b, node 2 is chosen to be attached to bar 3, and the degree of freedom 6 is now equal to the section rotation of bar 3 and the stiffness matrix of bar 2 should be modified.

Consider the bar described in Figure 4.51. The rotation of node 2 of the

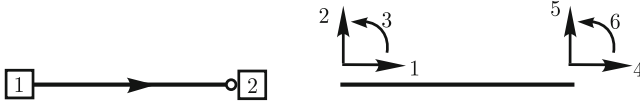


Fig. 4.51. Bar with built-in condition at local node one and pin condition at local node 2

bar is free; that is, there is no bending moment at the end section of the bar. We can construct this stiffness matrix column by column imposing unit end displacements/rotations. Columns 1 and 4 are obtained as for the stiffness matrix given in (4.176).

We detail the derivation of the fifth column which is obtained by imposing $u_5 = 1, u_1 = u_2 = u_3 = u_4 = 0$. We should take into account that $M(L) = 0$. The axial displacements are trivially zero as given by equation (4.170), *i.e.*,

$$u(\tilde{x}) = 0 \quad \rightarrow \quad N(\tilde{x}) = 0.$$

For the transverse displacements, we refer to the solution derived in Example 4.9 which gives the solution sought when we take $\delta = -1$ leading to

$$w(\tilde{x}) = h_5(\tilde{x}) + \frac{3}{2L} h_6(\tilde{x}) = -\frac{\tilde{x}^3}{2L^3} + \frac{3\tilde{x}^2}{2L^2}.$$

Therefore

$$M(\tilde{x}) = EIw''(\tilde{x}) = \frac{EI}{L^3} (3L - 3\tilde{x})$$

$$M(0) = \frac{3EI}{L^2}, \quad M(L) = 0$$

$$V(\tilde{x}) = EIw'''(\tilde{x}) = -\frac{3EI}{L^3}.$$

The results are summarized in Figure 4.52. In analogous manner the remaining columns are obtained and we summarize the results in Figure 4.53. Therefore, the stiffness matrix is given by

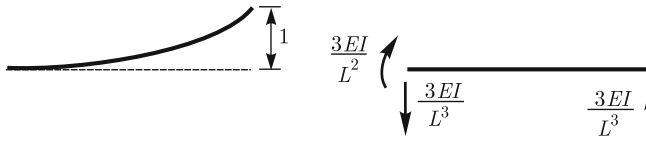


Fig. 4.52. Solution that leads to the fifth column of \mathbf{k}

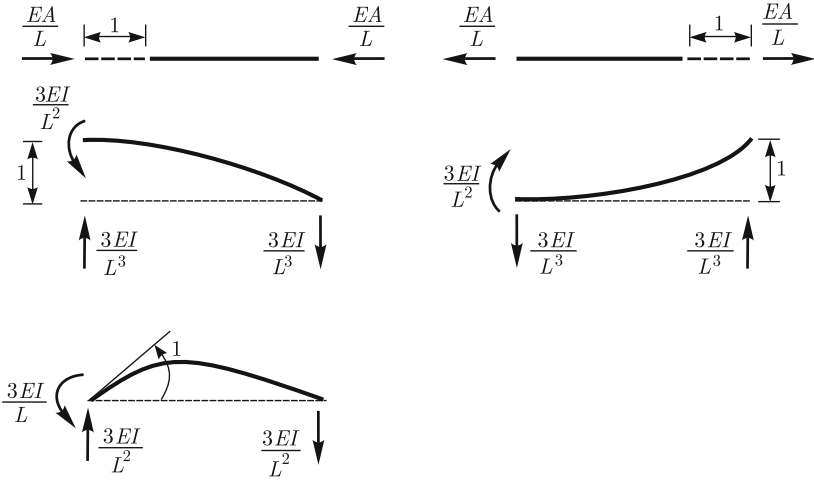


Fig. 4.53. Bar end forces for unit end displacements

$$\tilde{\mathbf{k}} = \begin{bmatrix} \frac{EA}{L} & 0 & 0 & -\frac{EA}{L} & 0 & 0 \\ 0 & \frac{3EI}{L^3} & \frac{3EI}{L^2} & 0 & -\frac{3EI}{L^3} & 0 \\ 0 & \frac{3EI}{L^2} & \frac{3EI}{L} & 0 & -\frac{3EI}{L^2} & 0 \\ -\frac{EA}{L} & 0 & 0 & \frac{EA}{L} & 0 & 0 \\ 0 & -\frac{3EI}{L^3} & -\frac{3EI}{L^2} & 0 & \frac{3EI}{L^3} & 0 \\ 0 & 0 & 0 & 0 & 0 & 0 \end{bmatrix}. \quad (4.183)$$

Note that the degree of freedom 6 no longer exists for the beam element; hence column six has all zero entries. Of course, there is an explicit understanding that when such a bar is used in an assemblage, the rotational stiffness of node 2 must come from other bars.

When the local node 1 is pinned as shown in Figure 4.54 the stiffness matrix can be obtained analogously and is given by

$$\tilde{\mathbf{k}} = \begin{bmatrix} \frac{EA}{L} & 0 & 0 & -\frac{EA}{L} & 0 & 0 \\ 0 & \frac{3EI}{L^3} & 0 & 0 & -\frac{3EI}{L^3} & \frac{3EI}{L^2} \\ 0 & 0 & 0 & 0 & 0 & 0 \\ -\frac{EA}{L} & 0 & 0 & \frac{EA}{L} & 0 & 0 \\ 0 & -\frac{3EI}{L^3} & 0 & 0 & \frac{3EI}{L^3} & -\frac{3EI}{L^2} \\ 0 & \frac{3EI}{L^2} & 0 & 0 & -\frac{3EI}{L^2} & \frac{3EI}{L} \end{bmatrix}. \quad (4.184)$$

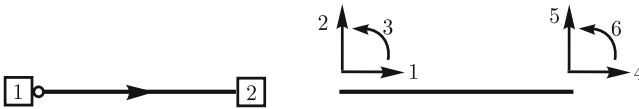


Fig. 4.54. Bar with pin condition at local node 1 and built-in condition at local node 2

Example 4.15

Consider again the structure defined in Figure 4.39, with the additional loads introduced in Example 4.14, but now with a pin connection as shown in Figure 4.55. Obtain the displacements of the free degrees of freedom.

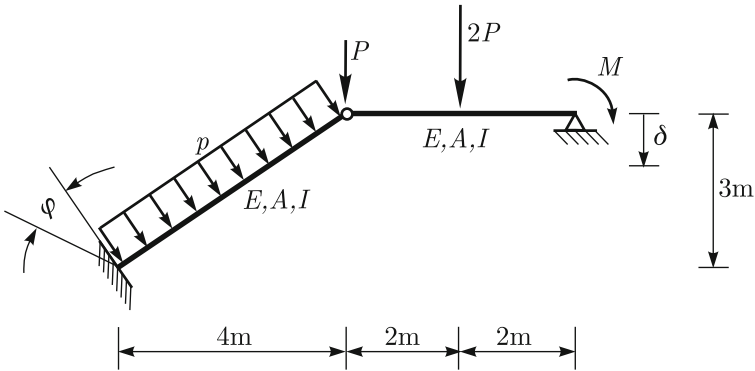


Fig. 4.55. Problem description having a pin connection.

Considering the numbering choices given in Figure 4.40 evaluate the nodal displacements. The rotation of the section of the inclined bar adjacent to the pin is to be predicted.

Solution

The modeling choices are shown in Figure 4.56. Note that the rotation of

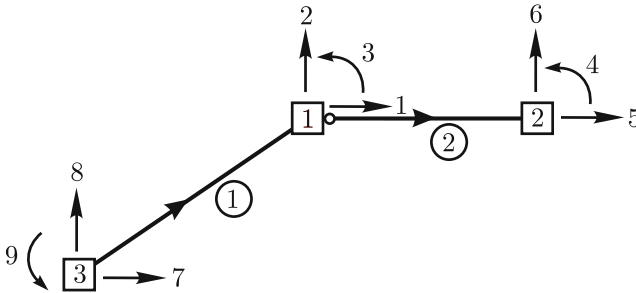


Fig. 4.56. Model definitions

node 1 given by U_3 is the rotation of the section of the inclined bar adjacent to the pin.

There are two modifications that should be introduced. The end conditions of bar 2 should be pinned – built-in (see Figure 4.54) and can be obtained using (4.184)

$$\tilde{\mathbf{k}}^{(2)} = \begin{bmatrix} 600000 & 0 & 0 & -600000 & 0 & 0 \\ 0 & 3375 & 0 & 0 & -3375 & 13500 \\ 0 & 0 & 0 & 0 & 0 & 0 \\ -600000 & 0 & 0 & 600000 & 0 & 0 \\ 0 & -3375 & 0 & 0 & 3375 & -13500 \\ 0 & 13500 & 0 & 0 & -13500 & 54000 \end{bmatrix}.$$

The other modification refers to the evaluation of $\tilde{\mathbf{f}}_0^{(2)}$. Since, in the superposition, the pin has to be taken into account. The condition that leads to $\tilde{\mathbf{f}}_0^{(2)}$ is shown in Figure 4.57 and therefore

$$\tilde{\mathbf{f}}_0^{(2)T} = \left[0 \quad \frac{10P}{16} \quad 0 \quad 0 \quad \frac{22P}{16} \quad -\frac{6Pa}{16} \right].$$

Introducing the modifications above and following the same solution steps which have been used, we obtain

$$\mathbf{U}_a^T = \left[4.481 \times 10^{-4} \quad -1.501 \times 10^{-3} \quad 1.229 \times 10^{-3} \quad -1.338 \times 10^{-3} \right].$$

□

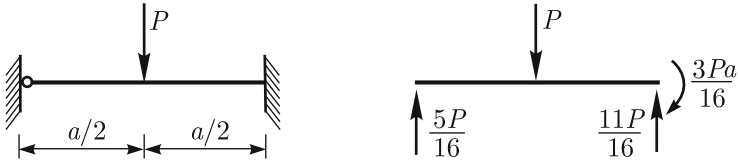


Fig. 4.57. Solution required for evaluation of $\tilde{\mathbf{f}}_0^{(2)}$

4.2.5 Bars subjected to 3-D actions

In this section we study the behavior of a straight prismatic bar subjected to arbitrary transverse and axial loads. The objective is to derive the stiffness matrix of the bar for these conditions.

Bending and axial actions

In Section 4.2.2 we introduced the Bernoulli-Euler beam model for planar conditions, *i.e.*, we assumed that the bar has a vertical plane of symmetry, that the transversely distributed load was acting in the plane of symmetry and that the bar axis remains in the plane of symmetry.

Now consider the situation summarized in Figure 4.58. The x axis is taken along the section centroid⁵ and since there are no section symmetries, the y and z axes are arbitrarily chosen. The transverse load is decomposed into p_y and p_z acting along directions y and z respectively. The axial loading is denoted by f_x . The stress resultants are shown in Figure 4.58 for a generic section with outward normal given by \mathbf{e}_x . Actually, there are many ways in which these stress resultants may be defined. In order to obtain analogous differential equilibrium equations to those of the planar beam problem, we choose the conventions of Figure 4.58.

The differential equilibrium equations are

$$\frac{dN}{dx} + f_x = 0 \tag{4.185}$$

$$\frac{dV_y}{dx} = p_y, \quad \frac{dV_z}{dx} = p_z \tag{4.186}$$

$$\frac{dM_y}{dx} = V_z, \quad \frac{dM_z}{dx} = -V_y. \tag{4.187}$$

The strain compatibility relations can be obtained considering the rotations of fibers on the cross-section which are aligned with the y and z axes as shown in Figure 4.59.

Note that

⁵ We assume that either the shear center coincides with the centroid or it is close enough to the centroid that the induced warping displacements can be neglected (see Section 4.2.6 for the definition of the shear center)

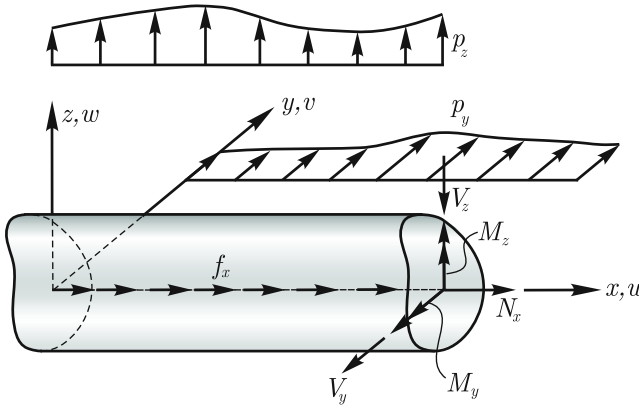


Fig. 4.58. Loading and stress resultant definitions

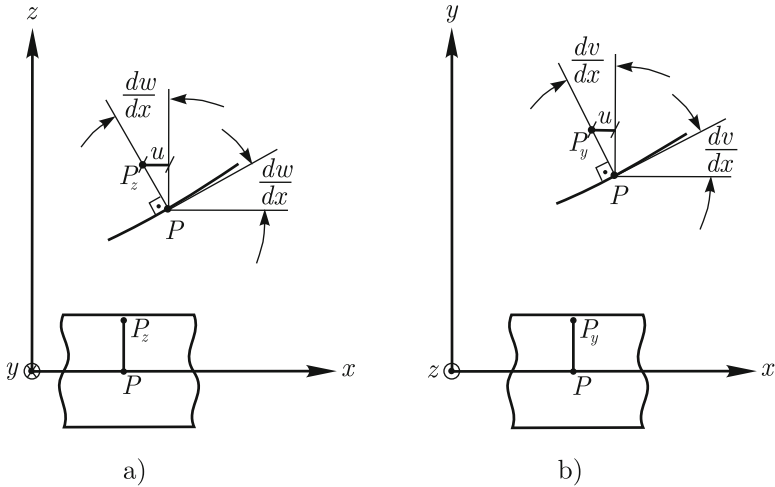


Fig. 4.59. Rotation of fibers aligned with axes y and z

$$v(x, y, z) = v(x) \tag{4.188}$$

$$w(x, y, z) = w(x). \tag{4.189}$$

The kinematics summarized in Figure 4.59 leads to

$$u(x, y, z) = u_0(x) - y \frac{dv}{dx} - z \frac{dw}{dx} \tag{4.190}$$

where $u_0(x)$ is the displacement in the x direction of points on the bar axis. Note that for a given cross-section u_0 , $\frac{dv}{dx}$ and $\frac{dw}{dx}$ are constant values and equations (4.188), (4.189) and (4.190) show, as assumed, that the cross-section remains plane. Orthogonality to the deformed axis, corresponding to the Bernoulli-Euler hypothesis, can be directly inferred from Figure 4.59.

The longitudinal strain is given by

$$\varepsilon_{xx} = \frac{\partial u}{\partial x} = \frac{du_0}{dx} - y \frac{d^2v}{dx^2} - z \frac{d^2w}{dx^2}$$

and Hooke's law leads to

$$\tau_{xx} = E \left(\frac{du_0}{dx} - y \frac{d^2v}{dx^2} - z \frac{d^2w}{dx^2} \right).$$

The stress resultants can be evaluated by integration of the stresses over the cross-sections. The axial force is given by

$$N(x) = \int_A \tau_{xx} dA = EA \frac{du_0}{dx} \quad (4.191)$$

since the x axis passes through the centroid.

The moment M_y is given by

$$M_y = \int_A \tau_{xx} (-z) dA = -E \frac{du_0}{dx} \int_A z dA + E \frac{d^2v}{dx^2} \int_A yz dA + E \frac{d^2w}{dx^2} \int_A z^2 dA. \quad (4.192)$$

We can define

$$I_y = \int_A z^2 dA, \quad I_{yz} = \int_A yz dA \quad (4.193)$$

where I_y is the moment of inertia of the section with respect to y and I_{yz} is the product of inertia of the section with respect to y and z .

Introducing (4.193) into (4.192) we obtain

$$M_y = EI_y \frac{d^2w}{dx^2} + EI_{yz} \frac{d^2v}{dx^2}. \quad (4.194)$$

The moment M_z is given by

$$M_z = \int_A \tau_{xx} (-y) dA = E \frac{du_0}{dx} \int_A y dA + E \frac{d^2v}{dx^2} \int_A y^2 dA + E \frac{d^2w}{dx^2} \int_A yz dA$$

which upon the definition of the moment of inertia with respect to z as

$$I_z = \int_A y^2 dA$$

leads to

$$M_z = EI_z \frac{d^2v}{dx^2} + EI_{yz} \frac{d^2w}{dx^2}. \quad (4.195)$$

We note that the equilibrium equations (4.185) to (4.187) and equations (4.191), (4.194) and (4.195) which represent the compatibility and constitutive relations give all the required conditions for the model and can be used to find solutions when appropriate boundary conditions are specified.

Equations (4.194) and (4.195) can be placed in a simpler form if a particular set of axes is chosen. It is possible to show that we can always find a position for the y and z axes by rotating them about the centroid of the section such that the product of inertia vanishes, that is

$$I_{yz} = 0. \quad (4.196)$$

The axes y and z for which (4.196) holds are the *principal axes of inertia* of the cross-section. For these axes, equations (4.194) and (4.195) become

$$M_y = EI_y \frac{d^2 w}{dx^2}, \quad M_z = EI_z \frac{d^2 v}{dx^2}.$$

Comparing the above equations with equation (4.147) which is applicable for planar situations, we can see that the solution for 3-D bars in bending can be obtained as the superposition of two planar bending problems, as detailed in Section 4.4.2, which should be defined for the planes xy and xz with y and z being the principal axes of the cross-section.

Torsional actions

In Section 3.6 we studied the torsion problem of a prismatic bar. The formulation led to the exact 3-D elasticity solution as long as the torsional actions are introduced at the end sections as a specific field of shear surface forces which is mechanically equivalent to a torsional moment only. Additionally, the cross-sections should be free to warp.

These conditions are frequently violated in practical problems. For example, the bar is not free to warp at the bar ends where it is either connected to other bars or its section is restrained. However, as long as the cross-sections are not thin walled, these end perturbations affect the solution only in a small region close to the bar ends (see Timoshenko and Goodier, 1970) and we can assume that the bar section rotations are governed by

$$\frac{d\theta_x}{dx} = \frac{M_x}{EI_t} \quad (4.197)$$

where, referring to Figure 4.58, the end section torsional moments are given by $\mathbf{M} = M_x \mathbf{e}_x$ and $-\mathbf{M}$, θ_x is the section rotation about the x axis and I_t is the torsional moment of inertia of the cross-section (see Section 3.6).

Matrix formulation for a 3-D bar

We can obtain the stiffness matrix of a bar subjected to 3-D actions in an analogous manner to the 2-D bar solving the applicable differential equations for unit end displacements.

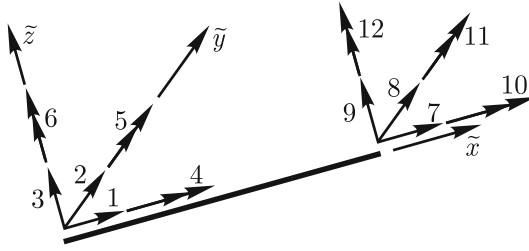


Fig. 4.60. Degrees of freedom for a 3-D bar

In Figure 4.60 the end section degrees of freedom are summarized. The local reference system is chosen such that \tilde{x} is taken along the section centroid and \tilde{y} and \tilde{z} are the principal axes of the bar cross-section.

We do not detail the evaluation of the stiffness coefficients since the bending solutions in planes $\tilde{x}\tilde{z}$ and $\tilde{y}\tilde{z}$ are identical to that of the planar beam. The axial solution is the same and for the torsion, we use (4.197) with unit end rotations. Therefore, the stiffness matrix is given on the next page.

We note that we can solve 3-D bar structures of arbitrary complexity with the matrix formulation. Of course, all the matrix procedures that were detailed for truss structures and for planar frames are directly applicable for 3-D bar structures.

4.2.6 Thin walled bars

Thin walled bars are used widely in engineering practice due to their efficient load carrying capabilities. In this section, we discuss some basic behaviors which are important for the modeling of thin walled bar structures. These behaviors, besides being essential for the modeling of thin walled bars, can be used to establish low-order models of complex structures. For example, the gross structural behavior of some buildings can be represented by an equivalent thin walled bar.

Bending behavior

A thin walled bar may be naturally obtained as a result of modifying the distribution of material over the cross-section to improve the bar stiffness with respect to bending. In Figure 4.61a, we show a highlighted region of a rectangular cross-section for which the normal stresses due to bending are significantly smaller than in the outer regions (refer to equation (4.145) for the linear normal stress distribution in bending) and, hence, in the highlighted region the material is not being used as effectively as in the outer regions. In Figure 4.61b, we show an I section whose area is the same as that of the rectangular section of Figure 4.61a. Let I_a and I_b be the moments of inertia of the rectangular and of the I section, respectively, and let us compare the

$$\frac{(w_{\max})_b}{(w_{\max})_a} = \frac{I_a}{I_b} = 0.0634 \tag{4.198}$$

and due to equation (4.145) the ratio between the maximum normal stresses is

$$\frac{(\tau_{n,\max})_b}{(\tau_{n,\max})_a} = \frac{I_a}{I_b} \frac{h_b}{h_a} = 0.176 \tag{4.199}$$

where $h_a = w$ and $h_b = h + t_f$. Although these evaluations are very basic, the values given in (4.198) and (4.199) quantify the effectiveness of the I section to resist bending when compared to the rectangular section.

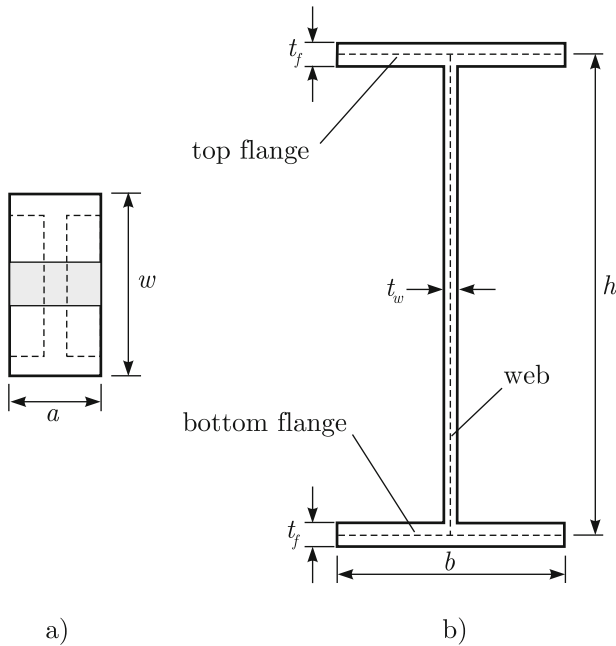


Fig. 4.61. Rectangular and I section of same area whose geometric data is given by $a = 6.615$ in, $w = 13.229$ in, $b = 16.655$ in, $h = 35.06$ in, $t_w = 0.945$ in, $t_f = 1.680$ in

The shear stress distribution due to bending for the I beam and, in fact, for any open thin walled section can be evaluated as detailed in Example 4.5. However, the “plane sectioning” (refer to Figure 4.21) should be taken orthogonal to the midlines of the flange/web and the shear stresses are assumed to be constant at these sections. We exemplify the sectioning in Figure 4.62a, and in Figure 4.62b we show the distribution of shear stresses where

$$\tau_f = \frac{bhV}{4I}, \quad \tau_{w_1} = \frac{bht_fV}{2It_w}, \quad \tau_{w_2} = \left(\frac{bt_f}{t_w} + \frac{h}{4} \right) \frac{Vh}{2I}.$$

Of course, I is the moment of inertia and V the shear force. For every point

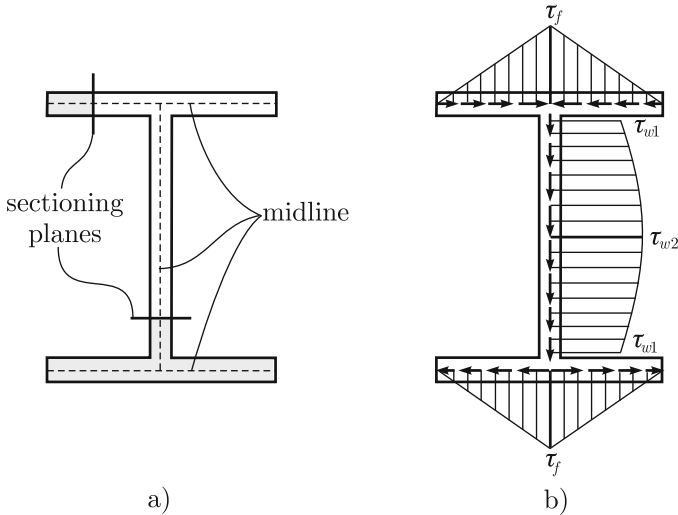


Fig. 4.62. a) Typical sectioning planes; b) Distribution of shear stresses

of the midline of the flange/web we define the shear flow as

$$f_s = \tau_s t$$

where τ_s is the magnitude of the shear stress and t is the thickness of the flange/web.

Shear center

An important concept associated with the distribution of shear stresses due to bending in a thin walled bar is the *shear center*. Consider a bar with the cross-section described in Figure 4.63a subjected to bending induced by a transverse vertical force distribution. The distribution of shear stresses is shown in Figure 4.63b where

$$\tau_f = \frac{bhV}{4I}, \quad \tau_{w1} = \frac{bht_f V}{2It_w}, \quad \tau_{w2} = \left(\frac{bt_f}{t_w} + \frac{h}{4} \right) \frac{Vh}{2I}.$$

The resultants at the web and at the flanges can be evaluated by integration of the shear stresses and are shown in Figure 4.64a.

If we reduce these forces to a generic point D on the horizontal axis of symmetry, we obtain the vertical force R_w which is equal to the shear force V and a moment given by

$$M_D = R_w d - R_f h.$$

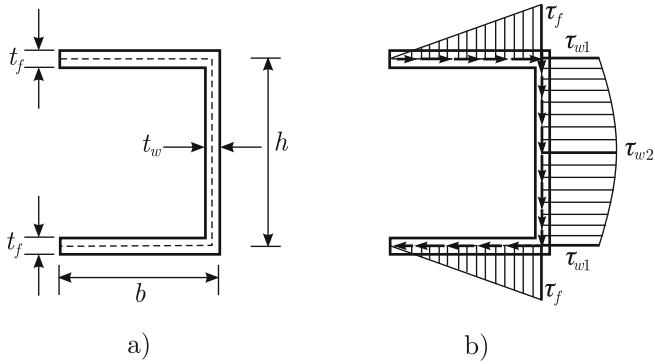


Fig. 4.63. a) Cross-section definition; b) Shear stress distribution

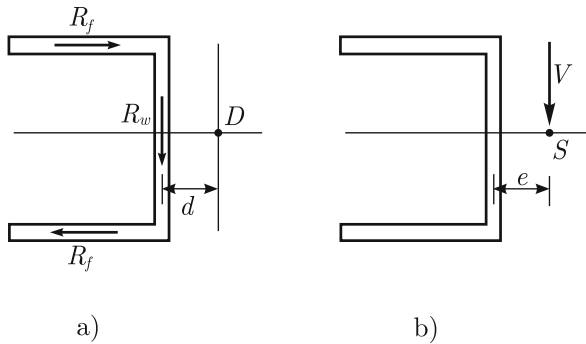


Fig. 4.64. a) Shear resultants; b) Location of the shear center

There is a position of point D for which $M_D = 0$, *i.e.*,

$$d = e = \frac{R_f h}{R_w}.$$

The value e determines the position of point D referred to as S – the shear center of the section.

Note that the shear center gives the position through which the resultant force – associated with all external loading to the section – should pass in order for there to be no twisting; that is, the resulting shear stress distribution is induced by bending alone. In Figure 4.63b, we summarize the situation for which only shear stresses induced by bending are developed.

Hence, if the resultant associated with all external loading does not pass through the shear center, shear stresses associated with torsion are induced.

We also note that, in general, the shear center and the center of gravity do not coincide. They coincide when there is a vertical plane of symmetry for the section.

Torsional behavior

The modeling of the torsional behavior of thin walled bars can be quite delicate. This behavior is drastically different depending on whether the cross-section is open or closed. Also, for open sections the restrained warping may affect the stress distribution in the whole bar. We first discuss the Saint Venant approach for open and closed sections and then introduce the modeling of restrained warping.

Open sections

The membrane analogy discussed in Section 3.6 is extremely useful to determine the shear stress distribution at an open⁶ thin walled section which is free to warp.

Consider, for example, the C section (“C” for channel) discussed above. In Figure 4.65, we show schematically the deformed shape of the membrane for this section. Except for the end regions and the corners, the membrane deforms as for the thin rectangular section studied in Example 3.9 and we obtain

$$I_t = 2I_t^f + I_t^w = 2\frac{bt_f^3}{3} + \frac{ht_w^3}{3}$$

and the maximum shear stress at the flange and web are given respectively by

$$\tau_{\max}^f = \frac{3M_t}{bt_f^2} \frac{I_t^f}{I_t}, \quad \tau_{\max}^w = \frac{3M_t}{bt_w^2} \frac{I_t^w}{I_t}.$$

In Figure 4.65b, we show schematically the shear stress distribution. We note that the methodology above can be applied for a thin walled section of n segments of length b_i and width t_i . In such a case

$$I_t = \sum_{i=1}^n \frac{b_i t_i^3}{3} \tag{4.200}$$

and the maximum shear stress for segment i

$$\tau_{\max}^i = \frac{M_t}{I_t^i} t_i \frac{I_t^i}{I_t} = \frac{M_t}{I_t} t_i. \tag{4.201}$$

⁶ When the midline of a thin walled section is a closed curve we say that the section is closed, otherwise the section is open

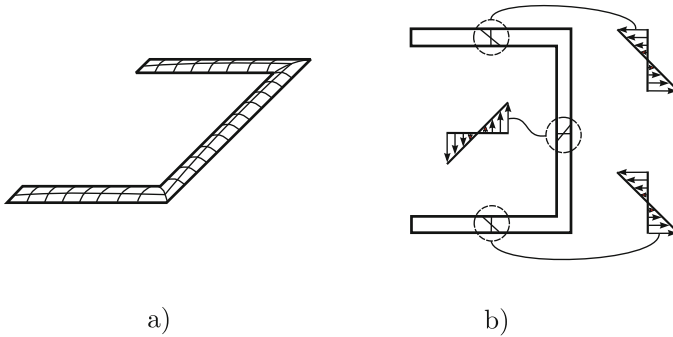


Fig. 4.65. a) Deformed shape of membrane; b) Distribution of shear stresses

Closed sections

We recall that in Section 3.6 we studied the uniform torsion of bars of arbitrary cross-sections. However, we made the implicit assumption that there were no holes in the cross-sections, *i.e.*, the cross-sectional region is simply connected.

The uniform torsion theory can be extended to be applicable to the more general cross-sections having holes. An interesting approach is to use the membrane analogy placing a rigid plate to cover each hole⁷. For example, consider the elliptical section with an elliptical hole as shown in Figure 4.66a where the elliptical hole is highlighted to emphasize that a rigid plate is placed there and in Figure 4.66b we show a side view. For thin walled sections we can assume that a section of the deformed shape of the membrane between the outer boundary and the rigid plate is a straight line.

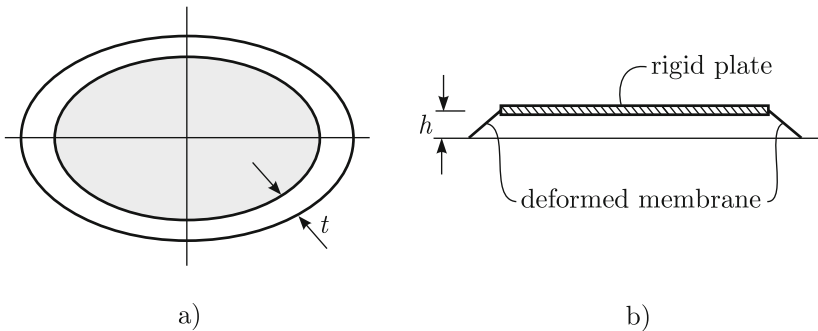


Fig. 4.66. a) Elliptical cross section with hole; b) Deformed membrane

⁷ In the general case, additional conditions should also be enforced to use the membrane analogy. However, it suffices to introduce the rigid plate for the thin walled closed sections (see Timoshenko and Gere, 1961)

The distribution of shear stresses can be directly inferred from the properties discussed in Section 3.6. In Figure 4.67a, a generic level curve of the membrane is shown and therefore the shear stresses are tangent to this curve and of constant magnitude (see equation (3.152)) and it is easily shown (see Timoshenko and Goodier, 1970) that

$$\tau_s = \frac{M_t}{2A_m t} \quad (4.202)$$

where A_m is the area enclosed by the midline of the wall as shown in Figure 4.67b. It can be shown that

$$I_t = \frac{M_t}{G\theta'} = \frac{4(A_m)^2 t}{L_m} \quad (4.203)$$

where L_m is the length of the midline.

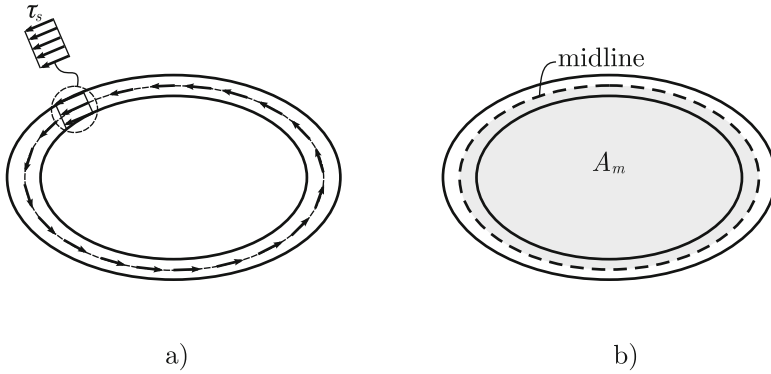


Fig. 4.67. a) Distribution of shear stresses; b) Geometric definitions

It is very interesting to compare the behavior of closed and open thin walled sections with respect to torsion. For that, we choose the simplest closed section – a thin walled circular tube. The open section is obtained by cutting the wall as shown in Figure 4.68b. For a given moment M_t , we can evaluate the I_t and the τ_{\max} for both situations. Using (4.200) we obtain for the open section

$$I_t^o = \frac{2\pi r t^3}{3}$$

and (4.203) gives for the closed section

$$I_t^c = \frac{4(\pi r^2)^2 t}{2\pi r} = \frac{4\pi^2 r^4 t}{2\pi r} = 2\pi r^3 t.$$

Therefore, the ratio between the torsional moments of inertia is

$$\frac{I_t^c}{I_t^o} = 3 \left(\frac{r}{t} \right)^2.$$

This ratio is very large for usual sections. For example, considering a tubular

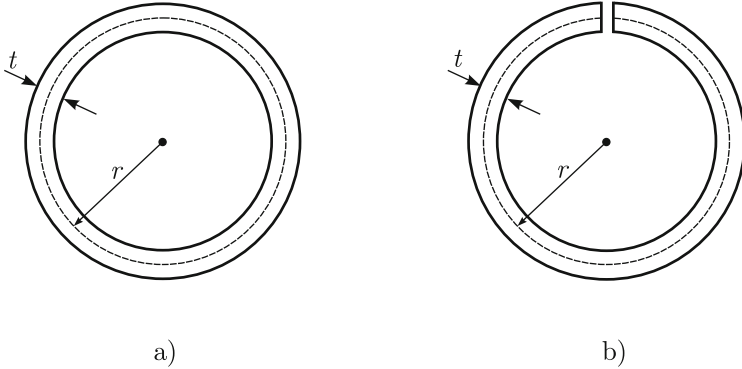


Fig. 4.68. Thin walled circular tubes: a) “closed” and b) “open”

section of $r = 12.375$ in and $t = 0.375$ in we obtain a ratio of 3267. Therefore the torsional stiffness of the closed section is much larger than that of the open section. This result could have been anticipated using the membrane analogy since I_t is proportional to the volume under the deformed membrane.

The maximum shear stress for the open section is given by (4.201)

$$\tau_{\max}^o = \frac{M_t}{I_t} t$$

and for the closed section by (4.202)

$$\tau_{\max}^c = \frac{M_t}{2\pi r^2 t}$$

leading to

$$\frac{\tau_{\max}^c}{\tau_{\max}^o} = \frac{1}{3} \frac{t}{r}$$

which is a small ratio. For the tubular section described above we obtain for this ratio 0.01.

In Figure 4.69 we summarize the distribution of shear stresses for both cases. Note that the closed section resists torsion very efficiently, because the shear flow has a lever arm of r for the resisting moment. On the other hand, for the open section, the shear flow is interrupted as the cutting plane

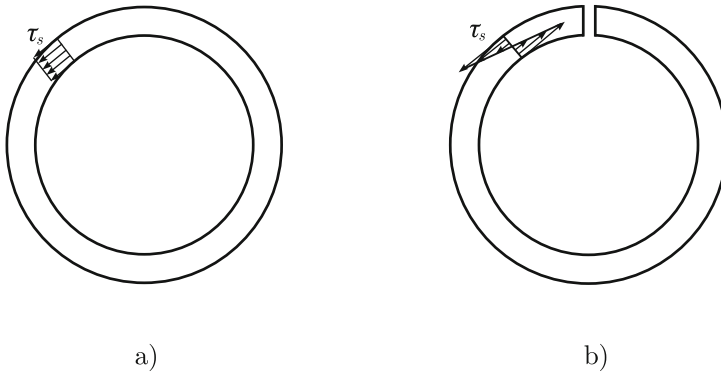


Fig. 4.69. a) Shear stresses for closed section; b) Shear stresses for open section. The magnitude of τ_s is not shown to scale

partially separates the section, and the shear flow has only a lever arm of the order of the wall thickness.

The differences in behavior with respect to torsion of closed and open sections were examined above for a particular case. However, they are representative of the qualitative behavior of general closed and open sections. Hence, for structural problems where torsion is an issue, closed sections are very efficient. For example, in bridges for which both bending and torsion are relevant, box sections are effective.

Warping effects

The modeling of torsion discussed so far is based on Saint Venant's uniform torsion model introduced in Section 3.6. In this theory it is assumed that the cross-sections are free to warp, *i.e.*, there are no kinematic restrictions preventing the out-of-plane displacements.

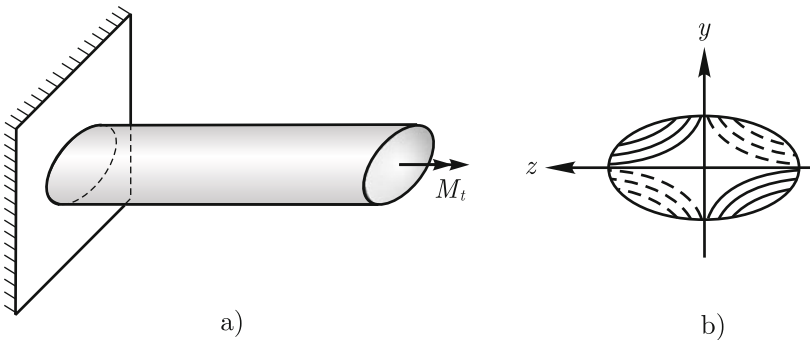


Fig. 4.70. a) Built-in bar of elliptical cross section subjected to torsion; b) Isolines of warping displacements predicted by Saint Venant's theory

Consider, for example, the case of a bar of elliptical cross-section subjected to a torsional moment at one end and built-in at the other, as summarized in Figure 4.70a. In Figure 4.70b, we show the isolines of warping displacements derived in Section 3.6 based on Saint Venant’s theory. Of course, at the built-in end the warping displacements are kinematically prevented giving rise to a field of normal stresses with zero resultant. It can be shown (Timoshenko and Goodier, 1970) that for the elliptical section these normal stresses result in a perturbation of the Saint Venant solution which rapidly diminishes in magnitude as we move away from the built-in end. This is the case for solid and thin walled closed cross-sections, but not for thin walled open sections.

In order to obtain insight into the behavior of open sections consider the situation summarized in Figure 4.71. A top view of the deformation of the bar predicted by Saint Venant’s theory is shown in Figure 4.71b. Of course, such deformation is incompatible with the built-in end. In Figure 4.72a we show qualitatively the distribution of normal stresses at the built-in section.

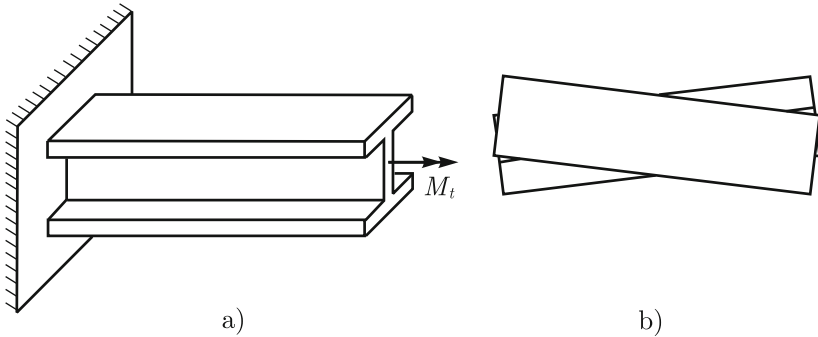


Fig. 4.71. a) Built-in bar of I section subjected to torsion; b) Top view of the deformation predicted by Saint Venant’s theory

Although the overall resultant of this stress distribution at the cross-section is null, the stresses give rise to bending moments of intensity M acting on the upper and lower flanges as summarized in Figure 4.72b. In fact, these bending moments acting at the rectangular cross-sections of the flanges induce the required deformation to counter, at the built-in end, the warping of the Saint Venant solution shown in Figure 4.71b. The quantity

$$B = Mh$$

is called the bimoment. To illustrate the interaction between the bimoment and the part of the torsional moment acting at a section we show in Figure 4.73 the equilibrium of an element of infinitesimally small length extracted from the I beam. We note that shear forces V are induced in the flanges associated with the variation of M . Of course,

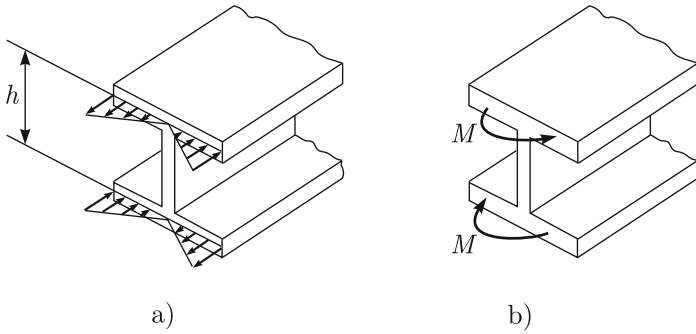


Fig. 4.72. a) Distribution of normal stresses at flange at built-in section; b) Moment resultant at flanges

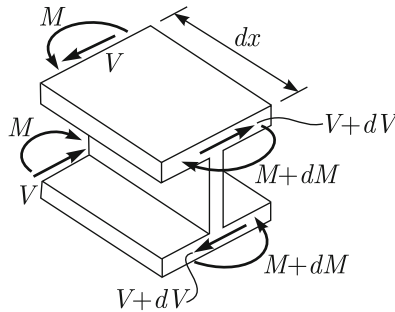


Fig. 4.73. Stress resultants at flanges

$$V = \frac{dM}{dx}.$$

Note that the shear forces acting at a section are equivalent to a torsional moment

$$(M_t)_w = Vh = h \frac{dM}{dx} = \frac{d(Mh)}{dx} = \frac{dB}{dx}$$

i.e., the variation of the bimoment induces a twisting moment distribution $(M_t)_w$ referred to as warping torsional moment since it is associated with restrained warping. The total torsional moment at a section can be written as

$$M_t = (M_t)_w + (M_t)_s$$

where $(M_t)_s$ is the moment of the Saint Venant part of the solution.

The complete formulation of the torsion problem of open sections with restrained warping is out of the scope of this book. For that, we refer the reader to Murray, 1985.

Our objective was to give some insight into the effect of restraining the warping for bars of open sections and how it influences the overall solution. This insight can be important when solving models and when establishing higher-order 3-D models.

4.2.7 Curved bar model

In this section we present the curved bar model and discuss basic behaviors of curved structures. The fundamental concepts introduced serve as a reference for many curved structural forms such as shell structures.

Basic facts

Referring to the straight bar model, transverse loads, such as those shown in Figure 4.74, are transferred to the supports by the beam through bending.

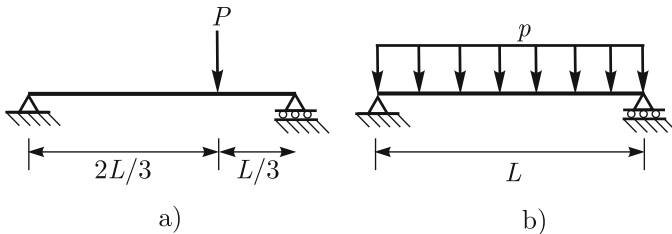


Fig. 4.74. Sample transverse loads applied to straight bars

Bending is not an efficient way of transferring load. We recall that the normal stress distribution due to bending at a bar cross-section is linear with the extreme values occurring at the outer fibers. Since the stress magnitude that can be supported by a given material is limited, in the case of bending this limit value is attained first at the outer fibers and there is a significant portion of the cross-section, around the centroid, for which the stresses are much lower than the limit values.

In contrast, when we have an axial load on the bar, the stress distribution is constant over the cross-section and all fibers simultaneously attain the stress limit value.

Suppose we consider the supports and the load of Figure 4.74a and that we would like to transfer such load to the supports without bending. We could try to do so with a cable, since cables can not sustain any bending. Although everyone has an intuitive understanding of what a cable is, in our context a cable can be understood as a very slender bar which is so flexible that it can not sustain any bending. If we place a cable linking the supports of Figure 4.74a we can not find an equilibrated position since as the section of the cable under the load starts moving downwards the right support moves

left horizontally. However, if we modify the right support to be fixed, the cable will find an equilibrated position as shown in Figure 4.75a and the axial forces in the cable can be evaluated by equilibrium. In fact equilibrium in the horizontal direction leads to

$$T_1 \cos \alpha = T_2 \cos \beta = H$$

and in the vertical to

$$P = T_1 \sin \alpha + T_2 \sin \beta$$

and we obtain

$$T_1 = \frac{P}{(\sin \alpha + \tan \beta \cos \alpha)}, \quad T_2 = \frac{P}{(\sin \beta + \tan \alpha \cos \beta)}.$$

Of course, to find the value of h (or α or β) we need to consider the section

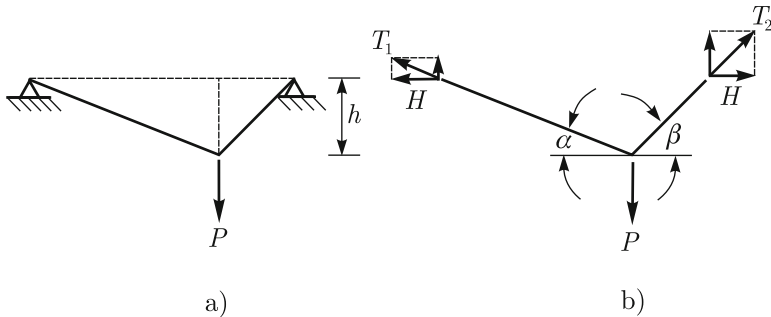


Fig. 4.75. Cable equilibrated configuration for a transverse concentrated load

properties and the material of the cable⁸.

An important observation which is always valid is that, to be able to equilibrate a vertical load with axial forces only, a horizontal reactive component at the supports is required which is called the thrust, in Figure 4.75b given by H . The equilibrated shape of the cable is called a funicular shape and h , the largest vertical displacement, is referred to as the sag. Let us find the funicular shape for the cable subjected to a uniformly distributed transverse load, see Figure 4.74b. Taking advantage of symmetry, an equilibrated configuration is shown in Figure 4.76. Of course, if this shape is funicular the bending moment at a generic section has to be zero. Hence,

$$M(x) = -(px) \frac{x}{2} + \frac{pL}{2}x - Hy(x) = 0$$

⁸ The value of h may be relatively large compared with the span for a rubber like cable and also for a steel cable when it is loose before the application of the load, that is, its length is greater than the span

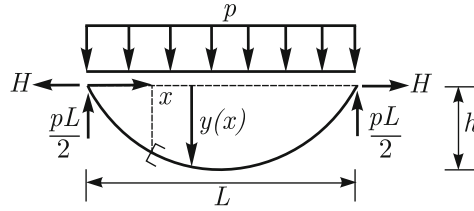


Fig. 4.76. Cable equilibrated configuration for a uniformly distributed load

which leads to

$$y(x) = \frac{p}{2H} (xL - x^2). \quad (4.204)$$

Therefore the funicular shape of a cable subjected to a uniformly distributed pressure is parabolic. We note that the sag is related to the value of the thrust. In fact, from equation (4.204)

$$h = y\left(\frac{L}{2}\right) = \frac{p}{2H} \left(\frac{L^2}{2} - \frac{L^2}{4}\right) = \frac{pL^2}{8H}$$

or

$$H = \frac{pL^2}{8h}.$$

Consider the funicular shape developed by the cable either in Figure 4.75b or 4.76. Instead of the very small cross-section of the cable, let us consider bars with a much larger cross-section whose axes coincide in its initial configuration with the funicular shape considered. Of course, in this case the cross-section is assumed to be large enough such that the displacements are small and, therefore, equilibrium is imposed in the undeformed configuration.

Now suppose we turn these bar structures over with respect to a horizontal line at the support level. In Figure 4.77 we summarize the resulting structures which are now referred to as arch structures. The structure of Figure 4.77a is called a polygonal arch since it consists of straight bars. The structure of Figure 4.77b is simply referred to as an arch; it is actually a curved bar structure.

The fundamental change that occurs when we turn the structures of Figure 4.75 over is that the axial forces developed in the bars go from tension to compression. This is a crucial distinction since structural materials behave differently in tension than in compression, especially with respect to their ultimate strength. In fact, historically, arches have had a tremendous importance in constructions since, for centuries, many construction materials have had a very low strength in tension.

The shape that leads to compression only in arch structures is referred to as “the line of pressure”. We note that the line of pressure is load dependent.

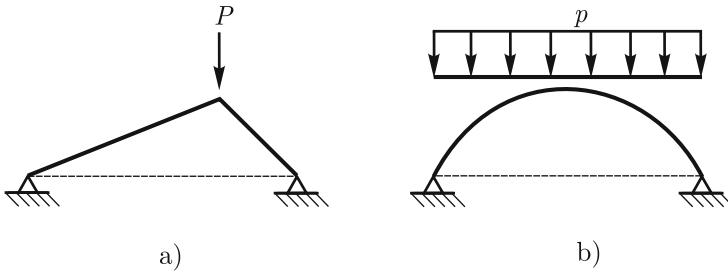


Fig. 4.77. Arch structures

For example, if we change the position of the concentrated load acting onto the arch of Figure 4.77a, bending is induced. Similarly, if a concentrated load acts onto the arch of Figure 4.77b bending is also induced. Here, cable structures behave differently, since when the load changes the cable changes its shape in such a way that the funicular shape for this new loading is always reached.

Consider the arch of Figure 4.77b whose bar axis is the line of pressure for the uniformly distributed load and is given by equation (4.204). A concentrated load is now applied as shown in Figure 4.78a. Of course, the axis of

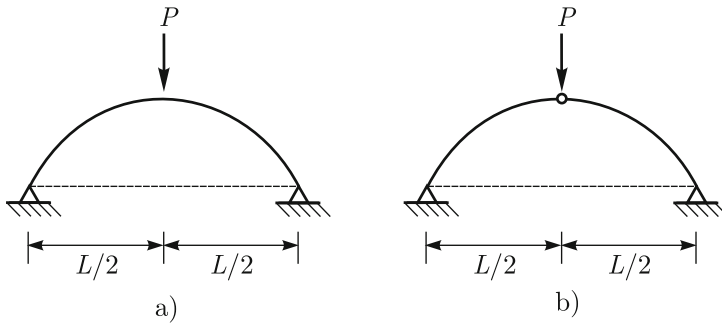


Fig. 4.78. Arches subjected to a concentrated load

this arch does not correspond to the pressure line for the concentrated load, since for this load the line of pressure is given by a polygonal arch defined by two straight bars from the point of load application to the supports.

We realize that we cannot solve this arch problem directly and find the internal forces since the structure is statically indeterminate. Therefore, to solve this problem we need to first discuss the formulation of the curved bar model which is addressed later in this section.

Let us for now transform the arch of Figure 4.78a into a statically determinate arch by introducing a pin type joint or hinge as shown in Figure 4.78b.

This kind of arch is called a three hinged arch and represents an important structural arrangement with wide engineering applications. We discuss the three hinged arch below, since insight into the behavior of arch structures is gained by means of this simple statically determinate structure.

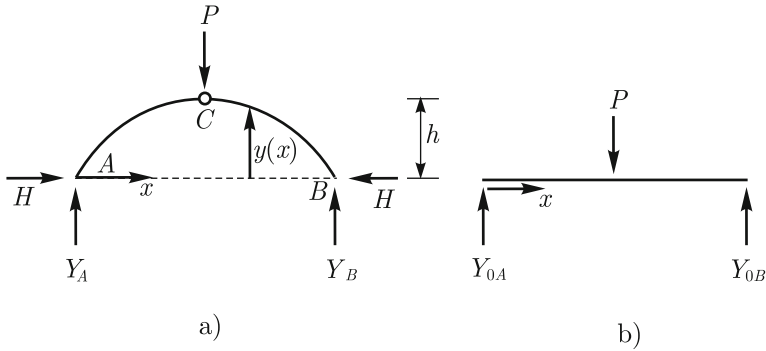


Fig. 4.79. a) Three hinged arch; b) Straight beam

Although we analyse the particular structure shown in Figure 4.78b, the solution procedure used applies for three hinged arches in general. In Figure 4.79a, we introduce the reactions taking into consideration that, as the external load is vertical, the horizontal reactions at the supports need to be self-equilibrated. To obtain insight into how the loads are transferred by an arch when compared to a straight beam, we consider the straight beam of Figure 4.79b.

To evaluate the vertical reactions for the arch we use equilibrium in the vertical direction

$$\sum F_y = 0 \quad \Rightarrow \quad Y_A + Y_B - P = 0$$

and moment equilibrium about A

$$\sum M_A = 0 \quad \Rightarrow \quad Y_B \cdot L - P \frac{L}{2} = 0.$$

These equations are the same that lead to reactions of the straight bar of Figure 4.79b. Therefore, in general,

$$Y_A = Y_{0A}$$

$$Y_B = Y_{0B}.$$

The additional condition to be considered is

$$M_C = 0$$

which is given by

$$M_C = M_{0C} - Hh = 0$$

where M_{0C} is the moment at the section of the straight beam corresponding to the hinge, that is, $M_{0C} = Y_B \cdot \frac{L}{2}$. Therefore,

$$H = \frac{M_{0C}}{h}.$$

The moment at a generic section of the arch is written as

$$M(x) = M_0(x) - Hy(x) \quad (4.205)$$

where $M_0(x)$ gives the moment distribution for the straight beam. Therefore, the moment for the arch is diminished with respect to that of the straight beam by the amount $Hy(x)$. In Figure 4.80a we graphically show the superposition given by equation (4.205) and in Figure 4.80b the moment diagram of the straight beam. The decrease in moment magnitudes in the arch with respect to the straight beam is clearly seen.

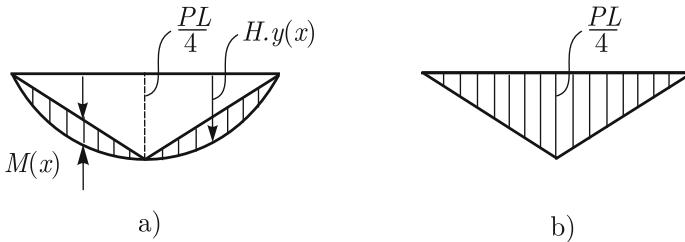


Fig. 4.80. Moment diagrams for arch and straight beam

Before we close this section, we would like to highlight some important facts. Due to the curved bar axis, it is possible to transfer certain transverse loads to the supports by developing axial forces only.

It is essential that the supports provide horizontal reactions which are called thrusts. Otherwise bending is developed.

We also note that even when the geometry of the arch does not correspond to the pressure line for a given load, the bending moment developed in the arch can be significantly lower than that of a straight bar of same span.

Differential formulation of a curved planar bar

Consider the curved bar problem described in Figure 4.81. The bar has a plane of symmetry and the bar axis is a curve in this plane. The bar axis is going through the centroid of the cross-section of the bar. The externally

applied distributed loads are applied at the bar axis in the plane of symmetry and can be decomposed into a normal component p_z and a tangential component p_x . For every point along the axis, we define a local coordinate system xz , x being tangential to the axis and z orthogonal. At the bar ends either prescribed displacements/rotations or force boundary conditions are applied.

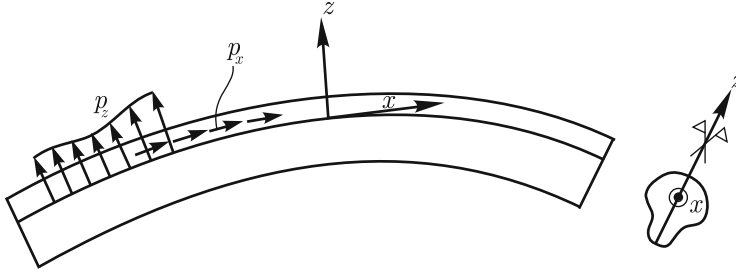


Fig. 4.81. Some definitions for curved bar problem; the axis goes through the centroid of the cross-section

Except for considering now a curved bar, the remaining definitions are analogous to those used for a straight bar. The basic kinematic hypothesis of the Bernoulli-Euler beam theory that sections initially orthogonal to the bar axis remain undeformed and orthogonal to this axis during deformations is also adopted.

Before we present the formulation, let us recall some basic facts for a planar curve. Consider a generic planar curve as shown in Figure 4.82. Let s be the arc-length coordinate along the curve. For any point on the curve, say point P , we can define a circle centered at point C located on a straight line defined by the normal to the curve at P . The radius of the circle and, hence, point C are defined to make the circle coincide with the curve at and in the vicinity of point P . A typical situation is summarized in Figure 4.82.

The radius r of the circle is called the radius of curvature of the curve at point P and the point C the center of curvature, and we have

$$ds = r d\theta. \tag{4.206}$$

The curvature κ at point P is given by

$$\kappa = \frac{d\theta}{ds} = \frac{1}{r}. \tag{4.207}$$

Kinematics

Consider a differential element of the bar, see Figure 4.83a. Since (4.206) holds we also have

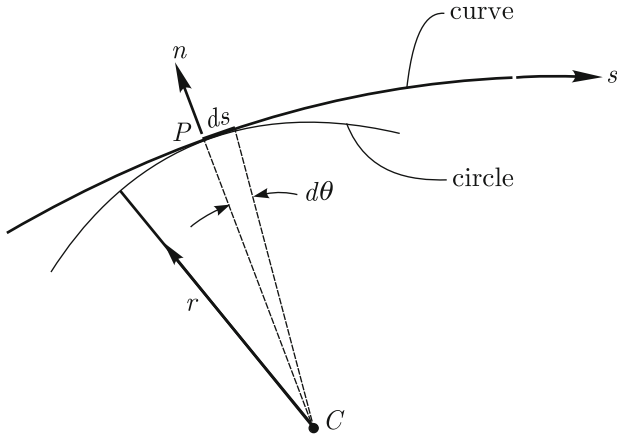


Fig. 4.82. Radius of curvature definitions for point P

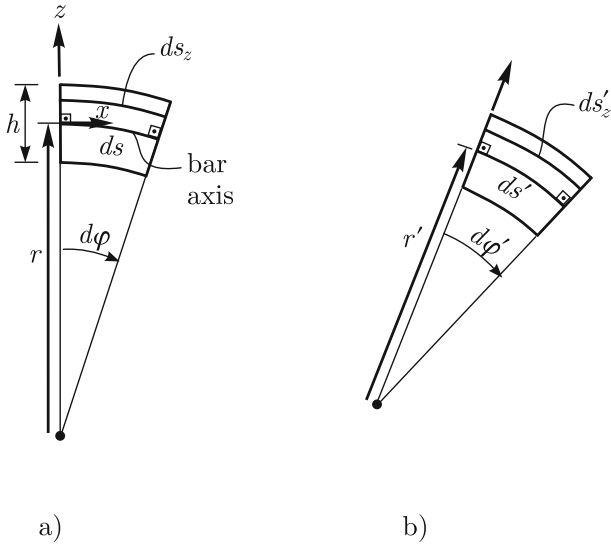


Fig. 4.83. Deformed and undeformed configurations for a differential element

$$ds_z = (r + z)d\varphi \tag{4.208}$$

where ds_z is the differential arc length at a distance z from the axis.

The deformed configuration of the differential element of Figure 4.83a is shown in Figure 4.83b. We note that the Bernoulli-Euler hypothesis is used to characterize the deformed configuration and a prime indicates that the quantities are associated with the deformed configuration.

The strain in the tangential direction at the bar axis is given by

$$\varepsilon_{xx_0} = \frac{ds' - ds}{ds} \quad (4.209)$$

and as a function of z by

$$\varepsilon_{xx} = \frac{ds'_z - ds_z}{ds_z}. \quad (4.210)$$

Using equations (4.206) and (4.208), we obtain

$$ds_z = \left(1 + \frac{z}{r}\right) ds. \quad (4.211)$$

In an analogous manner, we can write for the deformed configuration

$$ds'_z = \left(1 + \frac{z}{r'}\right) ds'. \quad (4.212)$$

Taking into account that relation (4.209) can be re-written as

$$ds' = (1 + \varepsilon_{xx_0}) ds$$

and substituting (4.211) and (4.212) into (4.210) yields

$$\varepsilon_{xx} = \frac{\left(1 + \frac{z}{r'}\right) (1 + \varepsilon_{xx_0}) - \left(1 + \frac{z}{r}\right)}{\left(1 + \frac{z}{r}\right)}$$

which can be re-written as

$$\varepsilon_{xx} = \frac{\varepsilon_{xx_0}}{\left(1 + \frac{z}{r}\right)} + \frac{z}{\left(1 + \frac{z}{r}\right)} \left((1 + \varepsilon_{xx_0}) \frac{1}{r'} - \frac{1}{r} \right). \quad (4.213)$$

We now want to focus on situations where the thickness of the bar is small compared with the ratio of curvature of the bar axis, that is, $h/r \ll 1.0$ and also where we can neglect the stretching of the axis on the change of curvature⁹ (see Timoshenko and Woinowsky-Krieger, 1959). Then expression (4.213) simplifies to

$$\varepsilon_{xx} = \varepsilon_{xx_0} + z \left(\frac{1}{r'} - \frac{1}{r} \right). \quad (4.214)$$

Let χ be the change in curvature due to deformations, *i.e.*,

$$\chi = \frac{1}{r'} - \frac{1}{r}. \quad (4.215)$$

⁹ The exact linearized expression for the change in curvature actually includes the stretching of the axis and is given in Chapelle and Bathe, 2010a

Introducing (4.215) into (4.214) yields

$$\varepsilon_{xx} = \varepsilon_{xx_0} + z\chi. \tag{4.216}$$

Therefore, we see that the tangential strain can be interpreted as the axial strain plus a term which is proportional to the distance of the longitudinal fiber to the axis times the change in curvature.

Let us introduce the kinematic variables u and w which give the displacements of points of the axis along x and z , *i.e.*, along the tangential and normal directions, and use small strain conditions. We would like to obtain the strain ε_{xx} as a function of these kinematic variables. Referring to Figure 4.84, the contributions for ε_{xx_0} are given by

$$\varepsilon_{xx_0} = \frac{du + (w + r)d\varphi - rd\varphi}{rd\varphi} = \frac{du}{ds} + \frac{w}{r}. \tag{4.217}$$

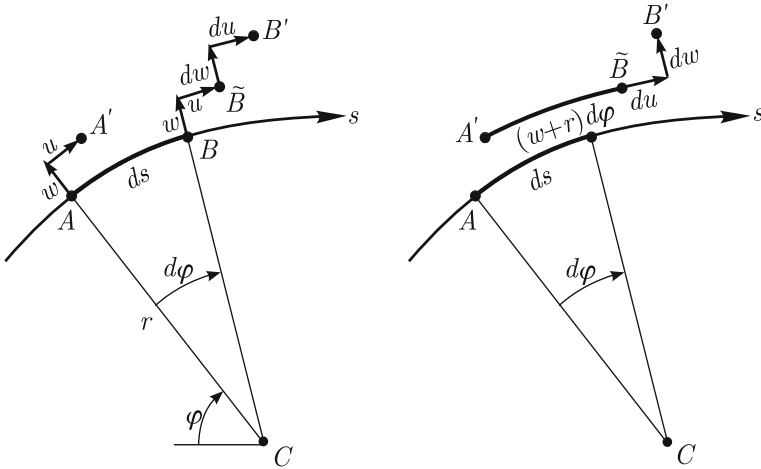


Fig. 4.84. Displacements and displacement increments for a generic differential arc length increment on the axis

To evaluate the change in curvature, we introduce an additional variable which we will eliminate later, namely the section rotation $\beta(s)$, see Figure 4.85. We also use the assumptions that lead to (4.214) and of small deformations and strains.

Then we have at a section the displacements

$$u_\varphi(\varphi, r, z) = u(\varphi) - z\beta(\varphi) \tag{4.218}$$

and of course

$$u_r(\varphi, r, z) = w(\varphi).$$

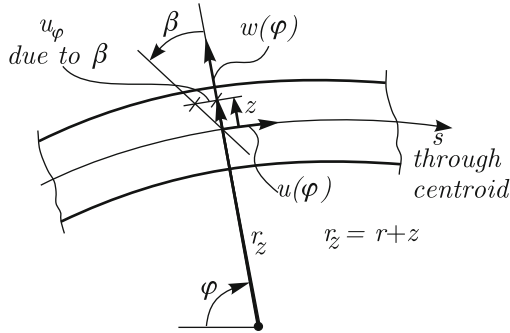


Fig. 4.85. Deformations of the beam

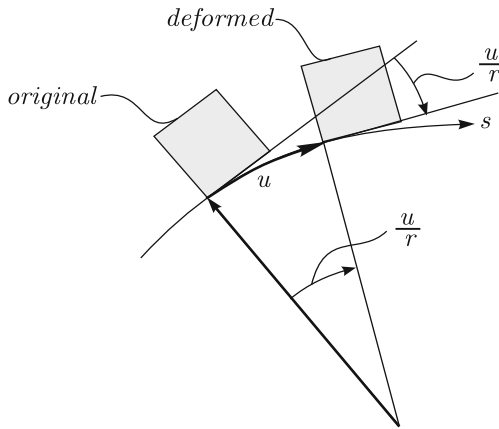


Fig. 4.86. Shear component due to displacement u

The normal strain is then given by (see Section 4.1.3)

$$\varepsilon_{xx}(\varphi, r, z) = \frac{w}{r_z} + \frac{1}{r_z} \frac{\partial u_\varphi}{\partial \varphi}$$

where we recognize the first term to be straining due to the radial displacement, and the second term to be the usual normal strain.

Since $r_z = r + z$, and using (4.218), we obtain

$$\varepsilon_{xx} = \frac{1}{1 + z/r} \left(\frac{w(\varphi)}{r} + \frac{1}{r} \frac{\partial u(\varphi)}{\partial \varphi} - \frac{z}{r} \frac{\partial \beta(\varphi)}{\partial \varphi} \right)$$

Assuming that $h/r \ll 1.0$, we thus have

$$\varepsilon_{xx} = \frac{w}{r} + \frac{1}{r} \frac{\partial u}{\partial \varphi} - \frac{z}{r} \frac{\partial \beta}{\partial \varphi}.$$

However, our assumption is that of Bernoulli-Euler theory, that the shear strain is zero (that is, originally straight fibers normal to the axis remain

normal to the axis during deformations). This requires that the shear given by

$$\gamma = \frac{1}{r+z} \frac{\partial w}{\partial \varphi} + \frac{\partial u_\varphi}{\partial z} - \frac{u_\varphi}{r+z}$$

be zero. Here the first two terms correspond to the usual shear strain components in a Cartesian coordinate system (see Section 3.2.5). The last term corresponds to the fact that the s -axis changes direction.

Assuming again $h/r \ll 1.0$, we obtain

$$\gamma = \frac{1}{r} \frac{\partial w}{\partial \varphi} + \frac{\partial u_\varphi}{\partial z} - \frac{u}{r}$$

where we use u instead of u_φ in the last term, resulting into a constant shear strain at a section. We give an interpretation of the u/r term in Figure 4.86. Substituting from (4.218) and using the condition that γ be zero, we obtain

$$\beta = \frac{1}{r} \frac{\partial w}{\partial \varphi} - \frac{u}{r} \quad (4.219)$$

and hence

$$\varepsilon_{xx} = \frac{w}{r} + \frac{1}{r} \frac{du}{d\varphi} - \frac{z}{r} \frac{d}{d\varphi} \left(\frac{1}{r} \frac{dw}{d\varphi} - \frac{u}{r} \right) \quad (4.220)$$

where u and w , measured at the axis of the beam, are only a function of φ . This strain relationship corresponds to (4.216) with¹⁰

$$\begin{aligned} \varepsilon_{xx_0} &= \frac{w}{r} + \frac{du}{ds} \\ \chi &= -\frac{1}{r} \frac{d}{d\varphi} \left(\frac{1}{r} \frac{dw}{d\varphi} - \frac{u}{r} \right) \end{aligned} \quad (4.221)$$

and ε_{xx_0} was already given in (4.217).

We note that, both, the tangential and normal displacements contribute to the strain along the axis ($z = 0$) and to the change in curvature. This fact contrasts with the situation for the straight bar where the strain along the axis depends only on the tangential displacement and the curvature change depends only on the transverse displacement (analogous to the normal displacement in the curved bar). As a consequence curved structures – and in particular shell structures – are much more difficult to analyze than straight or flat structures (straight beams and plates).

¹⁰ Note that, regarding the sign convention, the w -dependent term corresponds to a *decrease* in the original curvature (corresponding to a positive moment M). For a straight bar, a positive moment M causes an *increase* in curvature, but from zero curvature (see (4.134)); hence the sign convention is consistent, and we use the same convention for plates and shells

Constitutive relation and stress resultants

Hooke's law applies for the tangential direction, *i.e.*,

$$\tau_{xx} = E\varepsilon_{xx} \quad (4.222)$$

and using (4.216) we obtain

$$\tau_{xx} = E(\varepsilon_{xx_0} + z\chi) = E\varepsilon_{xx_0} + zE\chi. \quad (4.223)$$

The axial force N is given by

$$N = \int_A \tau_{xx} dA = EA\varepsilon_{xx_0} \quad (4.224)$$

and the bending moment by

$$M = \int_A -\tau_{xx}z dA = -EI\chi. \quad (4.225)$$

We note that the linear distribution of normal stress given in equation (4.223) is only valid when the section height of the beam is small compared with the radius of curvature of the axis (see the derivation from (4.218) to (4.221)). If the height of the beam is not small with respect to the radius of curvature the distribution of normal stress will no longer be linear. Actually we would obtain a hyperbolic distribution of normal stress along the beam height. However, the difference in stress predictions is only significant for situations where the ratio h/r is large. For example, when we consider the bending of a rectangular cross-section with $h/r = 1/4$, the difference in stress predictions at the extreme fibers is only about 8%.

Equilibrium

We consider the equilibrium of a differential element as shown in Figure 4.87. Equilibrium in the tangential and normal directions can be written as

$$-N + (N + dN) - Vd\theta + p_x ds = 0$$

$$V - (V + dV) - Nd\theta + p_z ds = 0$$

which leads to

$$\frac{dN}{ds} - \frac{V}{r} = -p_x \quad (4.226)$$

$$\frac{dV}{ds} + \frac{N}{r} = p_z \quad (4.227)$$

and moment equilibrium about point Q can be written as

$$-M + (M + dM) - Vds = 0$$

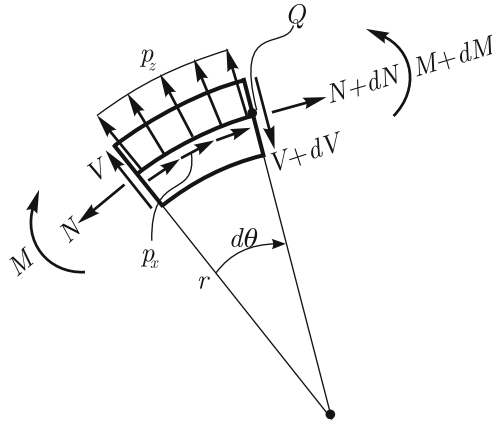


Fig. 4.87. Equilibrium of a differential element

leading to

$$\frac{dM}{ds} = V. \tag{4.228}$$

We note that due to the curved axis, equilibrium leads to coupled equations for the internal forces in contrast to the conditions for a straight bar for which the equilibrium of the axial forces is independent of that of the moment and shear forces.

Summarizing, equation (4.220) represents the strain compatibility conditions, equations (4.224) and (4.225) the constitutive relations, and equations (4.226) to (4.228) the equilibrium conditions. Therefore, when the boundary conditions at the end sections are introduced we have the complete formulation since all the requirements have been taken into account.

Of course, we could derive the stiffness matrix for a given curved bar solving the above differential formulation for unit end displacements/rotations as for the straight bar.

Our motivation to present the formulation of the curved bar problem was mainly to gain insight into how to tackle the analysis of curved bars including the basic assumptions used. Therefore we will not elaborate on the solution of the formulation, except for presenting the solution of a very simple problem as an illustration. Note that when the kinematic boundary conditions make the curved bar structure statically determinate, we can directly determine the internal forces and the solution becomes much simpler. In fact, substituting (4.217) and (4.221) into (4.224) and (4.225) respectively, we obtain

$$\frac{du}{ds} + \frac{w}{r} = \frac{N}{EA} \tag{4.229}$$

$$\frac{d^2w}{ds^2} - \frac{d}{ds} \left(\frac{u}{r} \right) = \frac{M}{EI} \tag{4.230}$$

with M and N known functions.

Example 4.16

Determine the displacement w for the circular cantilever beam shown in Figure 4.88.

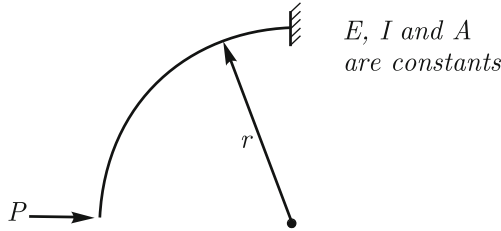


Fig. 4.88. Circular cantilever beam problem

Solution

We first determine the axial force and bending moment along the bar. Referring to Figure 4.89

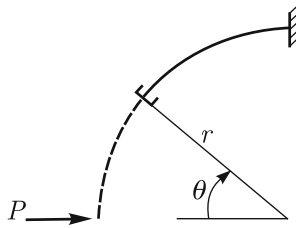


Fig. 4.89. Generic section of curved cantilever

$$N = -P \sin \theta \tag{4.231}$$

$$M = -Pr \sin \theta. \tag{4.232}$$

Since the radius of curvature is constant, we have that

$$s = \theta r$$

$$\frac{d(\cdot)}{ds} = \frac{d(\cdot)}{d\theta} \frac{d\theta}{ds} = \frac{1}{r} \frac{d(\cdot)}{d\theta}. \tag{4.233}$$

Hence, using (4.233) and substituting (4.229) into (4.230) yields

$$\frac{d^2w}{d\theta^2} + w = r^2 \frac{M}{EI} + r \frac{N}{EA}$$

and introducing (4.231) and (4.232), we obtain

$$\frac{d^2w}{d\theta^2} + w = -\frac{Pr}{E} \left(\frac{r^2}{I} + \frac{1}{A} \right) \sin \theta. \quad (4.234)$$

A particular solution of equation (4.234) is given by

$$w_p = -\frac{k}{2} \theta \cos \theta$$

where $k = -\frac{Pr}{E} \left(\frac{r^2}{I} + \frac{1}{A} \right)$. The general solution of (4.234) can be written as

$$w = C_0 \sin \theta + C_1 \cos \theta - \frac{k}{2} \theta \cos \theta$$

where C_0 and C_1 are constants to be determined. The two kinematic boundary conditions at $\theta = \pi/2$ are

$$w \left(\frac{\pi}{2} \right) = 0, \quad \frac{dw}{ds} \left(\frac{\pi}{2} \right) = 0$$

leading to

$$C_0 = 0 \quad \text{and} \quad C_1 = \frac{\pi k}{4}$$

and finally

$$w = -\frac{k}{2} \cos \theta \left(\theta - \frac{\pi}{2} \right) = \frac{Pr}{2E} \left(\frac{r^2}{I} + \frac{1}{A} \right) \cos \theta \left(\theta - \frac{\pi}{2} \right).$$

Of course, we could now use the solution for w and equation (4.229) to evaluate u by a simple integration considering that $u(\pi/2) = 0$.

□

4.2.8 The Timoshenko beam model

We recall that the Bernoulli-Euler beam model was used to describe the behavior of bars subjected to transverse loading. The model considers the change of curvature of the beam axis induced by the bending moment. This deformation dominates the overall bar deformation as long as the bar is slender. As the height of the bar section h increases with respect to the characteristic bar length L the deformation induced by shear becomes no longer negligible and when h/L is about $\frac{1}{10}$ shear deformations need frequently to be included.

The Timoshenko beam model considers shear deformations. Its fundamental hypothesis is that the bar cross-sections which are initially orthogonal to the bar axis remain plane but not necessarily orthogonal to the deformed bar axis.

The loading and geometrical definitions used for the Bernoulli-Euler beam model are adopted here. The kinematic hypothesis is shown in Figure 4.90¹¹.

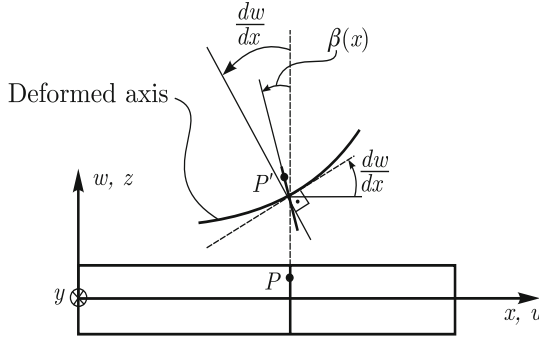


Fig. 4.90. Kinematics of beam sections for the Timoshenko beam model

We note that in addition to $w(x)$, which gives the transverse displacement of the beam axis, a new kinematic variable $\beta(x)$ which gives the section rotation with respect to the vertical direction is defined. Hence, we can write

$$u = -z\beta(x).$$

Hooke's law is also adopted for the longitudinal fibers leading to

$$\tau_{xx} = E\varepsilon_{xx} = -Ez\frac{d\beta}{dx}.$$

We can evaluate the transverse shear strain

$$\gamma_{xz} = \frac{\partial u}{\partial z} + \frac{\partial w}{\partial x} = \frac{dw}{dx} - \beta$$

and, therefore,

$$\tau_{xz} = G\gamma_{xz} = G\left(\frac{dw}{dx} - \beta\right).$$

According to these hypotheses the shear stresses are constant over the cross-section. However, the shear stresses must be zero at the top and bottom of the section, and we recall that, by static considerations alone, the Bernoulli-Euler model predicts a parabolic distribution of the transverse shear stresses for a rectangular cross-section.

¹¹ This same kinematic description was used in Figure 4.85

In order to retain the simple nature of the model while accounting for the deformations due to transverse shear strains, the value of γ_{xz} above is interpreted as a constant shear strain over a shear area A_s , where

$$k = \frac{A_s}{A}$$

and A is the actual cross-sectional area. Then the shear force is given by

$$V = \int_{A_s} -\tau_{xz} dA = -kGA \left(\frac{dw}{dx} - \beta \right). \quad (4.235)$$

The value of k depends on the stress/strain distributions over the cross-section and therefore depends on the cross-sectional shape. There are different procedures to evaluate k and we refer to Cowper, 1966 for a review of different methods¹². In Bathe, 1996 a simple procedure is applied to obtain $k = 5/6$ for a rectangular cross-section.

The bending moment is given by

$$M = \int_A -Ez \frac{d\beta}{dx} (-z) dA = EI \frac{d\beta}{dx} \quad (4.236)$$

and the axial force is zero.

Considering the equilibrium in the transverse direction, we obtain

$$\frac{dV}{dx} = p$$

and from (4.235)

$$-kGA \frac{d}{dx} \left(\frac{dw}{dx} - \beta \right) = p.$$

Moment equilibrium leads to

$$\frac{dM}{dx} = V. \quad (4.237)$$

Using equation (4.235), (4.236) and (4.237), we arrive at

$$EI \frac{d^2\beta}{dx^2} = -kGA \left(\frac{dw}{dx} - \beta \right).$$

Introducing the boundary conditions, we can summarize the Timoshenko beam model formulation.

¹² A value obtained, which depends on the Poisson ratio, is $k = \frac{10+10\nu}{12+11\nu}$

Differential formulation of the Timoshenko beam model

Given the transversely distributed loading $p(x)$, find $\beta(x)$, $w(x)$ such that

$$-kGA \frac{d}{dx} \left(\frac{dw}{dx} - \beta \right) = p(x) \quad (4.238)$$

$$EI \frac{d^2 \beta}{dx^2} = -kGA \left(\frac{dw}{dx} - \beta \right) \quad (4.239)$$

for all x . At $x = 0$

$$\beta(0) = \beta_0 \quad \text{or} \quad M(0) = -M_0$$

$$w(0) = w_0 \quad \text{or} \quad V(0) = Q_0$$

and at $x = L$

$$\beta(L) = \beta_L \quad \text{or} \quad M(L) = M_L$$

$$w(L) = w_L \quad \text{or} \quad V(L) = -Q_L$$

where β_0 , β_L are imposed rotations, w_0 , w_L imposed transverse displacements, M_0 , M_L prescribed moments and Q_0 , Q_L prescribed transverse forces¹³.

Example 4.17

Consider a bar with length L modeled as a Timoshenko beam. There is no transverse load and the following end displacements and rotations are imposed

$$w_0 = \delta, w_L = 0, \beta_0 = 0, \beta_L = 0$$

Solution

Since $p(x)$ is zero, equation (4.238) becomes

$$\frac{dw}{dx} - \beta = C_1 \quad (4.240)$$

¹³ The conventions for prescribed moments and forces are the same as those used for the Bernoulli-Euler beam model, see equations (4.136) to (4.140)

where C_1 is an integration constant. Substituting (4.240) into (4.239), we obtain

$$\frac{d^2\beta}{dx^2} = -\frac{kGA}{EI}C_1. \quad (4.241)$$

Integrating (4.241) twice and imposing $\beta(0) = 0$, we arrive at

$$\beta(x) = -\frac{kGA}{2EI}C_1x^2 + C_2x \quad (4.242)$$

where C_2 is also an integration constant. Now, substituting (4.242) into (4.240), integrating the resulting equation once and imposing the boundary condition $w(0) = \delta$, we obtain

$$w(x) = -\frac{kGA}{6EI}C_1x^3 + \frac{C_2}{2}x^2 + C_1x + \delta. \quad (4.243)$$

Considering the two remaining boundary conditions, $\beta(L) = 0$ and $w(L) = 0$, we obtain from (4.242) and (4.243)

$$-\frac{kGAL^2}{2EI}C_1 + LC_2 = 0$$

and

$$\left(-\frac{kGAL^3}{6EI} + L\right)C_1 + \frac{L^2}{2}C_2 = -\delta$$

which can be solved for C_1 and C_2 which substituted into (4.242) and (4.243) leads to the solution

$$w(x) = \left(\frac{2x^3}{L^3(1+2g)} - \frac{3x^2}{L^2(1+2g)} - \frac{2xg}{L(1+2g)} + 1\right)\delta$$

$$\beta(x) = \left(\frac{6x^2}{L^3(1+2g)} - \frac{6x}{L^2(1+2g)}\right)\delta$$

where $g = \frac{6EI}{kGAL^2}$. In Example 4.7, this same problem was solved for the Bernoulli-Euler beam model. Comparing the solution for $w(x)$ given above with that of the Bernoulli-Euler beam model given in equation (4.167), we conclude that these solutions are consistent since when the shear rigidity given by GA is made large compared to the bending rigidity, given by EI , the solution based on Timoshenko beam theory approaches the solution based on Bernoulli-Euler beam theory and in the limit case, $GA \rightarrow \infty$, both solutions are the same.

□

As before, we can impose unit end displacements to derive a stiffness matrix for the Timoshenko beam. Using the bar nodal degrees of freedom

convention of Figure 4.27, we can directly obtain the second column of the stiffness matrix from the solution of Example 4.7 imposing $\delta = 1$ and evaluating the end forces. In fact

$$\begin{aligned} M(0) &= EI \frac{d\beta}{dx}(0) = -\frac{6EI}{L^2(1+2g)} \\ M(L) &= EI \frac{d\beta}{dx}(L) = \frac{6EI}{L^2(1+2g)} \\ V(0) &= -kGA \left(\frac{dw}{dx} - \beta \right) \Big|_{x=0} = \frac{12EI}{L^3(1+2g)} = V(L). \end{aligned}$$

Therefore

$$\tilde{\mathbf{k}}_{i2} = \begin{bmatrix} 0 \\ \frac{12EI}{L^3(1+2g)} \\ \frac{6EI}{L^2(1+2g)} \\ 0 \\ -\frac{12EI}{L^3(1+2g)} \\ \frac{6EI}{L^2(1+2g)} \end{bmatrix}.$$

If we proceed in an analogous manner, imposing unit end displacements/rotations for the remaining degrees of freedom and evaluating bar end forces and moments, we can construct the stiffness matrix for the Timoshenko beam

$$\tilde{\mathbf{k}} = \begin{bmatrix} \frac{EA}{L} & 0 & 0 & -\frac{EA}{L} & 0 & 0 \\ 0 & \frac{12EI}{L^3(1+2g)} & \frac{6EI}{L^2(1+2g)} & 0 & -\frac{12EI}{L^3(1+2g)} & \frac{6EI}{L^2(1+2g)} \\ 0 & \frac{6EI}{L^2(1+2g)} & \frac{2EI(2+g)}{L(1+2g)} & 0 & -\frac{6EI}{L^2(1+2g)} & \frac{2EI(1-g)}{L(1+2g)} \\ -\frac{EA}{L} & 0 & 0 & \frac{EA}{L} & 0 & 0 \\ 0 & -\frac{12EI}{L^3(1+2g)} & -\frac{6EI}{L^2(1+2g)} & 0 & \frac{12EI}{L^3(1+2g)} & -\frac{6EI}{L^2(1+2g)} \\ 0 & \frac{6EI}{L^2(1+2g)} & \frac{2EI(1-g)}{L(1+2g)} & 0 & -\frac{6EI}{L^2(1+2g)} & \frac{2EI(2+g)}{L(1+2g)} \end{bmatrix}.$$

Of course, the axial displacements are considered in the stiffness matrix above. We note that we can superpose the solution of the bar model under axial loading with either the Bernoulli-Euler or Timoshenko models since the sections do not rotate due to the axial loading.

Regarding comparisons in predictions obtained with the Bernoulli-Euler and Timoshenko models, we refer the reader to the modeling presented in Section 7.1.

4.3 Plates in bending

We first recall the plane stress model discussed in Section 4.1.2. The model was characterized geometrically as a thin plate and the mechanical loading had to act in the midsurface of the plate. These definitions were summarized in Figure 4.5.

The plate models we address in this section have the same geometries, however, the loading is acting transversely, *i.e.*, orthogonal to the midsurface of the plate, which induces bending, leading to a completely different structural behavior. While in the plane stress model the stresses are constant through the thickness, for the plate bending models, the stresses vary linearly through the thickness of the plate.

There is an interesting analogy between the behavior of bars and plates. The analogue of the bar subjected to axial loading is the plane stress model and that of the bar subjected to transverse loading is the plate bending model.

Insight into the behavior of a plate resisting transverse loading can be gained by interpreting the plate to act “like” beams in orthogonal directions as schematically shown in Figure 4.91. Of course, only the gross behavior is captured by this interpretation. We will return to this interpretation of the plate behavior later on in this section.

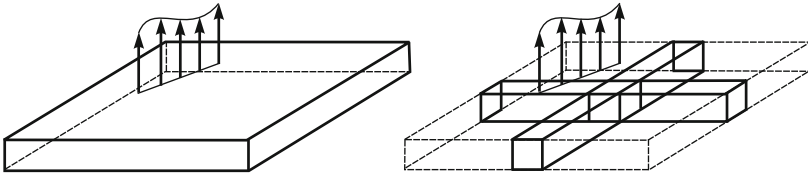


Fig. 4.91. Interpretation of bending behavior by beam action

The presentation of plate models is organized as follows. In the next section we discuss the Kirchhoff plate model which is the analogue of the Bernoulli-Euler beam model due to the similar kinematic hypothesis adopted. The emphasis is on model assumptions and on basic requirements. We derive the differential formulation of the model and, although solutions of the governing equations are not our primary objective, one classical solution is presented for illustrative purposes. A section is then dedicated to plate behavior. We end the presentation by briefly introducing the Reissner-Mindlin plate model which is the analogue of the Timoshenko beam model.

4.3.1 The Kirchhoff plate bending model

We restrict our discussion to the linear model. Therefore the displacements are assumed infinitesimally small and equilibrium is enforced in the undeformed configuration. The plate is supposed to be thin, *i.e.*, h , the thickness,

is small compared to a characteristic geometric dimension L of the midsurface of the plate. Typically, Kirchhoff theory gives good predictions when $h/L < 1/20$.

Kinematics

The fundamental kinematic hypothesis of the model is that straight material lines which are initially orthogonal to the midsurface of the plate are also straight and orthogonal to the deformed midsurface. Additionally, the displacements in the transverse direction do not vary along the thickness of the plate.

We consider a generic plate described in Figure 4.92. Let P be a generic point on the midsurface and let P_z be a point on a straight line from P orthogonal to the midsurface. The coordinates of P are $(x, y, 0)$ and of P_z are (x, y, z) . Suppose that the plate deforms under the action of the transversely distributed load $p(x, y)$ which is given per unit of midsurface area. In Figure 4.93a and 4.93b we show the deformed and undeformed configurations of the plate in the xz and yz planes, respectively.

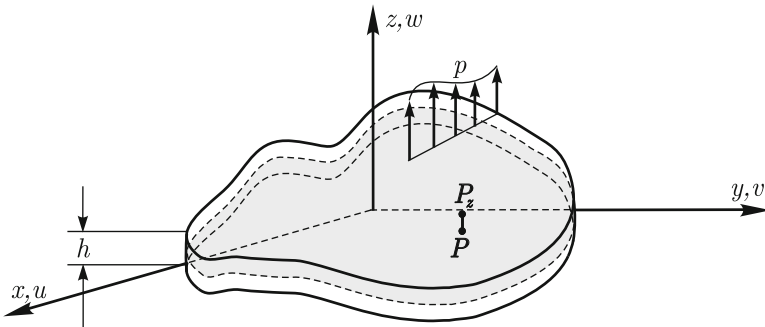


Fig. 4.92. Generic representation of a plate

Considering these definitions, the kinematic hypothesis translates into

$$w = w(x, y) \quad (4.244)$$

$$u = -z \frac{\partial w}{\partial x} \quad (4.245)$$

$$v = -z \frac{\partial w}{\partial y} \quad (4.246)$$

where we considered that the displacements are infinitesimally small.

Using the compatibility relations we obtain the strains

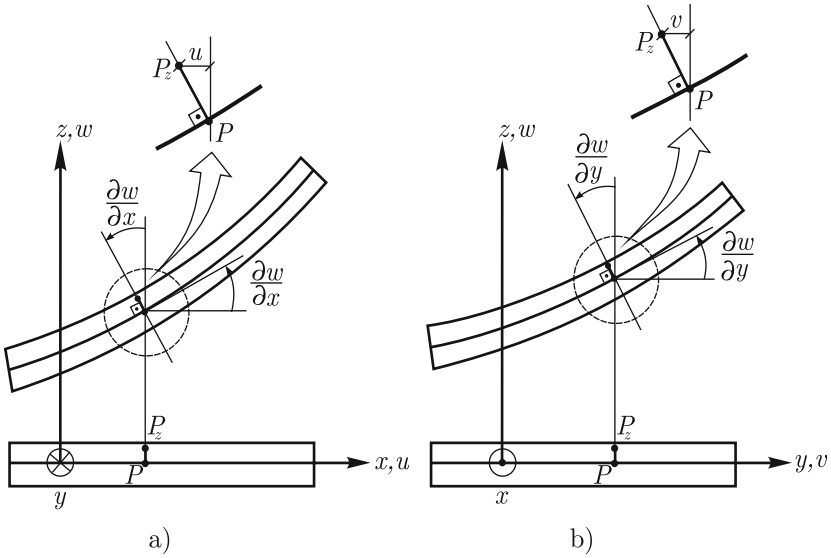


Fig. 4.93. Selected intersections of deformed and undeformed configurations of the plate with a vertical plane

$$\begin{aligned} \varepsilon_{xx} &= \frac{\partial u}{\partial x} = -z \frac{\partial^2 w}{\partial x^2} \\ \varepsilon_{yy} &= \frac{\partial v}{\partial y} = -z \frac{\partial^2 w}{\partial y^2} \\ \gamma_{xy} &= \frac{\partial u}{\partial y} + \frac{\partial v}{\partial x} = -2z \frac{\partial^2 w}{\partial x \partial y} \end{aligned}$$

and the remaining strain components are zero. We note that since we are considering infinitesimally small displacements the curvatures of the deformed midsurface are given by

$$\begin{aligned} \kappa_x &= \frac{\partial^2 w}{\partial x^2} \\ \kappa_y &= \frac{\partial^2 w}{\partial y^2} \\ \kappa_{xy} &= \frac{\partial^2 w}{\partial x \partial y} \\ \kappa_{yx} &= \kappa_{xy}. \end{aligned}$$

Constitutive equation

The theory assumes that the plate is composed of a stack of laminae, as schematically shown in Figure 4.94 for a part of the plate, and that each lamina is in a state of plane stress. Therefore

$$\tau_{xx} = \frac{E}{(1-\nu^2)} (\varepsilon_{xx} + \nu\varepsilon_{yy}) = -\frac{Ez}{(1-\nu^2)} \left(\frac{\partial^2 w}{\partial x^2} + \nu \frac{\partial^2 w}{\partial y^2} \right) \quad (4.247)$$

$$\tau_{yy} = \frac{E}{(1-\nu^2)} (\varepsilon_{yy} + \nu\varepsilon_{xx}) = -\frac{Ez}{(1-\nu^2)} \left(\frac{\partial^2 w}{\partial y^2} + \nu \frac{\partial^2 w}{\partial x^2} \right) \quad (4.248)$$

$$\tau_{xy} = \frac{E}{2(1+\nu)} \gamma_{xy} = -\frac{Ez}{(1+\nu)} \frac{\partial^2 w}{\partial x \partial y}. \quad (4.249)$$

Equations (4.247) to (4.249) show that the stresses vary linearly in the thickness direction.

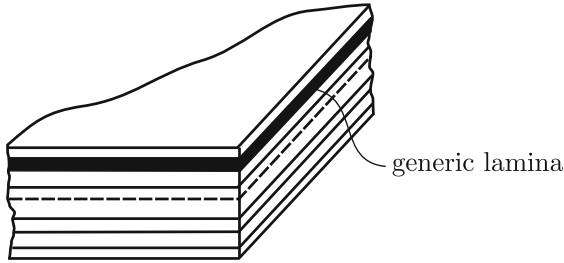


Fig. 4.94. Plate interpreted as a stack of laminae

Stress resultants

We extract a differential element from the plate and show in Figure 4.95a the stress distributions given by equations (4.247) to (4.249) when $\frac{\partial^2 w}{\partial x^2} > 0$, $\frac{\partial^2 w}{\partial y^2} > 0$ and $\frac{\partial^2 w}{\partial x \partial y} > 0$.

The moment resultant M_x per unit of length associated with the stress component τ_{xx} is

$$M_x = \int_{-h/2}^{+h/2} \tau_{xx}(-z) dz$$

where we use the same convention as for the beam: a positive value for the moment is associated with tension of the lower fibers, *i.e.*, below the midsurface of the plate. Using equation (4.247)

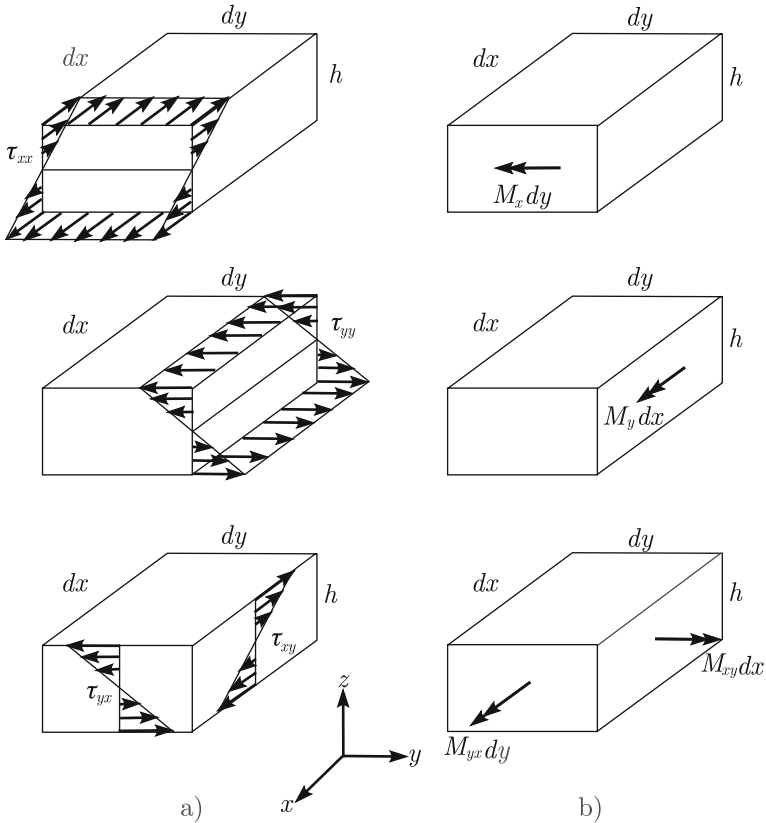


Fig. 4.95. Stress and stress resultant definitions; M_x, M_y and M_{yx} are positive whereas M_{xy} is negative for stresses shown

$$M_x = \frac{Eh^3}{12(1-\nu^2)} \left(\frac{\partial^2 w}{\partial x^2} + \nu \frac{\partial^2 w}{\partial y^2} \right) \tag{4.250}$$

and defining

$$D = \frac{Eh^3}{12(1-\nu^2)} \tag{4.251}$$

relation (4.250) becomes

$$M_x = D \left(\frac{\partial^2 w}{\partial x^2} + \nu \frac{\partial^2 w}{\partial y^2} \right). \tag{4.252}$$

Analogously, let M_y be the moment resultant per unit of length associated with τ_{yy} defined by

$$M_y = \int_{-h/2}^{+h/2} \tau_{yy} (-z) dz = D \left(\frac{\partial^2 w}{\partial y^2} + \nu \frac{\partial^2 w}{\partial x^2} \right). \tag{4.253}$$

Of course, both M_x and M_y are bending moments. Now let

$$M_{yx} = \int_{-h/2}^{+h/2} \tau_{yx}(-z) dz = D(1-\nu) \frac{\partial^2 w}{\partial x \partial y}. \quad (4.254)$$

We note that M_{yx} is a torsional moment per unit of length. This moment is also referred to as a twisting moment, and a positive value corresponds to the moment vector pointing out of the plate section on which the moment is acting. We also define

$$M_{xy} = \int_{-h/2}^{+h/2} \tau_{xy}z dz = -D(1-\nu) \frac{\partial^2 w}{\partial x \partial y} \quad (4.255)$$

where since $\tau_{xy} = \tau_{yx}$, we obtain

$$M_{yx} = -M_{xy}. \quad (4.256)$$

In Figure 4.95b we show the moments associated with the stress resultants defined above.

Equilibrium

The last requirement to be considered to complete the differential formulation is equilibrium. In Figure 4.96 we show the resultant forces and moments acting on a differential plate element which is shown twice in this figure merely for ease of visualization. We note that the shear resultants per unit of length, Q_x and Q_y , which are associated with the transverse shear stress components τ_{xz} and τ_{yz} respectively have been introduced. As for the shear force in the Bernoulli-Euler beam model, these shear forces do not enter the formulation through the constitutive relations since by the kinematic assumption the transverse shear strains are zero. However, they are required for equilibrium.

Imposing force equilibrium¹⁴ in the z direction, we obtain

$$-Q_x dy + \left(Q_x + \frac{\partial Q_x}{\partial x} dx \right) dy - Q_y dx + \left(Q_y + \frac{\partial Q_y}{\partial y} dy \right) dx + p dx dy = 0.$$

Simplifying the equation above, we arrive at

$$\frac{\partial Q_x}{\partial x} + \frac{\partial Q_y}{\partial y} = -p. \quad (4.257)$$

¹⁴ Note that the sign convention for the transverse shear force of plates and shells is here opposite to the convention used for beams. This sign convention for plates and shells is more natural considering the usual 3-D definition of strains, see Section 4.3.2

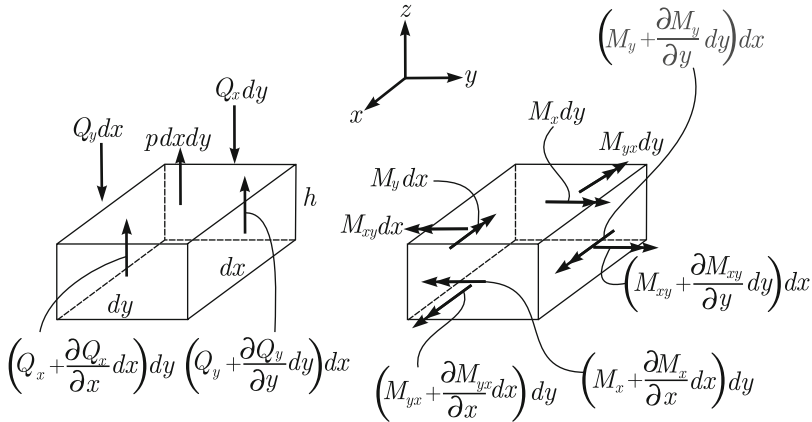


Fig. 4.96. Forces acting on a differential plate element.

Neglecting infinitesimals of higher-order, moment equilibrium about the x axis leads to

$$(Q_y dx) dy - M_y dx + \left(M_y + \frac{\partial M_y}{\partial y} dy \right) dx - M_{yx} dy + \left(M_{yx} + \frac{\partial M_{yx}}{\partial x} dx \right) dy = 0$$

which upon simplification gives

$$\frac{\partial M_y}{\partial y} + \frac{\partial M_{yx}}{\partial x} = -Q_y. \tag{4.258}$$

Finally, moment equilibrium in the y direction yields

$$-(Q_x dy) dx + M_x dy - \left(M_x + \frac{\partial M_x}{\partial x} dx \right) dy - M_{xy} dx + \left(M_{xy} + \frac{\partial M_{xy}}{\partial y} dy \right) dx = 0$$

$$\frac{\partial M_x}{\partial x} - \frac{\partial M_{xy}}{\partial y} = -Q_x. \tag{4.259}$$

Differential formulation

Summarizing, all requirements have been imposed, namely, compatibility (equations (4.244) to (4.246)), constitutive relations (equations (4.247) to (4.249)) and equilibrium (equations (4.257) to (4.259)). Therefore the differential equations of the Kirchhoff plate bending model were obtained.

It is usual to cast the complete formulation in terms of the transverse displacement $w(x, y)$ which is the only independent kinematic variable. For

that we take derivatives of equation (4.258) with respect to y and of (4.259) with respect to x , sum them and use equation (4.257) to obtain

$$\frac{\partial^2 M_x}{\partial x^2} - 2 \frac{\partial^2 M_{xy}}{\partial x \partial y} + \frac{\partial^2 M_y}{\partial y^2} = p. \quad (4.260)$$

We have also used that $M_{xy} = -M_{yx}$ to arrive at equation (4.260). Substituting (4.253), (4.254) and (4.255) into (4.260), we obtain

$$\frac{\partial^4 w}{\partial x^4} + 2 \frac{\partial^4 w}{\partial x^2 \partial y^2} + \frac{\partial^4 w}{\partial y^4} = \frac{p}{D} \quad (4.261)$$

which is known as the Lagrange equation for the plate bending problem.

We note that the interpretation of D as the flexural rigidity of the plate is now obvious. We also remark that when equation (4.261) subjected to the appropriate boundary conditions is solved, *i.e.*, $w(x, y)$ is determined, the complete solution is known since we can obtain the stresses, strains and resultant forces from the transverse displacement field as shown in the equations above. Even the transverse shear forces which are not obtained from the constitutive relations can be calculated from the transverse displacements (as for the Bernoulli-Euler beam model). Namely, substituting the expressions for the moments in terms of the transverse displacements (equations (4.250), (4.252) and (4.254) into equations (4.258) and (4.259)), we obtain

$$Q_x = -D \frac{\partial}{\partial x} \left(\frac{\partial^2 w}{\partial x^2} + \frac{\partial^2 w}{\partial y^2} \right) \quad (4.262)$$

and

$$Q_y = -D \frac{\partial}{\partial y} \left(\frac{\partial^2 w}{\partial x^2} + \frac{\partial^2 w}{\partial y^2} \right). \quad (4.263)$$

Boundary conditions

Let us examine very briefly the boundary conditions for the Kirchhoff model. Consider an edge, parallel to the y axis and therefore given by $x = a$.

The *clamped* or *built-in* condition corresponds to imposing that the transverse displacements and the rotations about the y axis of material lines, such as AB shown in Figure 4.97, are zero. Therefore, the boundary conditions are given by

$$w|_{x=a} = 0 \quad \text{and} \quad \left. \frac{\partial w}{\partial x} \right|_{x=a} = 0.$$

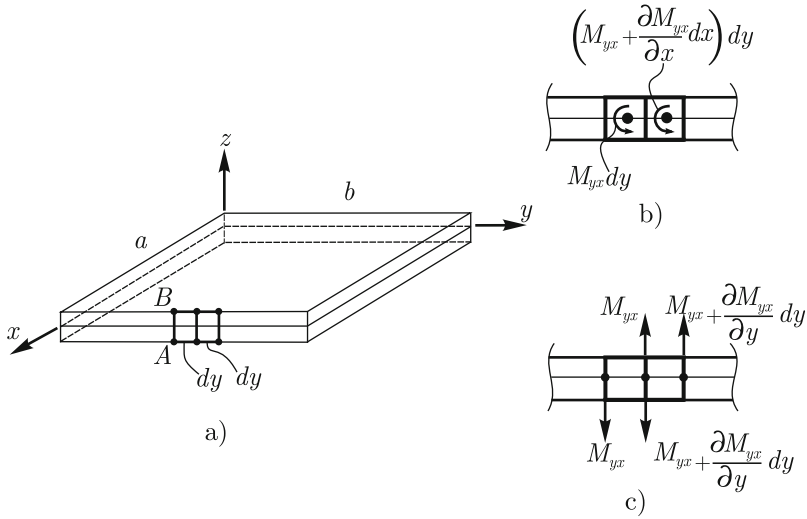


Fig. 4.97. Some definitions for a rectangular plate

Note that the condition on the rotation is imposed taking into account the kinematic assumption of the model.

Considering the *simply supported* condition, the transverse displacement should be restrained. For additional conditions, we observe that there are no kinematic restraints affecting the rotation about the y axis of material lines such as AB (see Figure 4.97), and there are no normal stresses τ_{xx} acting on the plate end section defined at $x = a$. Hence $M_x = 0$ at $x = a$. Summarizing, the two boundary conditions that represent the simply supported edge are

$$w|_{x=a} = 0 \tag{4.264}$$

and

$$M_x|_{x=a} = 0. \tag{4.265}$$

The last condition can also be expressed in terms of displacements when we consider equation (4.250) leading to

$$\frac{\partial^2 w}{\partial x^2} + \nu \frac{\partial^2 w}{\partial y^2} \Big|_{x=a} = 0$$

and because of (4.264) $\frac{\partial^2 w}{\partial y^2} \Big|_{x=a} = 0$, condition (4.265) becomes

$$\frac{\partial^2 w}{\partial x^2} \Big|_{x=a} = 0.$$

The last boundary condition to consider is the *free edge* condition. Since there are no kinematic restraints in this case, there are no stresses acting on

the plate end section defined by $x = a$. The stress components which could possibly act on this edge section are τ_{xx} , τ_{yx} and τ_{zx} . These components are associated with the stress resultants M_x , M_{yx} and Q_x . If we would enforce the condition that these stress resultants are zero, we would obtain three boundary conditions instead of the two obtained in the case of the clamped and the simply supported edges. Historically, this apparent inconsistency was object of much controversy. Mathematically, considering the order of the differential equation (4.261), only two conditions are required per edge. It was shown that one condition is given by $M_x|_{x=a} = 0$ and the second involves a combination of the stress resultants M_{yx} and Q_x . Kelvin and Tait (see Timoshenko and Woinowsky-Krieger, 1959) gave a mechanical interpretation of this second condition that we discuss below.

Consider two generic differential elements of the edge section shown in Figure 4.97a. In Figure 4.97b, the twisting moment resultant acting on these two differential elements are shown. Each of these moments are represented in Figure 4.97c by a mechanically equivalent force couple. Therefore, we can see that the twisting moment distribution acting at the edge can be represented by a mechanically equivalent distribution of shear forces given by

$$Q'_x = \frac{M_{yx} - \left(M_{yx} + \frac{\partial M_{yx}}{\partial y} dy \right)}{dy} \Bigg|_{x=a} = - \frac{\partial M_{yx}}{\partial y} \Bigg|_{x=a}.$$

The net shear force distribution V_x considering both Q_x and Q'_x is then given by

$$V_x = Q_x|_{x=a} + Q'_x = \left(Q_x - \frac{\partial M_{yx}}{\partial y} \right) \Bigg|_{x=a}$$

and the boundary condition for the free edge which combines both effects of Q_x and M_{yx} is

$$V_x = \left(Q_x - \frac{\partial M_{yx}}{\partial y} \right) \Bigg|_{x=a} = 0.$$

This condition can be expressed in terms of displacements. Using relations (4.254) and (4.262), we obtain

$$\left(\frac{\partial^3 w}{\partial x^3} \right) + (2 - \nu) \left(\frac{\partial^3 w}{\partial x \partial y^2} \right) \Bigg|_{x=a} = 0. \quad (4.266)$$

Below we show a sample solution of a classical plate bending problem.

Example 4.18

Find the solution for the rectangular plate problem of Figure 4.97a when the plate is simply supported at the four edges and subjected to a distributed pressure $p = p(x, y)$. Particularize the solution for $p(x, y) = p_0$.

Solution

The boundary conditions can be derived generalizing those for the simply supported edge studied above when we consider the four plate edges. Then, we obtain

$$w|_{x=0} = 0, \quad \left. \frac{\partial^2 w}{\partial x^2} \right|_{x=0} = 0 \quad (4.267)$$

$$w|_{y=0} = 0, \quad \left. \frac{\partial^2 w}{\partial y^2} \right|_{y=0} = 0 \quad (4.268)$$

$$w|_{x=a} = 0, \quad \left. \frac{\partial^2 w}{\partial x^2} \right|_{x=a} = 0 \quad (4.269)$$

$$w|_{y=b} = 0, \quad \left. \frac{\partial^2 w}{\partial y^2} \right|_{y=b} = 0. \quad (4.270)$$

We use a classical approach to derive solutions for plate bending problems which is to use a Fourier series to construct solutions.

Assume

$$w(x, y) = \sum_{m=1}^{\infty} \sum_{n=1}^{\infty} w_{mn} \sin \frac{m\pi x}{a} \sin \frac{n\pi y}{b}. \quad (4.271)$$

We can write (4.271) since it is a mathematical fact that every smooth function defined on a 2-D domain can be expanded in a Fourier series as above. The fundamental property is that given this particular functional form for $w(x, y)$, there exist constant coefficients w_{mn} such that if the double sum is performed up to m and n high enough, such sum will be arbitrarily close¹⁵ to $w(x, y)$.

Hence, our task is to determine the coefficients w_{mn} such that the sum given in (4.271) satisfies equation (4.261) and the boundary conditions given in equations (4.267) to (4.270). In fact, the Fourier series given in (4.271) was constructed such that it satisfies the boundary conditions independently of the values of w_{mn} . This property can be easily verified by checking that $w(x, y)$ written in the form of (4.271) satisfies conditions (4.267) to (4.270). In order to determine specific coefficients w_{mn} the load $p(x, y)$ should be characterized.

Given a smooth load distribution $p(x, y)$, it can also be expanded in a Fourier series as

$$p(x, y) = \sum_{m=1}^{\infty} \sum_{n=1}^{\infty} p_{mn} \sin \frac{m\pi x}{a} \sin \frac{n\pi y}{b} \quad (4.272)$$

¹⁵ Of course, what we mean by arbitrarily close can be made mathematically precise, see Chapelle and Bathe, 2010a. However, for our present purposes the intuitive idea of this concept suffices

where

$$p_{mn} = \frac{4}{ab} \int_0^a \int_0^b p(x, y) \sin \frac{m\pi x}{a} \sin \frac{n\pi y}{b} dx dy. \quad (4.273)$$

Substituting (4.271) and (4.272) into (4.261), and, of course, performing the derivatives involved, we obtain

$$\begin{aligned} & \sum_{m=1}^{\infty} \sum_{n=1}^{\infty} \left(\frac{m^4}{a^4} + \frac{2m^2n^2}{a^2b^2} + \frac{n^4}{b^4} \right) \pi^4 w_{mn} \sin \frac{m\pi x}{a} \sin \frac{n\pi y}{b} \\ &= \frac{1}{D} \sum_{m=1}^{\infty} \sum_{n=1}^{\infty} p_{mn} \sin \frac{m\pi x}{a} \sin \frac{n\pi y}{b}. \end{aligned}$$

Since the coefficients of the series on the left- and right-hand sides of the above equation should be the same, we obtain

$$w_{mn} = \frac{p_{mn}}{\pi^4 D \left(\frac{m^4}{a^4} + \frac{2m^2n^2}{a^2b^2} + \frac{n^4}{b^4} \right)}$$

and hence

$$w(x, y) = \frac{1}{\pi^4 D} \sum_{m=1}^{\infty} \sum_{n=1}^{\infty} \frac{p_{mn}}{\left(\frac{m^2}{a^2} + \frac{n^2}{b^2} \right)^2} \sin \frac{m\pi x}{a} \sin \frac{n\pi y}{b}. \quad (4.274)$$

When the load is uniform, *i.e.*, $p(x, y) = p_0$, we obtain from equation (4.273)

$$p_{mn} = \frac{16p_0}{\pi^2 mn} \quad m, n = 1, 3, 5, \dots$$

and $p_{mn} = 0$ for m or n an even number. Hence, from (4.274) we can write the solution as

$$w(x, y) = \frac{16p_0}{\pi^6 D} \sum_{m=1}^{\infty} \sum_{n=1}^{\infty} \frac{\sin \frac{m\pi x}{a} \sin \frac{n\pi y}{b}}{mn \left(\frac{m^2}{a^2} + \frac{n^2}{b^2} \right)^2}$$

where $m = 1, 3, 5, \dots$ and $n = 1, 3, 5, \dots$

As a historical remark, we note that it was Navier who first proposed this Fourier series solution for plate bending problems (see Timoshenko and Woinowsky-Krieger, 1959).

Of course, having evaluated $w(x, y)$ all stresses and stress resultants can be obtained.

□

Plate bending behavior

In the introductory part of this section we interpreted the gross behavior of a rectangular plate as being captured by orthogonal bars in bending (see Figure 4.91). Our objective here is to obtain further insight into the plate resisting mechanisms.

Consider a rectangular simply supported plate. Let us examine the behavior of the plate when modeled by bars of rectangular cross-sections as those shown in Figure 4.9. Considering a bar with axis parallel to the global x axis, we see that besides the moment M_x and the shear force Q_x which are directly associated with the bending of this beam (refer to equations (4.147) and (4.142)), torsional moments M_{xy} and the shear forces Q_y acting on the lateral faces of this beam contribute to its equilibrium.

To obtain insight into how these effects stiffen the plate when equilibrium and compatibility are imposed, we consider the structure of Figure 4.98a subjected to a uniform transverse load.

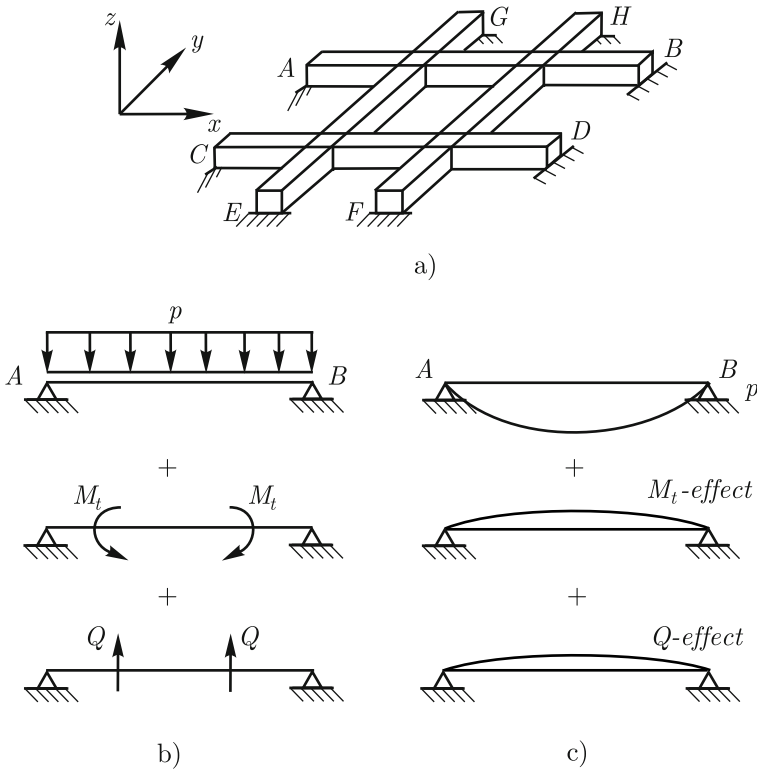


Fig. 4.98. Qualitative behavior of a rectangular plate based on a grid analogy

In Figure 4.98b, we show the actions onto bar AB . Besides the transverse load p , there are two additional contributions. The loads Q are a result of the compatibility of transverse displacements and represent the effect of the orthogonal beams working in bending. The moments M_t are a result of the compatibility of rotations. Namely, the section rotations of beam AB due to the transverse load induce rotations and torsion in the bars EG and FH . The sense of M_t indicated in Figure 4.98b reflects the fact that the bars EG and FH oppose the rotations due to the transverse load on the bar AB . Finally, in Figure 4.98c, we show, qualitatively, the transverse displacements induced by each load including the stiffening effect due to the M_t and Q effects.

Consider the rectangular plate in Figure 4.97. Let us examine the behavior of the plate as the relative size of the edges changes, *i.e.*, the relation a/b varies. Supposing that a/b is large, say $a/b > 5$, we show qualitatively in Figure 4.99 the deformations of two orthogonal slices of the midsurface. If we examine the contribution due to bending to equilibrate the transverse load, we conclude that the longer beam carries almost no loading, since for a simply supported beam the transverse stiffness is inversely proportional to L^3 where L is the beam length. Therefore, for a large portion of the plate, *i.e.*, the central part, away from the shorter edges, the resisting behavior corresponds to the bending along the short span and the plate behaves as a beam of large width. We note that the contribution of torsion for this part is also very small since $\frac{\partial^2 w}{\partial x \partial y}$ is close to zero and, hence, from equation (4.254), M_{xy} is very small. In fact, if we consider a plate infinitely long in the x direction, the deformation of the midsurface will be cylindrical (the end effects are at infinity), and $w = w(y)$. Hence $\frac{\partial^4 w}{\partial x^4} = 0$ and $\frac{\partial^4 w}{\partial x^2 \partial y^2} = 0$, and equation (4.261) becomes

$$\frac{d^4 w}{dy^4} = \frac{p}{D}$$

where, in essence, a beam of unit width is considered (see (4.136)). However, we use $D = E_* I$ with $E_* = E / (1 - \nu^2)$. Hence, a planar beam under plane strain conditions (refer to equation (4.58)) is solved (since anticlastic curvature is not allowed, see Figure 3.62). From a design perspective, it is relevant to note that for $a/b = 2$ the error incurred in assuming a large width beam behavior of the plate is of the order of 6.5%. Of course, this error decreases as a/b increases.

4.3.2 The Reissner-Mindlin plate bending model

As we mentioned, the Reissner-Mindlin plate model is the analogue of the Timoshenko beam model. This analogy is based on the kinematic hypothesis which includes modeling of transverse shear deformations. Hence, the Reissner-Mindlin model is adequate to model not only thin plates but also those which are moderately thick. All the assumptions used in the Kirchhoff model concerning linear analysis are also adopted here.

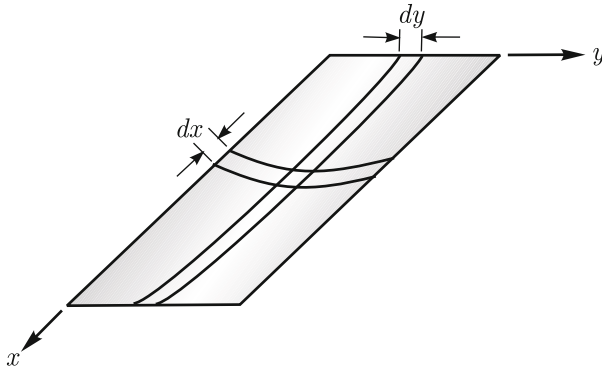


Fig. 4.99. Deformation of simply supported plate under uniform pressure for large a/b

Kinematics

The fundamental kinematic hypothesis of the model is that straight material lines which are initially orthogonal to the midsurface of the plate remain straight but not necessarily orthogonal to the deformed midsurface. Of course, we use the geometric and loading characterization of Figure 4.92, and Figure 4.100 is analogous to 4.93, but considering the kinematics of the Reissner-Mindlin model.

Note that $\beta_x(x, y)$ and $\beta_y(x, y)$ characterize the rotation of the material lines which are initially orthogonal to the midsurface. Again, we assume

$$w = w(x, y)$$

and referring to Figure 4.100, we can write

$$u = -z\beta_x(x, y)$$

$$v = -z\beta_y(x, y).$$

Therefore $w(x, y)$, $\beta_x(x, y)$ and $\beta_y(x, y)$ – all referred to the midsurface – are the three independent degrees of freedom of the model and completely characterize the displacement field.

Considering the strain compatibility relations, we can write

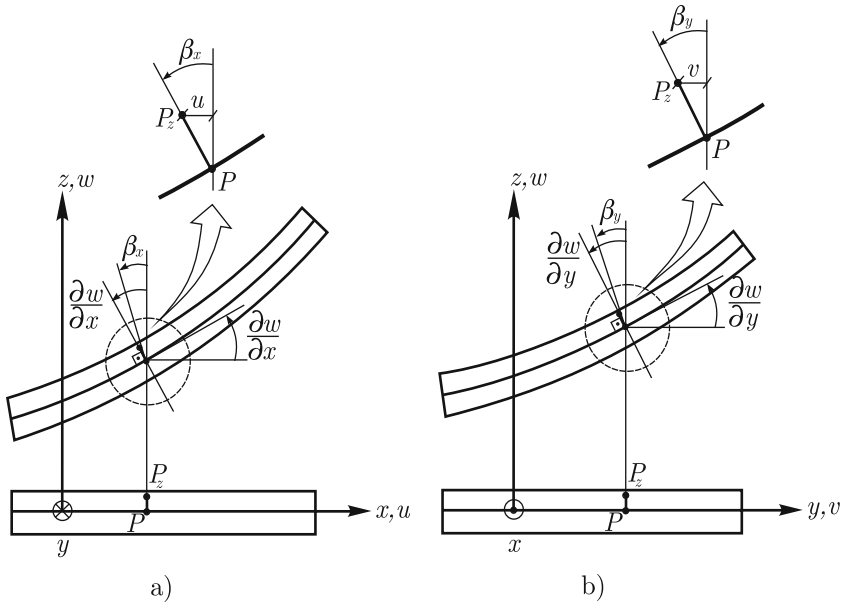


Fig. 4.100. Selected intersections of deformed and undeformed configurations of plate with a vertical plane. Reissner-Mindlin model

$$\begin{aligned} \varepsilon_{xx} &= \frac{\partial u}{\partial x} = -z \frac{\partial \beta_x}{\partial x} \\ \varepsilon_{yy} &= \frac{\partial v}{\partial y} = -z \frac{\partial \beta_y}{\partial y} \\ \gamma_{xy} &= \frac{\partial u}{\partial y} + \frac{\partial v}{\partial x} = -z \left(\frac{\partial \beta_x}{\partial y} + \frac{\partial \beta_y}{\partial x} \right) \\ \gamma_{xz} &= \frac{\partial u}{\partial z} + \frac{\partial w}{\partial x} = \frac{\partial w}{\partial x} - \beta_x \\ \gamma_{yz} &= \frac{\partial v}{\partial z} + \frac{\partial w}{\partial y} = \frac{\partial w}{\partial y} - \beta_y \end{aligned}$$

and $\varepsilon_{zz} = 0$.

Constitutive equation

The mechanical hypothesis of the Kirchhoff model assuming a plane stress condition of each lamina is used. Therefore

$$\begin{aligned}\tau_{xx} &= \frac{E}{(1-\nu^2)}(\varepsilon_{xx} + \nu\varepsilon_{yy}) = -\frac{Ez}{(1-\nu^2)}\left(\frac{\partial\beta_x}{\partial x} + \nu\frac{\partial\beta_y}{\partial y}\right) \\ \tau_{yy} &= \frac{E}{(1-\nu^2)}(\varepsilon_{yy} + \nu\varepsilon_{xx}) = -\frac{Ez}{(1-\nu^2)}\left(\frac{\partial\beta_y}{\partial y} + \nu\frac{\partial\beta_x}{\partial x}\right) \\ \tau_{xy} &= \frac{E}{2(1+\nu)}\gamma_{xy} = -\frac{Ez}{2(1+\nu)}\left(\frac{\partial\beta_x}{\partial y} + \frac{\partial\beta_y}{\partial x}\right).\end{aligned}$$

Additionally, we have the transverse shear relations which using the generalized Hooke's law can be written as

$$\begin{aligned}\tau_{xz} &= G\gamma_{xz} = G\left(\frac{\partial w}{\partial x} - \beta_x\right) = \frac{E}{2(1+\nu)}\left(\frac{\partial w}{\partial x} - \beta_x\right) \\ \tau_{yz} &= G\gamma_{yz} = G\left(\frac{\partial w}{\partial y} - \beta_y\right) = \frac{E}{2(1+\nu)}\left(\frac{\partial w}{\partial y} - \beta_y\right).\end{aligned}$$

Stress resultants

The stress resultants are the same as those of the Kirchhoff model and the relations between the stress resultants and the kinematic variables are

$$\begin{aligned}M_x &= D\left(\frac{\partial\beta_x}{\partial x} + \nu\frac{\partial\beta_y}{\partial y}\right) \\ M_y &= D\left(\frac{\partial\beta_y}{\partial y} + \nu\frac{\partial\beta_x}{\partial x}\right) \\ M_{yx} &= -M_{xy} = D\frac{(1-\nu)}{2}\left(\frac{\partial\beta_x}{\partial y} + \frac{\partial\beta_y}{\partial x}\right) \\ Q_x &= kGA\left(\frac{\partial w}{\partial x} - \beta_x\right) \\ Q_y &= kGA\left(\frac{\partial w}{\partial y} - \beta_y\right)\end{aligned}$$

where we have introduced the shear correction factor k which was defined for the Timoshenko beam model, see (4.235). Note that in the Reissner-Mindlin model the shear forces are obtained through the constitutive relations.

Equilibrium

The equilibrium conditions are those of the Kirchhoff model and are given by (4.257) to (4.259).

Boundary conditions

We note that due to the more general kinematic description in the Reissner-Mindlin model, we have three conditions to specify. As in the Kirchhoff model, let us examine the boundary conditions for an edge parallel to the y axis, *i.e.*, given by $x = a$.

For the *clamped* or *built-in* edge, we need to prevent the transverse displacements w and the rotation about the y axis of material lines such as AB of Figure 4.97. Therefore

$$w|_{x=a} = 0 \quad \text{and} \quad \beta_x|_{x=a} = 0.$$

Depending on the physical situation, these material lines such as AB may also be prevented to rotate about the x axis. Therefore, we either impose

$$\beta_y|_{x=a} = 0 \tag{4.275}$$

or

$$M_{yx}|_{x=a} = 0. \tag{4.276}$$

If we prevent the rotation β_y we have the “hard” condition and if we impose M_{yx} to be zero we have the “soft” condition.

For the *simply supported* edge, we would have

$$w|_{x=a} = 0 \quad \text{and} \quad M_x|_{x=a} = 0.$$

The third condition is also given by (4.275) and (4.276). Again (4.275) is called the “hard” condition while (4.276) is called the “soft” condition.

Finally, for the *free edge*, we have

$$M_x|_{x=a} = 0 \quad \text{and} \quad Q_x|_{x=a} = 0.$$

and either (4.275) or (4.276). Of course, if for our physical situation the plate section given by $x = a$ is stress free, then $M_{yx} = 0$ is the appropriate condition.

We note that, as we now have three independent kinematic variables, the free edge condition can be imposed in a more natural way than in the Kirchhoff model.

The differential formulation of the Reissner-Mindlin model is now complete since the compatibility, constitutive behavior, equilibrium and boundary conditions have been considered. Of course, the governing equations can be algebraically manipulated to arrive at a set of equations which are more convenient for the derivation of closed form solutions, but this is not our objective here.

The Reissner-Mindlin model is a hierarchically higher-order model when compared to the Kirchhoff model. One of the reasons is that it predicts transverse shear deformations. A less obvious improvement, which requires a more

detailed study of the Reissner-Mindlin model (see Häggblad and Bathe, 1990), is given by the nature of the solution close to the boundaries. There is a region near the boundary – referred to as the boundary layer region – where the solution for the stress resultants may vary significantly.

In order to obtain more insight into this boundary layer behavior, while examining a situation of engineering interest, let us study the shear force at an edge of a simply supported plate subjected to a constant uniform pressure. Considering the Kirchhoff model, there are two contributions: the force Q_x and that due to the rate of change of the twisting moment, *i.e.*, $Q'_x = -\frac{\partial M_{yx}}{\partial y}\Big|_{x=a}$ as discussed above. The actual values along the edges can be obtained from the solution $w(x, y)$, discussed in Example 4.18, using relations (4.254) and (4.262). In Figure 4.101a, we show these shear force contributions.

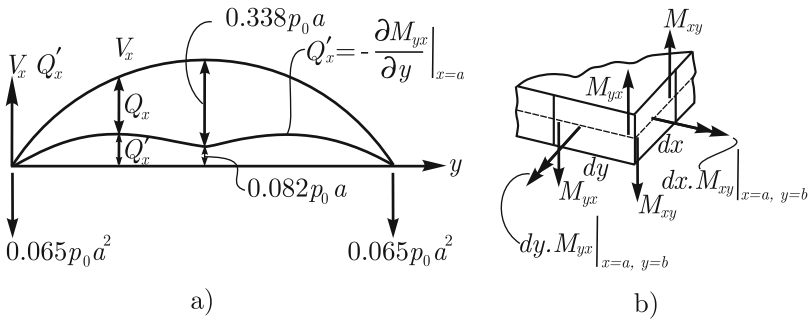


Fig. 4.101. Shear related quantities at edge of simply supported plate

If we refer to Figure 4.97 and, in particular, to Figure 4.97c we see that the shear force contribution given by $Q'_x = -\frac{\partial M_{yx}}{\partial y}\Big|_{x=a}$ is due to the balance of forces of two neighboring differential elements, not at a corner of the plate. That is, if we consider the differential element at the corner, such balance is no longer valid. In Figure 4.101b, we show the corner region. Here a concentrated reactive transverse force R is required for equilibrium

$$R = (M_{yx} - M_{xy})\Big|_{x=a, y=b} = 2M_{yx}\Big|_{x=a, y=b} = 2D(1 - \nu) \frac{\partial^2 w}{\partial x \partial y}\Big|_{x=a, y=b}.$$

In Figure 4.101a these reactions are shown for both corners. We note that these reactions and also the shear forces are those compatible with $p(x, y) = -p_0$, *i.e.*, with a constant distributed load of intensity p_0 acting downwards. A physical interpretation of the concentrated corner reaction is that the simply supported plate subjected to $p(x, y) = -p_0$, unless held down, would lift up at its corners.

Now, considering the Reissner-Mindlin model, we need first to decide if we impose hard or soft conditions. If we admit that the kinematic restraints are such that the material lines orthogonal to the midsurface along the edge given by $x = a$ can not rotate around the x axis, *i.e.*, $\beta_y = 0$ (hard condition), then we would obtain a distribution of reactive twisting moments M_{yx} which is equivalent to that of Kirchhoff theory. Also, the Q_x would be that of Kirchhoff theory and there would be no reactions at the corner ($R = 0$).

If we impose soft conditions, $M_{yx}|_{x=a} = 0$, we obtain the distribution of shear forces Q_x shown in Figure 4.102. We can see that the distribution of shear forces near the center tends to that of Kirchhoff theory which includes the effect of the torsional moment. As we approach a corner, the Reissner-Mindlin shear force inverts sense. There is no concentrated force at the corner

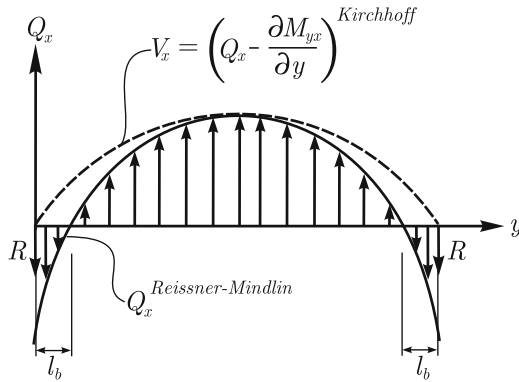


Fig. 4.102. Shear forces along simply supported edge for Kirchhoff and Reissner-Mindlin models

for the Reissner-Mindlin model and that shown in Figure 4.102 is from the Kirchhoff model.

Only from equilibrium considerations, we can conclude that V_x and R from the Kirchhoff model and Q_x from the Reissner-Mindlin model lead to the same resultant since they should equilibrate the same externally applied load. In other words, the corner concentrated reaction R of the Kirchhoff model is distributed along some distance from the corner as part of Q_x of the Reissner-Mindlin model. The magnitude of this distance depends on h/L . The situation shown in Figure 4.102 corresponds to a ratio h/L of the order of $1/10$. The quantity ℓ_b represents the length of the boundary layer. As the ratio h/L decreases ℓ_b also decreases and when h/L tends to zero, we approach the concentrated force situation predicted by the Kirchhoff model. We can clearly see, from the discussion above, that the Reissner-Mindlin model is a hierarchically higher-order model with respect to the Kirchhoff model regarding also the shear force predictions. Additional results regarding

boundary layers in Reissner-Mindlin plates can be found in Häggblad and Bathe, 1990 and Arnold and Falk, 1990.

4.4 Shells

Shell structures comprise a very broad subject. On the one hand, there is a wealth of nature and man made shells. The reader may easily list a number of shell structures. Examples are many, covering a wide range of length scales. We could mention microscopic living cells, sea shells, egg shells, human skulls, biomedical devices, ship hulls, aircraft fuselages, car bodies, roofs, among many others. On the other hand, there is a vast literature on this subject ranging from shell structural behavior to the analysis and design of shells. Therefore, we first would like to mention our objectives in this section.

Our aim is to present an introductory discussion of shell structures focused on basic structural behavior. We would like to help the reader to acquire some elementary understanding of the issues in shell models and to gain insight into expected shell behavior. This knowledge is very valuable when modeling shells. Of course, we suppose that the shell model solutions will be obtained by using finite element methods. Therefore, no emphasis is given to obtaining analytical solutions to shell mathematical models. The very few solutions that will be presented are given to obtain some basic understanding.

A shell structure is geometrically characterized by a thin solid whose domain is defined by a curved midsurface and a thickness h . The shell is acted upon by surface tractions and body forces and is kinematically supported, usually along part or all of its periphery. A generic shell is schematically described in Figure 4.103.

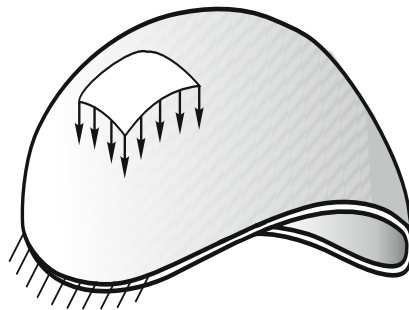


Fig. 4.103. A typical shell structure

The thickness h is supposed to be small. However, not too small that it would prevent the shell to sustain some level of compression and bending. In other words, we are not considering a membrane.

Below we discuss some basic geometrical facts required to introduce shell models. Next, we present an introductory discussion on shell mathematical models and on the formulation of the membrane-bending model. This formulation is then detailed for a class of problems – shells of revolution loaded axisymmetrically – and a few illustrative problems are solved.

4.4.1 Geometrical preliminaries

Let us consider a generic surface S . Let P be a point on the surface and \mathbf{n} be the unit normal to S at P . Let π be a plane which contains \mathbf{n} . The intersection of this plane with the surface gives a curve C_π . These definitions are shown in Figure 4.104.

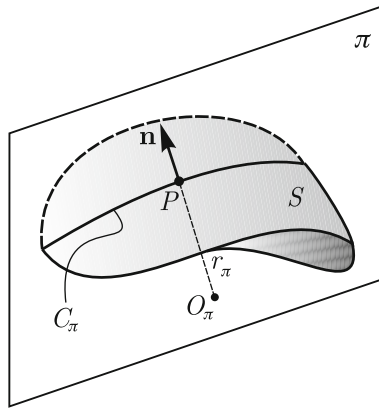


Fig. 4.104. Generic intersecting curve of surface S at point P

Considering the plane π , the curvature κ_π and the radius of curvature r_π at point P are well defined. We can also determine the center of curvature O_π for the curve C_π . Of course, there are infinitely many planes that contain the normal \mathbf{n} and for each of these planes we can characterize the intersecting curve and the associated curvature definitions.

It is always possible to determine the maximum and minimum values for the curvatures and radii of curvatures at a point, κ_1 , r_1 and κ_2 , r_2 which are called the principal curvatures and principal radii of curvatures. The planes associated with these extreme values are orthogonal to each other (see Chapelle and Bathe, 2010a).

An important geometrical quantity is the Gaussian curvature κ_G defined at a point by

$$\kappa_G = \kappa_1 \kappa_2.$$

There are important geometric properties associated with the algebraic value of κ_G . When $\kappa_G > 0$ all the centers of curvatures of the intersecting curves

are located on the same side of the tangent plane at that point, and the shell surface is called an *elliptic surface*. A dome like surface has this property for all points (see Figure 4.105).

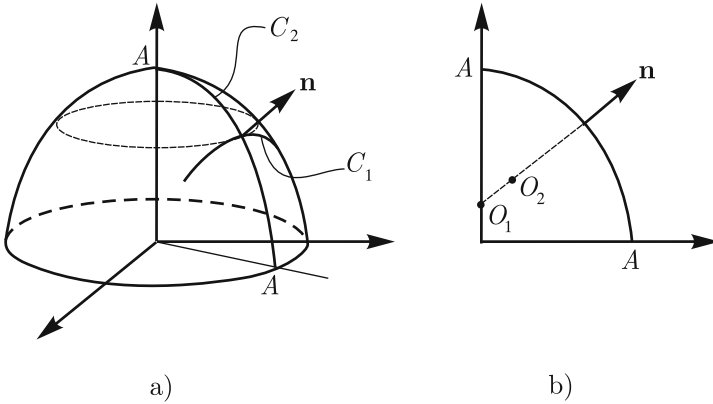


Fig. 4.105. Intersecting curves and centers of curvatures of the midsurface of a dome like structure; elliptic surface

When $\kappa_G < 0$ there are intersecting curves with centers of curvatures on opposite sides of the tangent plane at P , and the shell surface is called a *hyperbolic surface*. A saddle like surface is such an example as shown in Figure 4.106.

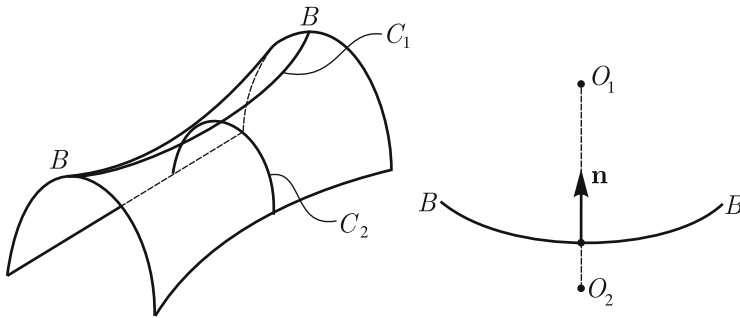


Fig. 4.106. Intersecting curves and centers of curvature for a saddle like surface; hyperbolic surface

Finally, $\kappa_G = 0$ corresponds to a surface with at least one curvature equal to zero (like for a cylinder or plate), and the shell surface is called a *parabolic surface*.

Therefore the algebraic value of κ_G helps to locally characterize a surface. Besides that, the algebraic value of κ_G of shell midsurfaces is one of the factors that greatly influences shell structural behavior.

4.4.2 Shell mathematical models

The particular choice of kinematic and mechanical hypotheses characterizes a given shell mathematical model. We adopt here the terminology used in Chapelle and Bathe, 2010a for the definitions of the mathematical models. There are two basic hypotheses which pertain to most shell mathematical models.

Kinematic hypothesis: Straight fibers initially orthogonal to the midsurface remain straight and unstretched during deformation. This kinematic assumption is called the Reissner-Mindlin kinematic assumption.

Mechanical hypothesis: The stress in the direction normal to the midsurface is zero.

The model characterized by these two assumptions is termed the *basic shell model*. While the displacement and rotation variables are referred to the shell midsurface, the strains and stresses of the *basic shell model* are given as for the 3-D continuum. When additional assumptions allow the analytical integration through the shell thickness, in a similar way as detailed for plates, the model is called the *shear-membrane-bending shell model* since these three behaviors can potentially arise.

When the kinematic hypothesis is stronger and it is further assumed that the straight lines initially orthogonal to the midsurface remain orthogonal to the midsurface after deformation, we have the *membrane-bending shell model* since transverse shear deformations are precluded. This kinematic hypothesis is known as the Kirchhoff-Love kinematic assumption, Love, 1934. We discuss below the membrane-bending shell model.

The membrane-bending shell model

Historically, this is an early shell model proposed; it is referred to as a classical shell model. There are many contributions associated with this model. Our presentation is closely based on the classical book of Timoshenko and Woinowsky-Krieger, 1959.

Stress resultants

Let us consider a generic point O on the midsurface of the shell. We choose a local Cartesian coordinate system such that z has the same direction as the normal at O and x and y are defined such that xz and yz are the planes associated with the principal curvatures at O . Let r_x and r_y be the principal

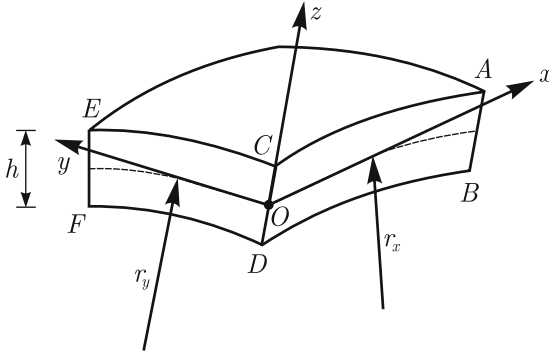


Fig. 4.107. A part extracted from the shell; r_x and r_y are radii of principal curvatures

radii of curvatures at O corresponding to the planes xz and yz respectively. In Figure 4.107, we show a differential element of the shell. The stress resultants per unit of length of coordinates along the midsurface acting on planes xz and yz are

$$N_x = \int_{-h/2}^{+h/2} \tau_{xx} \left(1 + \frac{z}{r_y} \right) dz \quad (4.277)$$

$$N_y = \int_{-h/2}^{+h/2} \tau_{yy} \left(1 + \frac{z}{r_x} \right) dz \quad (4.278)$$

$$N_{xy} = \int_{-h/2}^{+h/2} \tau_{xy} \left(1 + \frac{z}{r_x} \right) dz \quad (4.279)$$

$$N_{yx} = \int_{-h/2}^{+h/2} \tau_{yx} \left(1 + \frac{z}{r_y} \right) dz \quad (4.280)$$

$$Q_x = \int_{-h/2}^{+h/2} \tau_{zx} \left(1 + \frac{z}{r_y} \right) dz \quad (4.281)$$

$$Q_y = \int_{-h/2}^{+h/2} \tau_{zy} \left(1 + \frac{z}{r_x} \right) dz \quad (4.282)$$

$$M_x = \int_{-h/2}^{+h/2} \tau_{xx}(-z) \left(1 + \frac{z}{r_y} \right) dz \quad (4.283)$$

$$M_y = \int_{-h/2}^{+h/2} \tau_{yy}(-z) \left(1 + \frac{z}{r_x}\right) dz \quad (4.284)$$

$$M_{xy} = \int_{-h/2}^{+h/2} \tau_{xy} z \left(1 + \frac{z}{r_x}\right) dz \quad (4.285)$$

$$M_{yx} = \int_{-h/2}^{+h/2} \tau_{yx}(-z) \left(1 + \frac{z}{r_y}\right) dz. \quad (4.286)$$

In the resultant moment definitions the same sense conventions as for plates are used. Note that the stress resultants defined in equations (4.277) to (4.286) are the exact resultants associated with a given stress field. Since our presentation is restricted to thin shells, from now onwards we will neglect $\frac{z}{r_x}$ and $\frac{z}{r_y}$ with respect to 1, which implies obvious simplifications in the definitions of the stress resultants.

Kinematics

We adopt the Kirchhoff-Love kinematic assumption enunciated above and refer to Figure 4.83 where the deformation of a differential curved bar element was characterized. This same kinematics is used to describe the deformation of the shell sections $ABCD$ and $EFCD$ due to the analogous kinematic assumptions. In fact, Figure 4.83a can be used to characterize the undeformed configuration of either section $ABCD$ or $EFCD$ by considering instead of r , r_x or r_y respectively. The deformed configurations of these sections are given, in essence, by Figure 4.83b. Therefore, referring to equations (4.208) to (4.214), the shell strains are

$$\varepsilon_{xx} = \varepsilon_{xx_0} + z \left(\frac{1}{r'_x} - \frac{1}{r_x} \right) \quad (4.287)$$

$$\varepsilon_{yy} = \varepsilon_{yy_0} + z \left(\frac{1}{r'_y} - \frac{1}{r_y} \right) \quad (4.288)$$

where ε_{xx_0} and ε_{yy_0} are the strains at the midsurface. The approximations used for curved bars are employed here, *i.e.*, we are neglecting $\frac{z}{r_x}$, $\frac{z}{r_y}$, ε_{xx_0} and ε_{yy_0} with respect to 1. Note the complete analogy between (4.287), (4.288) and (4.214).

It is usual to define the changes of curvatures by

$$\chi_x = \frac{1}{r'_x} - \frac{1}{r_x}$$

$$\chi_y = \frac{1}{r'_y} - \frac{1}{r_y}.$$

Therefore equations (4.287) and (4.288) can be rewritten as

$$\varepsilon_{xx} = \varepsilon_{xx_0} + z\chi_x$$

$$\varepsilon_{yy} = \varepsilon_{yy_0} + z\chi_y.$$

In addition to these deformations of the shell, we still need to consider the deformations which induce shear strains in “planes” parallel to the mid-surface. Consider that line AB rotates with respect to CD about the x axis. Let χ_{xy} give this rotation per unit of length. This quantity is actually the twist of the deformed midsurface and the induced shear strain is given by

$$\gamma_{xy} = \gamma_{xy_0} + 2z\chi_{xy}$$

where γ_{xy_0} is the shear strain at the midsurface.

Constitutive relations

Using the plane stress constitutive assumption we have

$$\tau_{xx} = \frac{E}{1-\nu^2} [\varepsilon_{xx_0} + \nu\varepsilon_{yy_0} + z(\chi_x + \nu\chi_y)] \quad (4.289)$$

$$\tau_{yy} = \frac{E}{1-\nu^2} [\varepsilon_{yy_0} + \nu\varepsilon_{xx_0} + z(\chi_y + \nu\chi_x)] \quad (4.290)$$

$$\tau_{xy} = \frac{E}{2(1+\nu)} [\gamma_{xy_0} + 2z\chi_{xy}]. \quad (4.291)$$

Substituting relations (4.289) to (4.291) into (4.277) to (4.286) and performing the integration through the thickness, we obtain

$$N_x = \frac{Eh}{1-\nu^2} (\varepsilon_{xx_0} + \nu\varepsilon_{yy_0})$$

$$N_y = \frac{Eh}{1-\nu^2} (\varepsilon_{yy_0} + \nu\varepsilon_{xx_0})$$

$$N_{xy} = N_{yx} = \frac{Eh\gamma_{xy_0}}{2(1+\nu)}$$

$$M_x = -D(\chi_x + \nu\chi_y) \quad (4.292)$$

$$M_y = -D(\chi_y + \nu\chi_x) \quad (4.293)$$

$$M_{xy} = -M_{yx} = D(1-\nu)\chi_{xy}$$

where D gives the flexural rigidity of the shell, and is given by (4.251), as for the plate.

If we were to follow the approach used to formulate the previous structural models, the next step would be to impose equilibrium to obtain the differential formulation of the model. Then, to solve problems, the specific

shell midsurface geometry would need to be considered. We do not follow this approach due to the limited scope of our presentation. Instead, we present the formulation for a limited class of problems – shells of revolution loaded axisymmetrically.

Shell structures resist the external loads through membrane and bending internal actions. A special case is that of flat shells, that is, plates for which the transverse loads are resisted by bending while the in-plane loads are resisted by membrane internal actions. For curved midsurfaces this decoupling does not hold, see Section 4.2.7, and the loads are resisted by both membrane and bending actions. But, depending on the geometry of the midsurface, the boundary conditions and the loads, one of these internal actions – membrane or bending – may dominate.

Membrane actions dominate for example in shells of elliptic surfaces (for an example see Figure 4.105) when the loading can be resisted by membrane forces only and the restraints are applied all around the boundary and correspond to these internal membrane forces. In case the supports induce bending, these actions are local in the support regions. We discuss such a case below. However, if, for example, the elliptic shell is not supported all around the boundary and the external loading is inadmissible, then complex membrane and bending actions occur, see Bathe, Chapelle and Lee, 2003.

Considering hyperbolic surfaces (like the surface shown in Figure 4.106, which corresponds to half of a cooling tower), the boundary conditions and loading determine whether bending or membrane actions dominate. The same holds also for parabolic surfaces like cylinders. For a detailed discussion of the various cases that can arise, we refer to Chapelle and Bathe, 2010*a* and for numerical results see also Bathe and Lee, 2011, and Lee and Bathe, 2002.

Indeed, there are many different cases as to how a shell carries the externally applied loads – through bending, membrane or mixed stress state, varying over the shell surface, with possible boundary layers and internal layers of high stress gradients. Because of these various conditions that can arise, even just in linear analysis, the analysis of general shells considering linear and nonlinear behavior is a very challenging field in mechanics. We consider a relatively simple but practical and illustrative case of shell analyses below.

Clearly, from a structural design perspective resisting the loads primarily through membrane actions is most desirable and effective. Let us discuss one class of problems where this actually happens, namely, shells of revolution loaded axisymmetrically and supported on the whole boundary such that bending actions are small and mostly confined to the boundary only. This is a very special case of shell problems, but the discussion will illustrate some important general issues encountered in the analysis of shells. In our discussion we closely follow the work of Timoshenko and Woinowsky-Krieger, 1959.

4.4.3 Shells of revolution loaded axisymmetrically

In order to obtain insight into how transverse loads can be resisted by membrane actions in a shell of revolution loaded axisymmetrically consider a dome subjected to its own weight and to some surface loading as schematically described in Figure 4.108.

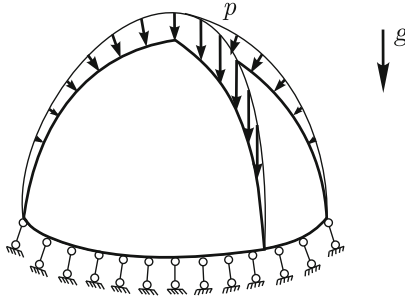


Fig. 4.108. A dome like structure

We compare the internal actions developed in an arch with those of a dome. In Figure 4.109a, we show a generic arch represented by its axis and in Figure 4.109c we describe a dome represented by its midsurface. This surface is obtained by revolving the curved axis of the arch around the vertical axis shown in Figure 4.109a.

The arch is acted on by the distributed load shown and since we assume that the arch axis does not correspond to the line of pressure for this load, bending will be developed in the arch as discussed in Section 4.2.7. The moment distribution is shown schematically in Figure 4.109b.

Consider now the distributed load acting on the shell, which is defined per unit of surface area, as schematically shown in Figure 4.109c. The spatial distribution of this load could be generated, for example, by revolving the load defined on the arch. We also show a force distribution at the lower shell boundary which equilibrates the applied load and whose evaluation is dealt with later on.

As we discuss in the sequel, as long as the applied distributed loading has a smooth variation, the shell “may” develop only internal forces tangential to its midsurface, that is, only membrane forces.

Let us examine two “slices” of the shell which are highlighted in Figure 4.109d. One is defined by the intersection of the shell with two meridian planes – planes which contain the vertical axis. The other is given by the intersection of the shell with two parallel planes – planes which are orthogonal to the vertical axis.

Assume now that the reactions on the periphery are such that only membrane forces develop in the shell, and consider the internal actions at the

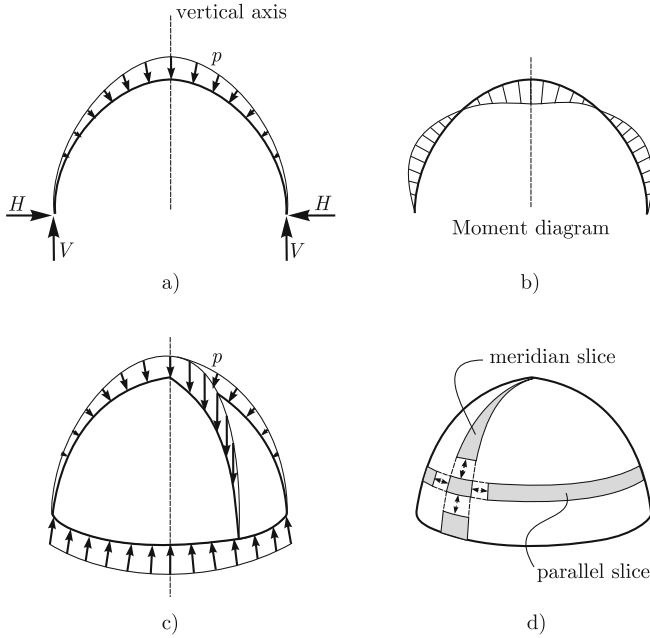


Fig. 4.109. Arch and shell actions

intersection of these two slices in Figure 4.109d. Then, an interesting interpretation for the shell resisting the load is as follows. The meridian slice behaves like an arch and the membrane forces on this slice due to the action of the parallel slices are such that the net loading – external loading superposed onto the membrane forces from the parallel slices – has as its line of pressure the line defined by the geometry of the meridian slice. Of course, under these conditions there will be no bending developed in the shell.

We can appreciate that a shell resisting loads through membrane forces only is a very efficient structure and such state is that one ideally sought by the structural designer. However, these conditions are very difficult to meet in practice and therefore some bending is generally induced even in this type of shell.

Membrane theory

We assume from the onset that there is no bending and torsion, *i.e.*,

$$M_x = M_y = M_{xy} = 0.$$

Therefore, we seek a field of membrane stress resultants, *i.e.*, N_x , N_y , N_{xy} which equilibrates the applied loading and which leads to deformations that are compatible with the kinematic boundary conditions.

A shell is called a shell of revolution when its midsurface is a surface of revolution, *i.e.*, it is obtained by revolving a planar curve around an axis,

which lies in the plane of the curve, called the axis of revolution. The curve is called a meridian and this plane is referred to as a meridian plane. The load is axisymmetric when its distribution in all meridian planes is the same and it acts in these planes. We are considering surface tractions and body forces, but do not allow concentrated loads.

Under these geometrical and loading conditions the stress resultants and displacements also have an axial symmetry, *i.e.*, they are identical for each meridian plane. Further, if we cut the shell through a generic meridian plane there is no tendency of one part to slide with respect to the other and, hence, there are no shear stresses acting on any meridian plane.

Consider a differential element extracted from the shell as shown in Figure 4.110a and impose equilibrium. At the midsurface, the differential element

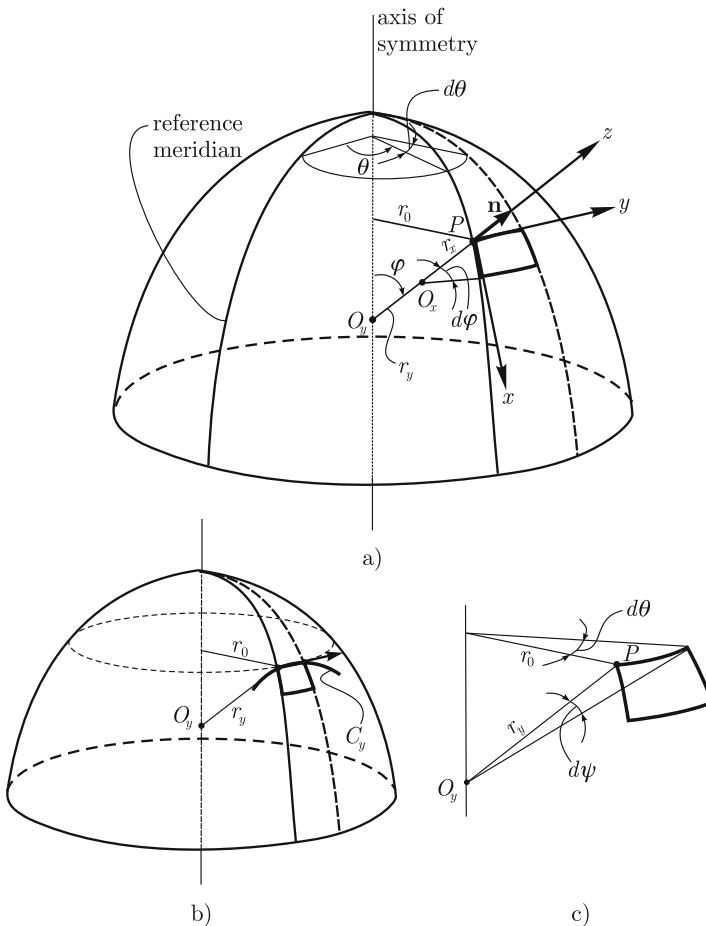


Fig. 4.110. Definitions for a shell of revolution

can be obtained by considering at point P a pair of meridian and a pair of parallel planes which are infinitesimally small distances apart.

It is possible to show that the meridian is always a principal curvature curve. We adopt a local coordinate system xyz with origin at P , z defined by the outward normal and x tangential to the meridian. The principal radius of curvature associated with the meridian is denoted by r_x with center O_x . In Figure 4.110b, the other principal normal section is shown. Its center of curvature O_y is located on the axis of symmetry. The parallel that passes through P is shown in Figure 4.110b and it is a geometrical fact that the parallel has the same unit tangent vector at P as the principal curve whose center is O_y . In Figure 4.110c a detail of 4.110a is shown which allows a better visualization of some quantities such as the differential angle increment $d\psi$ associated with the arc increment of the principal curve whose center is O_y . Also, r_0 is the radius of the parallel that contains the point P .

Let us first consider the equilibrium of the differential element in the z direction. Referring to Figures 4.111a to 4.111c, we can evaluate the contribution of the membrane forces. The contribution of N_x is given by

$$-(N_x + dN_x)(r_0 + dr_0) d\theta d\varphi$$

which, neglecting infinitesimals of higher-order, leads to

$$-N_x r_0 d\theta d\varphi. \tag{4.294}$$

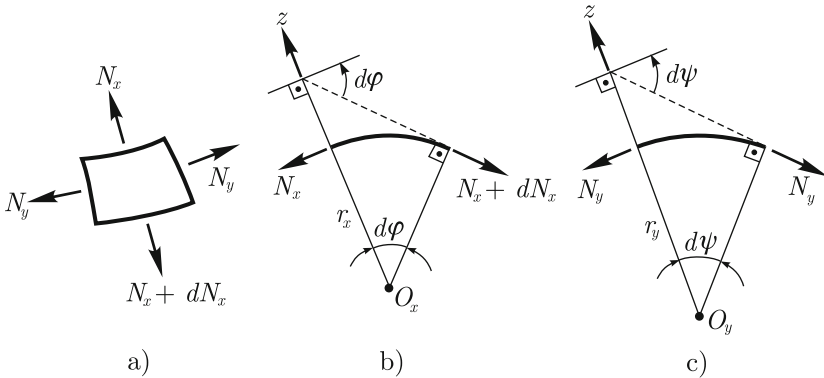


Fig. 4.111. Differential element and principal sections

We note that due to the axisymmetric nature of the solution, N_y is the same for every meridian plane. Its contribution is given by

$$-N_y r_x d\varphi d\psi. \tag{4.295}$$

Next consider the contribution of the external load. Let p_z be the component of the surface load which is normal to the shell midsurface and taken positive when oriented as the z axis. Its contribution is given by

$$p_z r_x d\varphi r_y d\psi. \quad (4.296)$$

From Figure 4.110c, we can write the geometrical relation

$$r_0 d\theta = r_y d\psi. \quad (4.297)$$

Therefore using (4.294) to (4.297), equilibrium in the z direction leads to

$$N_x r_y d\psi d\varphi + N_y r_x d\varphi d\psi = p_z r_x r_y d\varphi d\psi$$

which yields

$$\frac{N_x}{r_x} + \frac{N_y}{r_y} = p_z. \quad (4.298)$$

We choose to obtain the additional equilibrium condition isolating a convenient part of the shell. This part is defined as the portion of the shell which lies above the parallel circumference defined by the angle φ as summarized in Figure 4.112, where the intersection of this part with a meridian plane is shown. Due to the axisymmetric nature of the external loading, a mechanically equivalent force system to the external loading acting on the selected part is given by its resultant R acting along the symmetry axis as shown in Figure 4.112. Equilibrium in this direction can be written as

$$N_x \sin \varphi (2\pi r_y \sin \varphi) = R$$

or

$$N_x = \frac{R}{2\pi r_y (\sin \varphi)^2}. \quad (4.299)$$

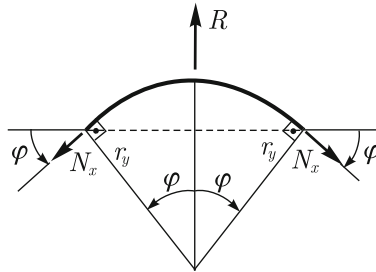


Fig. 4.112. Equilibrium of selected part of the shell

Equations (4.298) and (4.299) give the equilibrium conditions for the shell. Therefore, given the external load, these equations can be used to solve for the membrane forces. We demonstrate a typical solution in the following example.

Example 4.19¹⁶

Spherical domes are used extensively in engineering practice (*e.g.*, churches) and the major stresses developed are due to self-weight.

Consider the spherical dome in Figure 4.113a and find the membrane force distribution due to its own weight. Suppose that the required force distribution is applied at the periphery to guarantee equilibrium. The specific weight of the shell material is γ .

Find the membrane force distribution of the spherical dome characterized in Figure 4.113a subjected to its own weight. Suppose that the required force distribution is applied at the periphery to guarantee equilibrium. The specific weight of the shell material is γ .

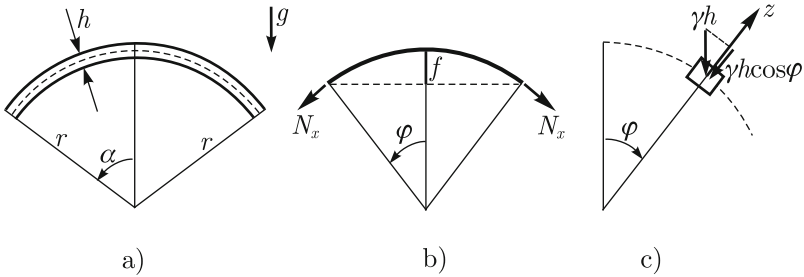


Fig. 4.113. a) Section of the dome; b) Selected part; c) Weight load of a differential element

Solution

We can evaluate the resultant force due to the dome weight for the part described in Figure 4.113b. The surface area of the midsurface of the spherical shell associated with this part is given by

$$S = 2\pi r f$$

and the resultant force, following the convention adopted in Figure 4.112, is given by

¹⁶ This example is also presented in Timoshenko and Woinowsky-Krieger, 1959

$$R = -2\pi r f h \gamma = -2\pi r^2 \gamma h (1 - \cos \varphi)$$

and therefore from equation (4.299)

$$N_x = \frac{-2\pi r^2 \gamma h (1 - \cos \varphi)}{2\pi r (\sin \varphi)^2} = -\frac{\gamma r h}{1 + \cos \varphi}. \tag{4.300}$$

Of course, for a spherical shell $r_x = r_y = r$. Referring to Figure 4.113c

$$p_z = -\gamma h \cos \varphi.$$

Considering equation (4.298), we obtain

$$\frac{-\gamma h}{1 + \cos \varphi} + \frac{N_y}{r} = -\gamma h \cos \varphi$$

and therefore

$$N_y = \gamma h r \frac{1 - \cos \varphi - \cos^2 \varphi}{1 + \cos \varphi}. \tag{4.301}$$

In Figure 4.114 we show the membrane force distributions obtained. We note

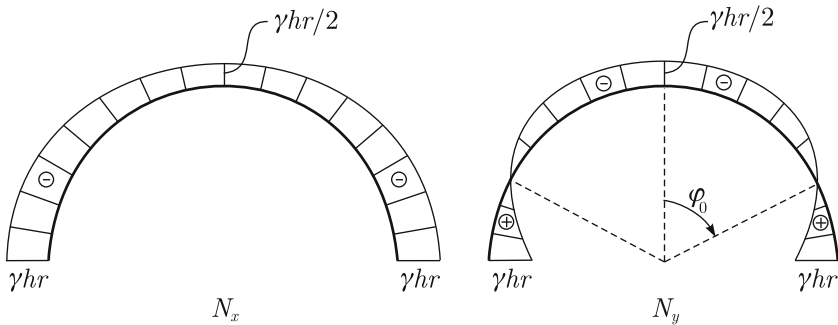


Fig. 4.114. Membrane forces for spherical shell problem

that N_x is always negative, *i.e.*, the meridian “slice” (refer to Figure 4.109d) works in compression. However, N_y changes from compression to tension when $\varphi = \varphi_0 \doteq 52^\circ$. Therefore, the parallel “slices” defined by $\varphi < \varphi_0$ work in compression while those given by $\varphi > \varphi_0$ work in tension. Of course, when $\alpha < \varphi_0$ the whole shell is in compression.

□

We next consider the solution of the displacements. Again, due to the axisymmetric conditions, the displacements are completely characterized if they are known for a meridian plane.

In Figure 4.115, we show a meridian extracted from the midsurface of the shell described in Figure 4.110a. Let u be the displacement in the tangential direction x and w be that in the normal direction. The displacement increments associated with the increment $d\varphi$ are also shown in this figure. We note the complete analogy with the displacements of the axis of a curved bar which are described in Figure 4.84. Actually the axial strain given by equation (4.217) corresponds to the midsurface strain ε_{xx_0} and, hence, it is given by

$$\varepsilon_{xx_0} = \frac{1}{r_x} \frac{du}{d\varphi} + \frac{w}{r_x}. \tag{4.302}$$

The circumferential strain ε_{yy_0} can be evaluated from the change in radius,

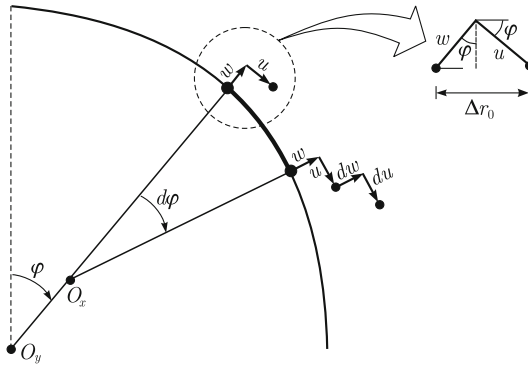


Fig. 4.115. Displacement conventions for a shell of revolution

Δr_0 , of the parallel considering the undeformed and deformed configurations. This change in radius is given by

$$\Delta r_0 = u \cos \varphi + w \sin \varphi$$

and

$$\begin{aligned} \varepsilon_{yy_0} &= \frac{\Delta r_0}{r_0} = \frac{u \cos \varphi + w \sin \varphi}{r_y \sin \varphi}. \\ \varepsilon_{yy_0} &= \frac{u}{r_y} \cot \varphi + \frac{w}{r_y}. \end{aligned} \tag{4.303}$$

We can eliminate w from equations (4.302) and (4.303) to arrive at

$$\frac{du}{d\varphi} - u \cot \varphi = r_x \varepsilon_{xx_0} - r_y \varepsilon_{yy_0}. \tag{4.304}$$

Using the plane stress constitutive relation (equation (4.44)) we have

$$\varepsilon_{xx_0} = \frac{1}{E} (\tau_{xx} - \nu\tau_{yy}) = \frac{1}{Eh} (N_x - \nu N_y) \quad (4.305)$$

$$\varepsilon_{yy_0} = \frac{1}{E} (\tau_{yy} - \nu\tau_{xx}) = \frac{1}{Eh} (N_y - \nu N_x). \quad (4.306)$$

Substituting (4.305) and (4.306) into (4.304), we obtain

$$\frac{du}{d\varphi} - u \cot \varphi = \frac{1}{Eh} [N_x (r_x + \nu r_y) - N_y (r_y + \nu r_x)]. \quad (4.307)$$

We can denote the right-hand side of (4.307) by $f(\varphi)$, *i.e.*,

$$f(\varphi) = \frac{1}{Eh} [N_x (r_x + \nu r_y) - N_y (r_y + \nu r_x)] \quad (4.308)$$

which is a known function when we suppose that the membrane forces have been determined by equilibrium. Hence, the displacement u can be obtained by solving the following ordinary differential equation

$$\frac{du}{d\varphi} - u \cot \varphi = f(\varphi) \quad (4.309)$$

subject to appropriate kinematic boundary conditions, and from equation (4.303) we obtain

$$w = r_y \varepsilon_{yy_0} - u \cot \varphi. \quad (4.310)$$

Example 4.20

Consider the spherical dome subjected to its own weight studied in Example 4.19. Find the displacement fields when the shell is supported in the tangential direction as indicated in Figure 4.116.

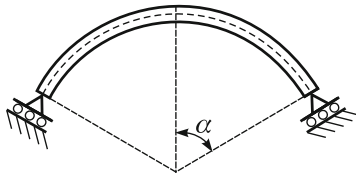


Fig. 4.116. Section of spherical dome with boundary conditions

Solution

Since the membrane forces have already been determined (see solution of Example 4.19), we can directly evaluate $f(\varphi)$ defined by equation (4.308) which leads to

$$f(\varphi) = \frac{(1 + \nu) \gamma r^2}{E} \left(\cos \varphi - \frac{2}{1 + \cos \varphi} \right) \quad (4.311)$$

and solving (4.309), we obtain

$$u = \frac{(1 + \nu) \gamma r^2}{E} \left[\sin \varphi \ln(1 + \cos \varphi) - \frac{\sin \varphi}{1 + \cos \varphi} \right] + C \sin \varphi. \quad (4.312)$$

Imposing the boundary condition $u(\alpha) = 0$, the constant C can be determined and it is given by

$$C = \frac{(1 + \nu) \gamma r^2}{E} \left[\frac{1}{1 + \cos \alpha} - \ln(1 + \cos \alpha) \right].$$

The displacement w is obtained from equation (4.310). Note that, as expected physically, the forces (expressed in (4.311)) and displacements u (given by (4.312)) and w (given by (4.310)) only vary with φ .

□

Using Examples 4.19 and 4.20, we have the solution of the spherical dome supported tangentially as described in Figure 4.116 within the membrane theory. However, if we change the supports such that the displacements are constrained in both directions, we can no longer obtain the solution using the membrane theory, since the solution obtained with this theory predicts a non-zero radial displacement at the supports. Of course, the transverse forces that would be developed at the supports associated with the restraint of the radial displacement w would induce bending and, hence, the membrane theory is no longer applicable since it neglects bending from the start. This observation prompts the discussion we present next.

Membrane-bending theory

In the membrane-bending model we need to consider, besides the membrane stress resultants N_x , N_y and N_{xy} which are already taken into account in the membrane theory, the moments M_x , M_y and M_{xy} and the transverse shear forces, Q_x and Q_y . Since in our simplified setting there are no shear stresses in any meridian plane the resultants to be considered are summarized in Figure 4.117a, which is a close up of the differential element of Figure 4.110. Equilibrium in the z direction is established as in the membrane theory but we need to include the shear force contribution. In Figure 4.117b, we repeat Figure 4.111b including the shear force. Therefore, equilibrium implies

$$\begin{aligned}
 & -N_x d\varphi r_0 d\theta + (Q_x + dQ_x)(r_0 + dr_0) d\theta - Q_x r_0 d\theta \\
 & -N_y r_x d\varphi \sin \varphi d\theta + p_z r_0 d\theta r_x d\varphi = 0
 \end{aligned}$$

which leads to

$$N_x r_0 + N_y r_x \sin \varphi - \frac{d}{d\varphi} (Q_x r_0) = p_z r_0 r_x. \tag{4.313}$$

The above equation, apart from the term $-\frac{d}{d\varphi} (Q_x r_0)$, is the same as equation

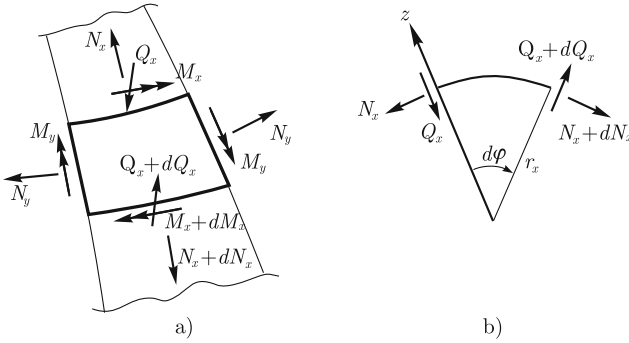


Fig. 4.117. a) Stress resultants acting in a differential element; b) Shear force appended to principal section defined by r_x

(4.298). Note, however, that the above equation was written in terms of r_0 instead of r_y because the additional term is more easily expressed considering r_0 .

For the membrane theory, we did not consider the differential equilibrium in the x direction, since the second differential equilibrium condition was imposed in resultant form. Now, however, we need to consider the equilibrium in the x direction which referring to Figures 4.117 and 4.118 can be written as

$$\begin{aligned}
 & -N_x r_0 d\theta + (N_x + dN_x)(r_0 + dr_0) d\theta - N_y r_x \cos \varphi d\varphi d\theta \\
 & + Q_x r_0 d\theta d\varphi + p_x r_0 r_x d\theta d\varphi = 0
 \end{aligned}$$

where p_x is the x direction component of the surface load. Then, we obtain

$$\frac{d}{d\varphi} (N_x r_0) - N_y r_x \cos \varphi + Q_x r_0 = -p_x r_0 r_x \tag{4.314}$$

and referring to Figures 4.117 and 4.119 moment equilibrium about the y axis gives

$$-(M_x + dM_x)(r_0 + dr_0) d\theta + M_x r_0 d\theta + M_y r_x \cos \varphi d\varphi d\theta$$

$$-Q_x r_0 r_x d\varphi d\theta = 0$$

leading to

$$\frac{d}{d\varphi} (M_x r_0) - M_y r_x \cos \varphi + Q_x r_x r_0 = 0. \tag{4.315}$$

Therefore equations (4.313), (4.314) and (4.315) represent the equilibrium conditions for the differential element.

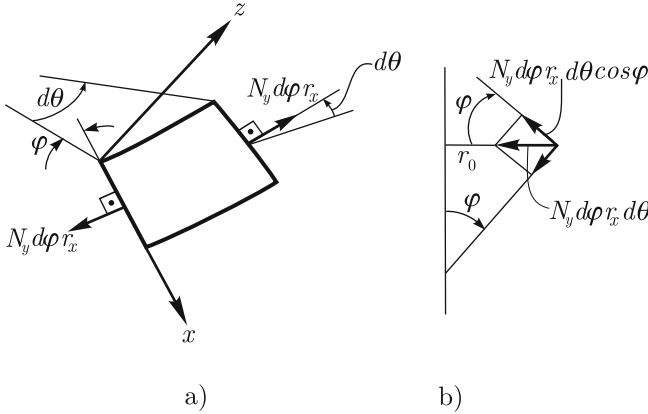


Fig. 4.118. Contribution of N_y to equilibrium in the x -direction, $N_y d\varphi r_x d\theta$ acts in the parallel plane and its $\cos \varphi$ component into the x -direction

The compatibility relations for the membrane strains have been already examined and are given by equations (4.302) and (4.303).

Using Hooke's law for the membrane components, we obtain

$$N_x = \frac{Eh}{1 - \nu^2} \left[\frac{1}{r_x} \left(\frac{du}{d\varphi} + w \right) + \frac{\nu}{r_y} (u \cot \varphi + w) \right] \tag{4.316}$$

$$N_y = \frac{Eh}{1 - \nu^2} \left[\frac{1}{r_y} (u \cot \varphi + w) + \frac{\nu}{r_x} \left(\frac{du}{d\varphi} + w \right) \right]. \tag{4.317}$$

The compatibility relations for the bending strains involve the changes in curvatures. Let us consider first the change in curvature of a meridian. We recognize that this change in curvature corresponds to the change in curvature of the axis of a curved bar. Adapting equation (4.221) to the shell quantities, we obtain

$$\chi_x = \frac{1}{r_x} \frac{d}{d\varphi} \left(\frac{u}{r_x} - \frac{dw}{r_x d\varphi} \right). \tag{4.318}$$

We note that in this evaluation of the change of curvature, the term $\left(\frac{u}{r_x} - \frac{dw}{r_x d\varphi} \right)$ corresponds to the angular change of the unit normal from the

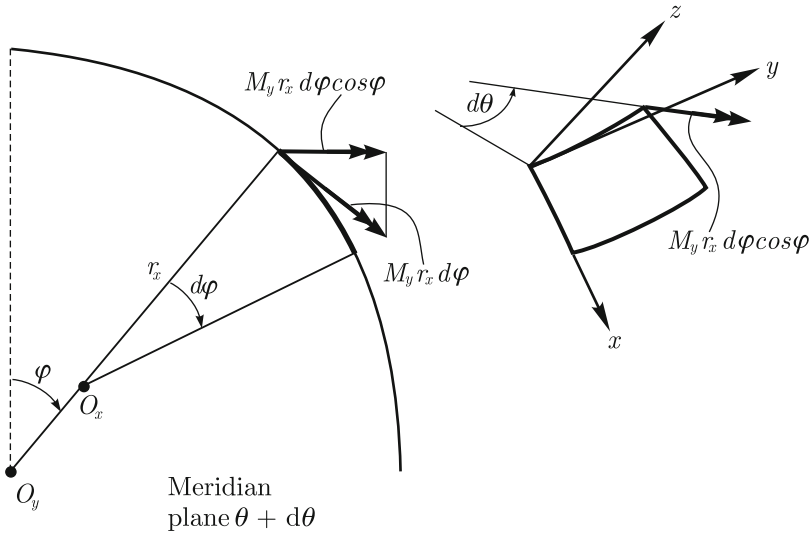


Fig. 4.119. Contribution of M_y to the moment equilibrium about the y axis

undeformed to deformed configuration. The rate of change in the x -direction gives χ_x . This same concept will be used for the evaluation of the change in curvature in the y direction, *i.e.*, we will compute the change in angle per unit of arc length along y .

Namely, referring to Figure 4.120, consider $\left(\frac{u}{r_x} - \frac{dw}{r_x d\varphi}\right)$ at point R ; it corresponds to the change in angle of an infinitesimal meridian arc. Of course, due to the symmetry of the deformation, both, this normal and the arc remain in the meridian plane. Therefore, the rotation vector which characterizes this rotation is orthogonal to the meridian plane at R as shown in Figure 4.121. This rotation vector has a projection on the x axis which is different from zero. In Figure 4.121 all quantities used to evaluate this projection are shown and we obtain

$$-\left(\frac{u}{r_x} - \frac{dw}{r_x d\varphi}\right) \cos \varphi d\theta$$

which gives the change in angle of the normal around the x axis when we move from point P to R . Therefore, we have

$$\chi_y = \left(\frac{u}{r_x} - \frac{dw}{r_x d\varphi}\right) \frac{\cos \varphi d\theta}{r_0 d\theta} \tag{4.319}$$

leading to

$$\chi_y = \left(\frac{u}{r_x} - \frac{dw}{r_x d\varphi}\right) \frac{\cos \varphi}{r_0} = \left(\frac{u}{r_x} - \frac{dw}{r_x d\varphi}\right) \frac{\cot \varphi}{r_y}. \tag{4.320}$$

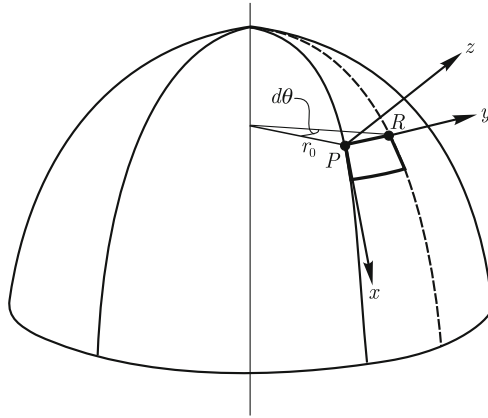


Fig. 4.120. Definition of points P and R for axisymmetrical shell

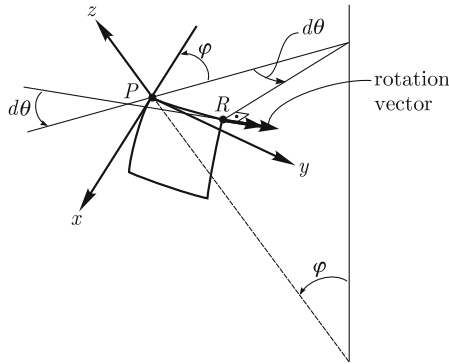


Fig. 4.121. Rotation vector at point R

Finally the bending moments can be evaluated using relation (4.292) and (4.293)

$$M_x = -D \left[\frac{1}{r_x} \frac{d}{d\varphi} \left(\frac{u}{r_x} - \frac{dw}{r_x d\varphi} \right) + \frac{\nu}{r_y} \left(\frac{u}{r_x} - \frac{dw}{r_x d\varphi} \right) \cot \varphi \right] \quad (4.321)$$

$$M_y = -D \left[\left(\frac{u}{r_x} - \frac{dw}{r_x d\varphi} \right) \frac{\cot \varphi}{r_y} + \frac{\nu}{r_x} \frac{d}{d\varphi} \left(\frac{u}{r_x} - \frac{dw}{r_x d\varphi} \right) \right]. \quad (4.322)$$

Now all conditions have been considered. Namely, equilibrium (equations (4.313), (4.314) and (4.315)), compatibility (equations (4.302), (4.303), (4.319) and (4.320)) and the constitutive (equations (4.316), (4.317), (4.321) and (4.322)). Therefore, these equations appended by appropriate boundary conditions represent the complete formulation.

We note that the substitution of equations (4.302), (4.303), (4.319), (4.320), (4.316), (4.317), (4.321) and (4.322) into (4.313), (4.314) and (4.315)

reduces the problem to three equations in the variables u , w and Q_x . The solution of these equations has been addressed in many references, for example, in the classical work of Timoshenko and Woinowsky-Krieger, 1959. Of course, our objective is not to discuss these solutions. Actually, we presented the formulations only to gain some insight into the variables and into the resisting mechanisms of a shell in bending.

Membrane versus bending

We next want to mention some issues related to the accuracy of the membrane theory when compared to the bending theory which is, of course, a hierarchically higher-order theory. This discussion is also based on the book of Timoshenko and Woinowsky-Krieger, 1959.

Consider the membrane theory solution of the spherical shell subjected to its own weight for the displacements u and w (Example 4.20). These displacements can be substituted into equations (4.321) and (4.322) to obtain an estimate of the bending moments which are, of course, neglected in the membrane theory. These bending moments are given by

$$M_x = M_y = \frac{\gamma h^2}{12} \frac{2 + \nu}{1 - \nu} \cos \varphi. \quad (4.323)$$

If we use these moments to evaluate the ratio between the bending stresses and the compressive membrane stresses predicted by the membrane theory and compute the maximum value, we arrive at $3.29h/r$ for $\nu = 0.3$. Therefore, since for thin shells the ratio of the thickness h to the radius of curvature r is small, these bending stresses are negligible.

An improved estimate for the membrane forces N_x and N_y can be obtained if the moment estimates given in (4.323) are substituted into the equilibrium equations ((4.313), (4.314) and (4.315)). A comparison of these membrane forces with those of (4.300) and (4.301) shows that they differ by quantities that are proportional to $\frac{h^2}{r^2}$, a difference which becomes also negligible for thin shells. Therefore, as long as the boundary conditions are compatible with the membrane theory and the shell is thin the above discussion indicates that the membrane theory provides good predictions.

The effect on the solution of violating the boundary conditions which are compatible with the membrane theory can also be assessed.

Consider the spherical shell described in Figure 4.122. We report solutions for the problems summarized in Figures 4.123a and 4.123b. These solutions are based on further approximations of the differential formulation presented for the bending problem, which are increasingly appropriate as the shell becomes thinner.

These approximate solutions may be obtained as shown in Timoshenko and Woinowsky-Krieger, 1959 and are, for the problem of Figure 4.123a,

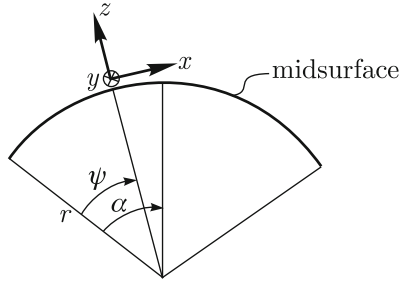


Fig. 4.122. Generic section of a spherical shell

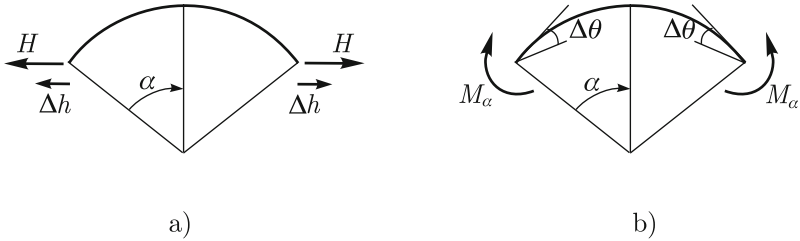


Fig. 4.123. End conditions for spherical shell problem: Δh is the displacement induced by H and $\Delta\theta$ is the rotation induced by M_α

$$N_x = -\sqrt{2} \cot(\alpha - \psi) \sin \alpha e^{-\lambda\psi} \sin\left(\lambda\psi - \frac{\pi}{4}\right) H$$

$$N_y = -2\lambda \sin \alpha e^{-\lambda\psi} \sin\left(\lambda\psi - \frac{\pi}{2}\right) H$$

$$M_x = \frac{r}{\lambda} \sin \alpha e^{-\lambda\psi} \sin(\lambda\psi) H$$

$$\Delta h = \frac{2r\lambda \sin^2 \alpha}{Eh} H$$

$$\Delta\theta = \frac{2\lambda^2 \sin \alpha}{Eh} H$$

and for the problem of Figure 4.123b

$$N_x = -\frac{2\lambda}{r} \cot(\alpha - \psi) e^{-\lambda\psi} \sin(\lambda\psi) M_\alpha$$

$$N_y = -\frac{2\sqrt{2}\lambda^2}{r} e^{-\lambda\psi} \sin\left(\lambda\psi - \frac{\pi}{4}\right) M_\alpha$$

$$M_x = \sqrt{2} e^{-\lambda\psi} \sin\left(\lambda\psi + \frac{\pi}{4}\right) M_\alpha$$

$$\Delta h = \frac{2\lambda^2 \sin \alpha}{Eh} M_\alpha$$

$$\Delta \theta = \frac{4\lambda^3 M_\alpha}{Erh}$$

where

$$\lambda^4 = 3(1 - \nu^2) \left(\frac{r}{h}\right)^2. \quad (4.324)$$

Examining the functional form of these solutions, we note that the membrane forces and the bending moments damp out as we move away from the edge due to the factor $e^{-\lambda\psi}$. Of course, as the shell becomes thinner, λ becomes larger and the significant part of these solutions is closer to the boundary.

These solutions can be used to consider restraints at the boundary which are different from those compatible with the membrane theory in a similar way as solving statically indeterminate structures (refer, for example, to the discussion of Section 4.2.3 and to the example given below).

Example 4.21

Consider the spherical dome subjected to its own weight as described in Example 4.19 now clamped at the periphery. Obtain the solution for the bending moment M_x and the membrane force N_x using the membrane theory solution superimposed to the solutions for the problems given in Figure 4.123. To obtain numerical values use $r = 20$ m, $h = 0.2$ m, $\alpha = 90^\circ$, $E = 2.1 \times 10^7$ kN/m², $\nu = 0.3$, $\gamma = 2.4g$ kN/m³ where $g = 9.81$ m/s².

Solution

For the clamped condition both Δh and $\Delta \theta$ (refer to Figure 4.123 for the definitions of Δh and $\Delta \theta$) should be zero. Therefore

$$(\Delta h)_m + (\Delta h)_{horiz} + (\Delta h)_{moment} = 0 \quad (4.325)$$

$$(\Delta \theta)_m + (\Delta \theta)_{horiz} + (\Delta \theta)_{moment} = 0 \quad (4.326)$$

where the subscript m refer to the membrane solution, “*horiz*” to the contribution of the horizontal force H given per unit of length and “*moment*” to the contribution of the moment M_α also given per unit of length. Then

$$(\Delta h)_{horiz} = \frac{2r\lambda \sin^2 \alpha}{Eh} H = F_{11}H$$

$$(\Delta h)_{moment} = \frac{2\lambda^2 \sin \alpha}{Eh} M_\alpha = F_{12}M_\alpha$$

$$(\Delta\theta)_{horiz} = \frac{2\lambda^2 \sin \alpha}{Eh} H = F_{21}H = F_{12}H$$

$$(\Delta\theta)_{moment} = \frac{4\lambda^3}{Erh} M_\alpha = F_{22}M_\alpha$$

where λ is given in (4.324).

The values of H and M_α come from the solutions of (4.325) and (4.326) which can be re-written as

$$F_{11}H + F_{12}M_\alpha = -(\Delta h)_m \quad (4.327)$$

$$F_{21}H + F_{22}M_\alpha = -(\Delta\theta)_m. \quad (4.328)$$

Since the flexibility coefficients F_{11} , F_{12} , F_{22} are given above, we only need to determine $(\Delta h)_m$ and $(\Delta\theta)_m$. Referring to (4.310), we can write

$$(\Delta h)_m = r_0 \varepsilon_{yy_0} = r_y \sin \alpha \varepsilon_{yy_0}$$

since $u = 0$ and using (4.306), we obtain

$$(\Delta h)_m = \frac{r_y \sin \alpha}{Eh} (N_y - \nu N_x). \quad (4.329)$$

Introducing the numerical values we obtain

$$(\Delta h)_m = 5.830 \times 10^{-4} \text{ m.}$$

The change of angle $(\Delta\theta)_m$ can be evaluated as the change of the normal at the section given by α . Referring to equation (4.318) and considering the convention defined in Figure 4.123b, we obtain

$$(\Delta\theta)_m = -\frac{u}{r_x} + \frac{1}{r_x} \frac{dw}{d\psi}.$$

Considering that at the section given by α , $u = 0$ and using equation (4.310), we obtain

$$(\Delta\theta)_m = \frac{1}{r_x} \left(\frac{d}{d\psi} (r_y \varepsilon_{yy_0}) - \frac{d}{d\psi} (u \cot \psi) \right)$$

leading to

$$(\Delta\theta)_m = \frac{1}{r_x} \left(\frac{d}{d\psi} \left(\frac{(\Delta h)_m}{\sin \psi} \right) - \frac{du}{d\psi} \cot \psi \right).$$

Using equation (4.307) we finally arrive at

$$(\Delta\theta)_m = \frac{1}{r_x} \left\{ \frac{d}{d\psi} \left(\frac{(\Delta h)_m}{\sin \psi} \right) - \frac{\cot \psi}{Eh} [N_x (r_x + \nu r_y) - N_y (r_y + \nu r_x)] \right\}.$$

Since $(\Delta h)_m$ is given in (4.329), we obtain

$$(\Delta\theta)_m = \frac{r\gamma}{E} (2 + \nu) \sin \alpha = 5.1572 \times 10^{-5} \text{ rad.}$$

The solution of (4.327) and (4.328) gives

$$H = -8.869 \text{ kN/m} \quad \text{and} \quad M_\alpha = 6.39 \text{ kN.}$$

If we plot N_x corresponding to the membrane solution and the value including the edge effects we would barely be able to distinguish both curves.

We obtain for M_x , which is identically zero in the membrane solution, the values shown in Figure 4.124. Note that the resulting moment has high

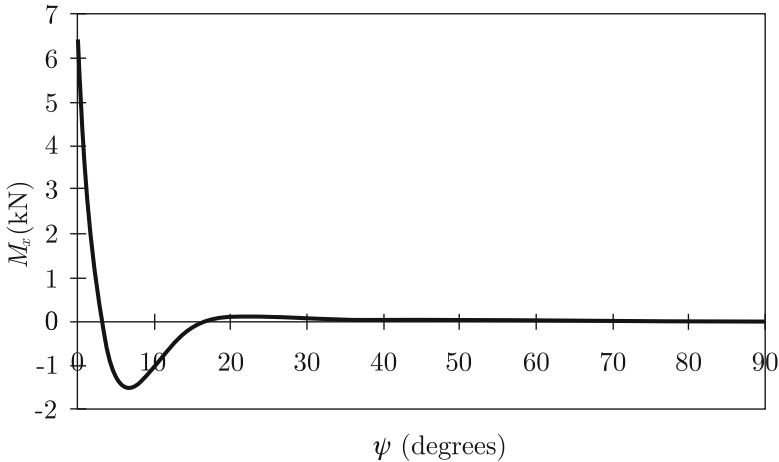


Fig. 4.124. Bending moment M_x for clamped shell

gradients near the edge but it is close to zero in the rest of the domain. □

4.4.4 Remarks on shell modeling of engineering structures

In this introductory presentation on shells, the emphasis was placed on basic facts and behaviors. The formulation of the membrane-bending model was discussed for a very limited class of problems; namely, axisymmetric shells loaded axisymmetrically. Nevertheless, insight was gained into the relevant variables of the model, resisting mechanisms, membrane and bending behaviors, edge effects, among others.

As mentioned, the presentation was structured having in mind that the reader who is faced with the modeling of a shell structure will most probably be solving the shell models through finite element analysis. Therefore, the most important objective of the presentation was to focus on some basic understanding of shell structural behavior.

Of course, the formulations and results given above should also help the reader to understand and use other formulations, considering more general shell geometries, loadings and boundary conditions.

If a shell finite element analysis is undertaken – and not considering yet the task of making sure that the finite element solution is close enough to the solution of the mathematical model, a task which will be dealt with later on and which is very challenging for shells – the analyst needs to be aware that the response of shell structures is in general very sensitive to the shell geometry, loading and boundary conditions. Also, the behavior is not always easy to anticipate since the propagation of edge and perturbation effects may vary significantly depending on the conditions mentioned above, for detailed discussions see Chapelle and Bathe, 2010*a*. Hence, the hierarchical modeling concepts are clearly very valuable in shell analyses – as indeed already illustrated by the relatively simple shell solutions given above.

4.5 Summary of the mathematical models for structural mechanics

We end this long chapter with a summary of the mathematical models discussed. The objective is to synthesize the main aspects of each model for future reference. We list the basic model assumptions as well as the main variables, organized as kinematic, strain and stress type variables.

For all models, we define: the displacement, or generalized displacement, as the column matrix \mathbf{u} which collects all independent kinematic variables of the model; the strain, or generalized strain, as the column matrix ε which collects the strain, or strain type, variables and the stress, or generalized stress, as the column matrix τ which collects the stress variables such as stresses and stress resultants.

Of course, as detailed in the presentation of each model, these stress type variables are used to enforce the equilibrium conditions. Also, the constitutive relations allow us to write

$$\tau = \mathbf{C}\varepsilon \tag{4.330}$$

and the strain compatibility is given by

$$\varepsilon = \partial_\varepsilon \mathbf{u}. \tag{4.331}$$

where we assume, as pointed out in Section 3.2.2, continuous displacements satisfying the displacement boundary conditions.

The specific forms of \mathbf{C} and ∂_ε for the models studied are presented in Tables 4.3 and 4.4.

Plane strain model

Hypotheses

- Solid is prismatic
- Displacement assumptions

$$u = u(x, y), v = v(x, y)$$

$$w = 0$$

- Restrictions on loading

Volume Lateral surface

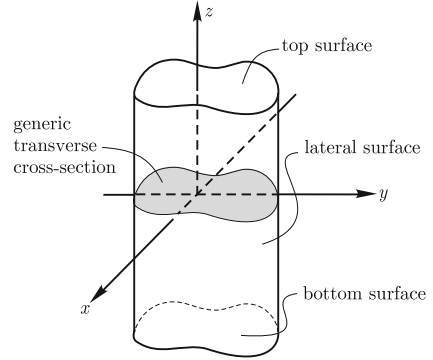
$$f_x^B = f_x^B(x, y) \quad f_x^S = f_x^S(x, y)$$

$$f_y^B = f_y^B(x, y) \quad f_y^S = f_y^S(x, y)$$

$$f_z^B = 0 \quad f_z^S = 0$$

Top and bottom surfaces

$$f_x^S = 0, f_y^S = 0$$



Primary variables

Displacements

$$\mathbf{u} = \begin{bmatrix} u(x, y) \\ v(x, y) \end{bmatrix}$$

Stresses

$$\boldsymbol{\tau} = \begin{bmatrix} \tau_{xx} \\ \tau_{yy} \\ \tau_{xy} \end{bmatrix}$$

Strains

$$\boldsymbol{\varepsilon} = \begin{bmatrix} \varepsilon_{xx} \\ \varepsilon_{yy} \\ \gamma_{xy} \end{bmatrix}$$

Remarks

Formulation is cast in the 2-D domain

Upon solution of \mathbf{u} , $\boldsymbol{\tau}$, $\boldsymbol{\varepsilon}$, we can evaluate $\tau_{zz} = \nu(\tau_{xx} + \tau_{yy})$

Remaining variables are zero: $w = 0, \varepsilon_{zz} = \gamma_{xz} = \gamma_{yz} = 0,$

$$\tau_{xz} = \tau_{yz} = 0$$

Solution is exactly the same as for the 3-D model when restrictions are satisfied

Plane stress model

Hypotheses

- Solid is a plate
- Stress assumptions

$$\tau_{zz} = \tau_{xz} = \tau_{yz} = 0$$

$$\tau_{xx} = \tau_{xx}(x, y)$$

$$\tau_{yy} = \tau_{yy}(x, y)$$

$$\tau_{xy} = \tau_{xy}(x, y)$$

- Restrictions on loading

Volume	Lateral surface
--------	-----------------

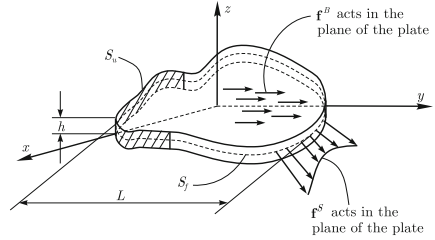
$f_x^B = f_x^B(x, y)$	$f_x^S = f_x^S(x, y)$
-----------------------	-----------------------

$f_y^B = f_y^B(x, y)$	$f_y^S = f_y^S(x, y)$
-----------------------	-----------------------

$f_z^B = 0$	$f_z^S = 0$
-------------	-------------

Top and bottom surfaces

$$f_x^S = 0, f_y^S = 0, f_z^S = 0$$



Primary variables

Displacements	Stresses	Strains
$\mathbf{u} = \begin{bmatrix} u(x, y) \\ v(x, y) \end{bmatrix}$	$\boldsymbol{\tau} = \begin{bmatrix} \tau_{xx} \\ \tau_{yy} \\ \tau_{xy} \end{bmatrix}$	$\boldsymbol{\varepsilon} = \begin{bmatrix} \varepsilon_{xx} \\ \varepsilon_{yy} \\ \gamma_{xy} \end{bmatrix}$

Remarks

Formulation is cast in the 2-D domain

Upon solution of \mathbf{u} , $\boldsymbol{\tau}$, $\boldsymbol{\varepsilon}$, we can evaluate: $\varepsilon_{zz} = -\frac{\nu}{E}(\tau_{xx} + \tau_{yy})$,
 w by integration of ε_{zz}

Remaining variables are zero: $\tau_{zz} = \tau_{xz} = \tau_{yz} = 0$,
 $\gamma_{xz} = \gamma_{yz} = 0$

Solution is only approximate compared with the solution of the 3-D model; however, it is close to the solution of the 3-D model

as long as the restrictions are satisfied and the plate is thin.

Additional solution terms of the 3-D exact solution are proportional to z^2 .

Axisymmetric model

Hypotheses

- Solid is of revolution
- Loading is axisymmetric

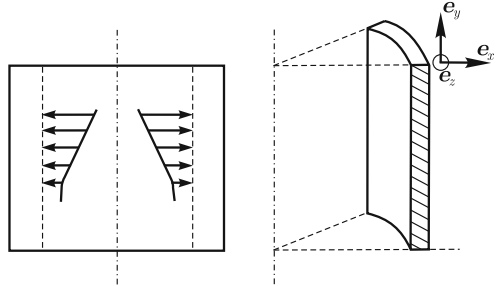
These hypotheses lead to

$$w = 0$$

$$\tau_{xz} = \tau_{yz} = 0$$

$$\gamma_{xz} = \gamma_{yz} = 0$$

$$\varepsilon_{zz} = \frac{u}{x}$$



Primary variables

Displacements

$$\mathbf{u} = \begin{bmatrix} u(x, y) \\ v(x, y) \end{bmatrix}$$

Stresses

$$\boldsymbol{\tau} = \begin{bmatrix} \tau_{xx} \\ \tau_{yy} \\ \tau_{xy} \\ \tau_{zz} \end{bmatrix}$$

Strains

$$\boldsymbol{\varepsilon} = \begin{bmatrix} \varepsilon_{xx} \\ \varepsilon_{yy} \\ \gamma_{xy} \\ \varepsilon_{zz} \end{bmatrix}$$

Remarks

Formulation is cast in the 2-D domain

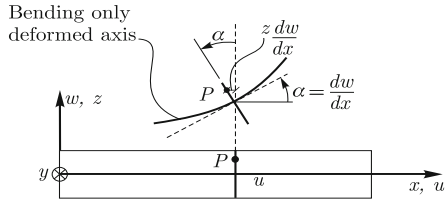
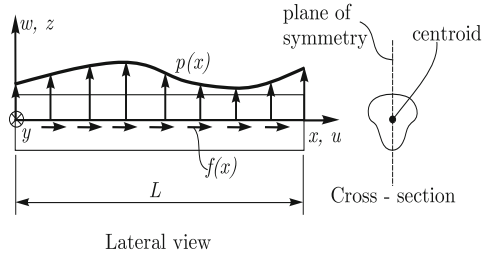
The solution for \mathbf{u} , $\boldsymbol{\tau}$, $\boldsymbol{\varepsilon}$ appended by $w = 0$, $\tau_{xz} = \tau_{yz} = 0$,

$\gamma_{xz} = \gamma_{yz} = 0$ is exactly the same as the solution of the 3-D model provided restrictions are satisfied

Bernoulli-Euler beam model

Hypotheses

- Solid is a straight bar
- Bar sections remain plane and orthogonal to the deformed axis
- Kinematics is fully described by:
 - $u(x)$ displacement of the axis in the x direction
 - $w(x)$ displacement of the axis in the z direction
- Loading
 - $p(x)$ transverse distributed load
 - $f(x)$ axial distributed load



Primary variables

Displacements	Generalized stresses	Generalized strains
$\mathbf{u} = \begin{bmatrix} u(x) \\ w(x) \end{bmatrix}$	$\boldsymbol{\tau} = \begin{bmatrix} N(x) \\ M(x) \end{bmatrix}$	$\boldsymbol{\varepsilon} = \begin{bmatrix} \varepsilon \\ \kappa \end{bmatrix}$

Remarks

Formulation is cast in the 1-D domain

There is no transverse shear strain, *i.e.*, $\gamma_{xz} = 0$

Note that κ gives the change in curvature χ since the initial curvature is zero (bar is straight)

Curved bar model

Hypotheses

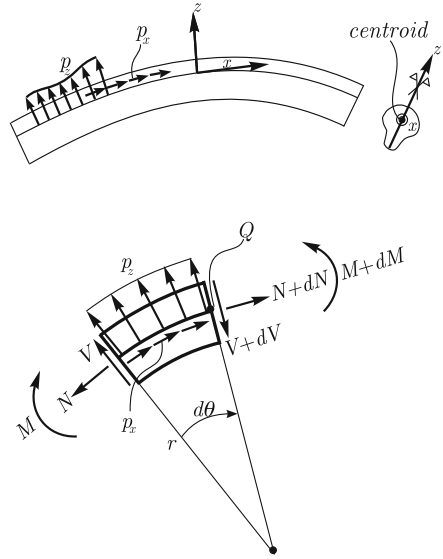
- Solid is a curved bar
- Bar sections remain plane and orthogonal to the deformed axis

• Kinematics is fully described by:

- $u(s)$ displacement of the axis in the tangential x direction
- $w(s)$ displacement of the axis in the normal z direction

• Loading

- $p_x(s)$ tangential distributed load
- $p_z(s)$ normal distributed load



Primary variables

Displacements	Generalized stresses	Generalized strains
$\mathbf{u} = \begin{bmatrix} u(s) \\ w(s) \end{bmatrix}$	$\boldsymbol{\tau} = \begin{bmatrix} N(s) \\ M(s) \end{bmatrix}$	$\boldsymbol{\varepsilon} = \begin{bmatrix} \varepsilon_{xx_0} \\ -\chi \end{bmatrix}$

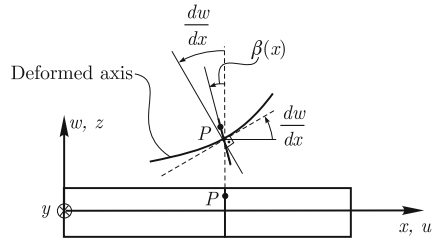
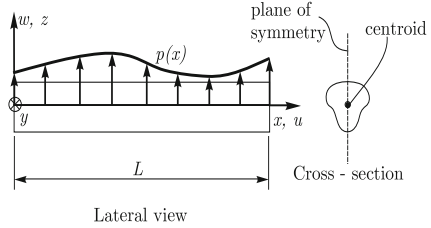
Remarks

- Formulation is cast in a 1-D curved domain
- There is no transverse shear strain, *i.e.*, $\gamma_{xz} = 0$
- Kinematic assumptions of Bernoulli-Euler model

Timoshenko beam model

Hypotheses

- Solid is a straight bar
- Bar sections remain plane but not necessarily orthogonal to the deformed axis
- Kinematics is fully described by:
 - $w(x)$ displacement of the axis in the z direction
 - $\beta(x)$ rotation of the cross-section
- Loading
 - $p(x)$ transverse distributed load



Primary variables

Displacements	Generalized stresses	Generalized strains
$\mathbf{u} = \begin{bmatrix} w(x) \\ \beta(x) \end{bmatrix}$	$\boldsymbol{\tau} = \begin{bmatrix} V(x) \\ M(x) \end{bmatrix}$	$\boldsymbol{\varepsilon} = \begin{bmatrix} \gamma_{xz} \\ \frac{d\beta}{dx} \end{bmatrix}$

Remarks

Formulation is cast in the 1-D domain

The model includes transverse shear deformations $\gamma_{xz} \neq 0$

The formulation can also be presented including the axial displacement $u(x)$ and the loading $f(x)$ as for the Bernoulli-Euler model

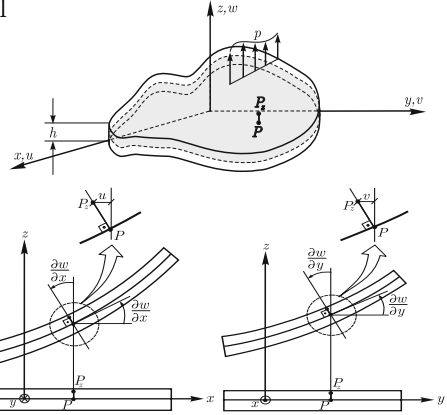
Kirchhoff plate model

Hypotheses

- Solid is a thin plate
- Straight material lines which are initially orthogonal to the midsurface of the plate remain straight and orthogonal to the deformed midsurface
- Displacements in the transverse direction do not vary along the thickness of the plate
- Each plate lamina is in a state of plane stress
- Kinematics is fully described by:

$$w = w(x, y)$$
- Loading

$$p(x, y) \quad \text{transverse loading per unit of surface area}$$



Primary variables

Displacements	Generalized stresses	Generalized strains
$\mathbf{u} = \begin{bmatrix} w(x, y) \end{bmatrix}$	$\boldsymbol{\tau} = \begin{bmatrix} M_x \\ M_y \\ M_{yx} \end{bmatrix}$	$\boldsymbol{\varepsilon} = \begin{bmatrix} \kappa_x \\ \kappa_y \\ \kappa_{yx} \end{bmatrix}$

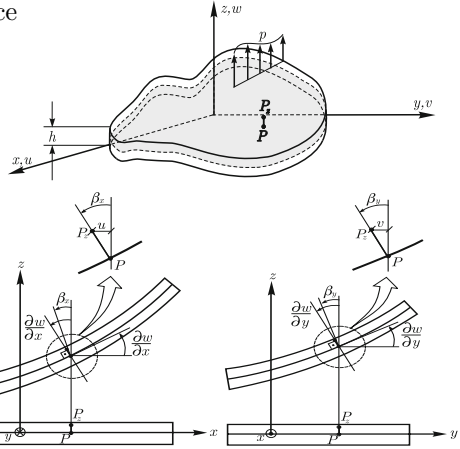
Remarks

Formulation is cast in a 2-D domain, the midsurface of the plate
 There are no transverse shear stresses: $\gamma_{xz} = \gamma_{yz} = 0$

Reissner-Mindlin plate model

Hypotheses

- Solid is a thin to moderately thick plate
- Straight material lines which are initially orthogonal to the midsurface of the plate remain straight but not necessarily orthogonal to the deformed midsurface
- For bending each plate lamina is in a state of plane stress
- Kinematics is fully described by:
 - $w = w(x, y)$
 - $\beta_x = \beta_x(x, y)$
 - $\beta_y = \beta_y(x, y)$
- Loading
 - $p(x, y)$ transverse loading per unit of surface area



Primary variables

Generalized displacements	Generalized stresses	Generalized strains
$\mathbf{u} = \begin{bmatrix} w(x, y) \\ \beta_x(x, y) \\ \beta_y(x, y) \end{bmatrix}$	$\boldsymbol{\tau} = \begin{bmatrix} M_x \\ M_y \\ Q_x \\ Q_y \end{bmatrix}$	$\boldsymbol{\varepsilon} = \begin{bmatrix} \frac{\partial \beta_x}{\partial x} \\ \frac{\partial \beta_y}{\partial y} \\ \frac{\partial \beta_x}{\partial y} + \frac{\partial \beta_y}{\partial x} \\ \gamma_{xz} \\ \gamma_{yz} \end{bmatrix}$

Remarks

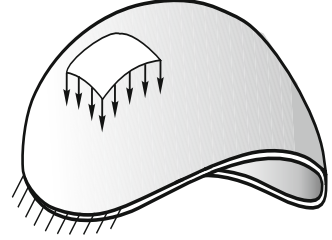
Formulation is cast in a 2-D domain, the midsurface of the plate

Shell models

Hypotheses

Basic shell model

- Solid is a shell with a midsurface
- Straight material lines initially orthogonal to the midsurface remain straight and unstretched during deformations
- Kinematic variables are referred to the shell midsurface
- The stress in the direction orthogonal to the midsurface is zero



Membrane-shear-bending model

Additional hypotheses permit the analytical integration through the shell thickness

Membrane-bending model

- Additional hypothesis: straight material lines initially orthogonal to the midsurface remain orthogonal to the midsurface during deformations
- Hence transverse shear strains are zero

Remarks

This summary for shells is only giving some basic model hypotheses since much more discussion would be required before we could present for each shell model a summary analogous to those presented for the other models, see Chapelle and Bathe, 2010a

Table 4.3. Definitions of \mathbf{C} and \mathcal{D}_ε for linear elasticity mathematical models

Mathematical model (displacements)	Constitutive matrix \mathbf{C}	Strain-displacement matrix \mathcal{D}_ε
3-D elasticity (u, v, w)	$\mathbf{C} = \frac{E(1-\nu)}{(1+\nu)(1-2\nu)} \begin{bmatrix} 1 & \frac{\nu}{1-\nu} & \frac{\nu}{1-\nu} & 0 & 0 & 0 \\ \frac{\nu}{1-\nu} & 1 & \frac{\nu}{1-\nu} & 0 & 0 & 0 \\ \frac{\nu}{1-\nu} & \frac{\nu}{1-\nu} & 1 & 0 & 0 & 0 \\ 0 & 0 & 0 & \frac{1-2\nu}{2(1-\nu)} & 0 & 0 \\ 0 & 0 & 0 & 0 & \frac{1-2\nu}{2(1-\nu)} & 0 \\ 0 & 0 & 0 & 0 & 0 & \frac{1-2\nu}{2(1-\nu)} \end{bmatrix}$	$\begin{bmatrix} \frac{\partial \cdot}{\partial x} & 0 & 0 \\ 0 & \frac{\partial \cdot}{\partial y} & 0 \\ 0 & 0 & \frac{\partial \cdot}{\partial z} \\ \frac{\partial \cdot}{\partial y} & \frac{\partial \cdot}{\partial x} & 0 \\ 0 & \frac{\partial \cdot}{\partial z} & \frac{\partial \cdot}{\partial y} \\ \frac{\partial \cdot}{\partial z} & 0 & \frac{\partial \cdot}{\partial x} \end{bmatrix}$
Plane strain (u, v)	$\frac{E(1-\nu)}{(1+\nu)(1-2\nu)} \begin{bmatrix} 1 & \frac{\nu}{1-\nu} & 0 \\ \frac{\nu}{1-\nu} & 1 & 0 \\ 0 & 0 & \frac{1-2\nu}{2(1-\nu)} \end{bmatrix}$	$\begin{bmatrix} \frac{\partial \cdot}{\partial x} & 0 \\ 0 & \frac{\partial \cdot}{\partial y} \\ \frac{\partial \cdot}{\partial y} & \frac{\partial \cdot}{\partial x} \end{bmatrix}$
Plane stress (u, v)	$\frac{E}{1-\nu^2} \begin{bmatrix} 1 & \nu & 0 \\ \nu & 1 & 0 \\ 0 & 0 & \frac{1-\nu}{2} \end{bmatrix}$	$\begin{bmatrix} \frac{\partial \cdot}{\partial x} & 0 \\ 0 & \frac{\partial \cdot}{\partial y} \\ \frac{\partial \cdot}{\partial y} & \frac{\partial \cdot}{\partial x} \end{bmatrix}$
Axisymmetric (u, v)	$\frac{E(1-\nu)}{(1+\nu)(1-2\nu)} \begin{bmatrix} 1 & \frac{\nu}{1-\nu} & 0 & \frac{\nu}{1-\nu} \\ \frac{\nu}{1-\nu} & 1 & 0 & \frac{\nu}{1-\nu} \\ 0 & 0 & \frac{1-2\nu}{2(1-\nu)} & 0 \\ \frac{\nu}{1-\nu} & \frac{\nu}{1-\nu} & 0 & 1 \end{bmatrix}$	$\begin{bmatrix} \frac{\partial \cdot}{\partial x} & 0 \\ 0 & \frac{\partial \cdot}{\partial y} \\ \frac{\partial \cdot}{\partial y} & \frac{\partial \cdot}{\partial x} \\ \frac{\partial \cdot}{\partial x} & 0 \end{bmatrix}$

Table 4.4. Definitions of \mathbf{C} and ∂_ε for structural mathematical models

Mathematical model (generalized displacements)	Generalized constitutive matrix \mathbf{C}	Generalized strain-displacement matrix ∂_ε
Bernoulli-Euler beam (u, w)	$\begin{bmatrix} EA & 0 \\ 0 & EI \end{bmatrix}$	$\begin{bmatrix} \frac{d \cdot}{dx} & 0 \\ 0 & \frac{d^2 \cdot}{dx^2} \end{bmatrix}$
Curved beam (u, w)	$\begin{bmatrix} EA & 0 \\ 0 & EI \end{bmatrix}$	$\begin{bmatrix} \frac{d \cdot}{ds} & \frac{\cdot}{r} \\ -\frac{d}{ds} \left(\frac{\cdot}{r} \right) & \frac{d^2 \cdot}{ds^2} \end{bmatrix}$
Timoshenko beam (w, β)	$\begin{bmatrix} kGA & 0 \\ 0 & EI \end{bmatrix}$	$\begin{bmatrix} \frac{d \cdot}{dx} & -1 \\ 0 & \frac{d \cdot}{dx} \end{bmatrix}$
Kirchhoff plate (w)	$D \begin{bmatrix} 1 & \nu & 0 \\ \nu & 1 & 0 \\ 0 & 0 & (1 - \nu) \end{bmatrix}$	$\begin{bmatrix} \frac{\partial^2 \cdot}{\partial x^2} \\ \frac{\partial^2 \cdot}{\partial y^2} \\ \frac{\partial^2 \cdot}{\partial x \partial y} \end{bmatrix}$
Reissner-Mindlin plate (w, β_x, β_y)	$\begin{bmatrix} D & \nu D & 0 & 0 & 0 \\ \nu D & D & 0 & 0 & 0 \\ 0 & 0 & \frac{D(1-\nu)}{2} & 0 & 0 \\ 0 & 0 & 0 & kGA & 0 \\ 0 & 0 & 0 & 0 & kGA \end{bmatrix}$	$\begin{bmatrix} 0 & \frac{\partial \cdot}{\partial x} & 0 \\ 0 & 0 & \frac{\partial \cdot}{\partial y} \\ 0 & \frac{\partial \cdot}{\partial y} & \frac{\partial \cdot}{\partial x} \\ \frac{\partial \cdot}{\partial x} & -1 & 0 \\ \frac{\partial \cdot}{\partial y} & 0 & -1 \end{bmatrix}$